A STUDY OF A- AND B-TYPE STARS IN THE SOUTHERN GALACTIC HALO

Thesis by

Jeffrey Ross Pier

In Partial Fulfillment of the Requirements

for the Degree of

Doctor of Philosophy

California Institute of Technology

Pasadena, California

1983

(Submitted October 18, 1982)

To Nancy, Catherine and Christina

ACKNOWLEDGEMENTS

I have benefitted immeasurably from the friendship and help of a great many people during the course of my graduate work. The faculty, support staff and fellow students have all helped make my years at Caltech not only richly rewarding academically and scientifically but have also helped foster my scientific curiosity in an atmosphere of openness and integrity. The privilege of working with such people is one of the great attractions that a career in science holds and I treasure it highly.

George Preston has guided the course of this work with innumerable insightful suggestions and an unflagging interest. I have always walked away from our conferences feeling refreshed, encouraged and full of new ideas. I am also grateful to George, as a very busy director of the Mount Wilson and Las Campanas Observatories, for a very generous allocation of his personal time and of observatory telescope time.

I appreciate helpful correspondence with Bruce Carney, with Robert Kurucz (who provided magnetic tapes of his model atmospheres), and with A. W. J. Cousins, Jim Hesser and Steve Shawl who provided me with materials in advance of publication.

Las Campanas Observatory is a very special place. The people there to whom I am especially indebted inlude Oscar Duhalde, Angel Guerra, Fernando Peralta, Ljubo Papic, Bill Robinson and Hernan Solis. I always look forward to returning to LCO for an opportunity to renew friendships and work at their splendid facility.

Many people at 813 Santa Barbara Street have contributed, especially Bob Brucato, Ken Clardy, Jerry Kristian, Armando Manduca,

Leonard Searle and Gary Yanik. A special word of thanks goes to Steve Shectman who designed and built the marvelous detector for the du Pont spectrograph and who also provided me with many useful suggestions on all aspects of this work.

The debt of gratitude I owe to the faculty and staff at Caltech cannot be adequately expressed in a reasonable amount of space but I want to make special mention of Professors Jesse Greenstein, Jim Gunn, Bev Oke and Wal Sargent, librarian Helen Knudson and VAX SYS$MANAGERS Tim Pearson and Mike Lesser.

I am grateful to Wal and Anneila Sargent, Steve Knapp, and the North Wilson Avenue Astronomical Ghetto (NWAAG) for the hospitality I enjoyed while much of this work was written.

I thank Marshall Cohen, Wal Sargent, Maarten Schmidt, the National Science Foundation and the U. S. Veteran's Administration for financial support.

Much of the time invested in graduate work is spent in the company of fellow graduate students and post-docs and it is from them that one learns the actual techniques of observing, computing, data reduction and analysis and with whom one develops a taste for Armenian food and late-night philosophical discussions. My graduate years have been enriched through associations with all graduate students and post-docs at Caltech and at MWLCO. Those who have made special contributions include, but are not limited to, Todd Boroson, Alex Filippenko, Richard Green, John Hoessel, Steve Kent, Dave Monet, Doug Rabin, Don Schneider, Abi Saha, Richard Simon, Richard Wade and Howard Yee. I am grateful to them all and look forward to their continued friendship.

ABSTRACT

A sample of over 200 stars of spectral types A and B has been selected for study. Drawn from the Preston and Shectman objective-prism survey of the southern galactic halo, the stars comprise a sample of halo objects selected without kinematic bias. Photoelectric UBV photometry has been obtained and the sample stars have apparent V magnitudes mostly in the range $13.5 \leq V \leq 15.5$. The (U-B)--(B-V) two-color diagram shows that the halo AB stars have colors similar to those of globular cluster blue horizontal-branch (BHB) stars.

Reticon spectroscopy of the sample confirms the BHB status of the large majority of the sample. Interesting non-BHB stars found include a few high luminosity A stars, several stars of low metallicity and apparently normal main-sequence gravities which may be field Population II blue stragglers, and ten metallic-line stars. A few normal A stars have been found as far as 2 to 3 kpc from the plane, but none beyond that distance. It is suggested that the metal-rich early-type population found by other authors belongs to a population of old disk stars with a scale height of over 1 kpc.

Interstellar Ca II K lines are found in many of the high-velocity stars. The interstellar components arise from low-velocity material associated with the disk.

The solar motion of the halo AB stars is -236 ± 39 km s^{-1} and the velocity ellipsoid is elongated towards the galactic center throughout the halo. By adding a list of halo objects drawn from other sources and solving for the solar motion a lower limit of -208 ± 20 km s^{-1} is set for the circular velocity at the solar radius. The solar motion solution is found to be metallicity-dependent. Anisotropy in the velocity ellipsoid is strongly indicated for the combined halo objects. The presence of this global anisotropy removes one of the arguments favoring a flattened halo. Since the gravitational potential of the disk increases the z component of velocity it is seen that at very early times in the history of the Galaxy the velocities were highly anisotropic (predominantly radial).

TABLE OF CONTENTS

INTRODUCTORY NOTE

The chapters comprising this thesis have been written essentially as individual papers to be submitted to refereed journals. Chapter 1 has, in fact, been accepted for publication and is scheduled to appear in the November, 1982 Astronomical Journal. Chapter 2 will be submitted to The Astrophysical Journal Supplement and Chapter 3 to The Astrophysical Journal.

Chapter 1

UBV PHOTOMETRY OF A- AND B-TYPE STARS IN THE SOUTHERN GALACTIC HALO

I. INTRODUCTION

Large-scale surveys of the halo constituents of the Galaxy have included classes of objects such as globular clusters, field subdwarfs and RR Lyrae stars. Kinman, Mahaffey, and Wirtanen (1982, hereinafter KMW) point out that studies of all three classes of objects suffer to some extent from selection effects and luminosity uncertainties. The existing subdwarf sample, for example, is limited to nearby stars due to their low intrinsic luminosities. Furthermore, many of them have been chosen on the basis of their high proper motions. (Nonetheless, much of our fundamental knowledge of halo kinematics and metallicities has come from studies of subdwarfs and there is little reason to doubt that the local subdwarf population is a fair representation of the overall subdwarf population in the halo field).

The globular cluster system is the archetype and touchstone for studies of the halo population. Nevertheless it is not clear that globular clusters and the halo field have the same evolutionary history (see Mould 1982 for a timely and comprehensive review of the entire stellar populations picture). Furthermore there exists considerable controversy regarding the size of the spreads in both the ages and the metallicities of the globular clusters.

One would like to be able to study a representative sample of field halo stars *in situ* and discern their kinematics and metallicities. One obvious candidate for such a study is the population of field RR Lyrae variable stars. Unfortunately, searches for faint RR Lyrae stars are necessarily long and difficult and require considerable amounts of telescope time. The Lick astrograph survey (KMW and many references therein) has been under way for over two decades and comprises a search of eight halo fields for variables out to ~ 20 kpc. This monumental work will no doubt prove to be of great importance to our understanding of galactic structure.

The ideal tracer of the halo would perhaps be one from a sample of intrinsically very luminous objects, substantial in number, which waves a straightforward and reliable metallicity banner and is easily distinguishable from foreground disk objects. Nature hasn't yet pointed the way toward such an object (although if one could devise an efficient means for distinguishing faint foreground red dwarfs from halo red giants it might start us in the right direction). Finding intrinsically luminous blue objects seems, at the moment, to be more promising.

Several colorometric searches towards the galactic poles have produced lists of faint blue objects (see, for example, Haro and Luyten 1962, and Chavira 1958 for studies of southern high latitude fields). Such lists are, however, greatly contaminated by nearby white dwarfs and hot subdwarfs, as well as by faint blue extragalactic objects. Objective-prism searches over limited areas (e.g., Philip and Sanduleak 1968; Slettebak and Brundage 1971) have produced lists of stars with

spectral types ranging mostly from late B through early F. The AB stars are both sufficiently luminous and numerous at large distances from the plane to provide a large enough sample for a major study. Additionally, as pointed out by Rodgers (1971), absolute magnitudes and radial velocities of AB stars can be determined confidently.

The Curtis Schmidt objective-prism search for metal poor stars (Preston and Shectman, 1979) is currently comprised of 80 fields distributed over the southern sky mostly south of galactic latitude -40^{o}, although a select few are at lower southern latitudes. Sixty-eight of these have been scanned so far. As a side product, several thousand field AB stars have been discovered in the southern galactic halo with B magnitudes in the range $12.5 \lesssim B \lesssim 15.5$. As classified by Preston and Shectman, "AB" stars are those whose spectra obtained through their H and K interference filter (~ 180 Å/mm at Ca II K λ3934) possess prominent H_{ε} λ3970 and a non- or marginally visible K line. The list of these objects provides a homogeneous sample of field halo objects selected without kinematic bias and in a magnitude range which, for the most part, assures their membership, or at the very least their present residence, in the halo.

This paper is the first in a series describing a photometric and spectroscopic study of a sample of about 200 AB stars drawn from the Preston and Shectman survey. Details regarding the survey itself will be published elsewhere (Preston, Shectman and Pier 1982). Section II below describes the sample chosen for the present work. Section III discusses the photometric observations and reductions of the data. Results are presented in Section IV.

II. THE SAMPLE

Seven regions of the sky were selected from the Preston and Shectman survey fields for which objective-prism plates had been obtained by mid-1980. Five of the regions lie on or near the meridional plane along galactic longitudes $l=0^{o}$ to $l=180^{o}$ from south of the galactic center through the southern polar cap to the anticenter. The other two regions lie near the longitudes of the solar apex and antapex. Within each of the seven regions a list of stars classified as AB by Preston was chosen. The goal was to observe $\gtrsim 30$ stars in each region. In some regions there weren't enough AB stars and a few mid-A spectral types were included.

In Table I are listed the 16 Curtis Schmidt (CS) fields which make up the seven survey regions. The 1950.0 equatorial and galactic (system II is used throughout) coordinates of the field centers and the number of stars for which UBV photometry has been obtained in each field are given.

The relative positions of all survey stars as well as those of numerous SAO positional reference stars per plate were determined using the XY machine at the offices of the Mount Wilson and Las Campanas Observatories in Pasadena, largely by S. Shectman although a few plates were measured by the present author. Positional accuracy thus determined is typically on the order of one arcsecond judging from the residuals of the reference stars after solving for the plate constants. Enlarged prints of the objective-prism plates served as finding charts.

III. OBSERVATIONS AND REDUCTIONS

(a) Observations

In order to (1) limit the sample to a well defined color range and (2) deduce photometric parallaxes for each object, photoelectric UBV photometry was obtained for the sample stars. All photoelectric observations were made at the Cassegrain focus of the 40" Swope Telescope at Las Campanas Observatory using the same single-channel dry ice cooled S20 cathode and FW130 photomultiplier in a pulse counting mode. The data were gathered over two observing seasons during the months of August and September of both 1980 and 1981. The same set of UBV filters was used for all observations; the filter combinations used are shown in Table II. Observations were made exclusively through a ~ 15 arcsecond circular aperture.

Data acquisition software was developed by the author for the photometry system's HP9830 computer which provided real-time error analysis to aid in monitoring the photometric quality of the observations. For each observation two error calculations were made: (1) the standard error from Poisson statistics of the accumulated dark, sky and sky+object counts; and (2) the observed variance among repeated observations through each filter. Each observation consisted of a minumum of two integrations through each filter both on and off the object. No integration was longer than 30 seconds. Offset guiding was not deemed necessary since the integrations were so short. Although the centering of the objects within the aperture was checked

frequently, the telescope tracked so well at small hour angles that in practice little or no correction was ever necessary. Repeated integrations for each object were accumulated to the point where theoretical Poisson statistics predicted a standard error of $\lesssim 1\%$ in each filter. For the very faintest stars the sky signal became, of course, very important and the required integration times impractically long. Consequently, in a few cases the criterion was relaxed to ~ 1.5-2.0% in the U filter.

UBV photometric standards were chosen from the Harvard E-region lists of Cousins [Cousins and Stoy (1962); see Vogt, Geisse, and Rojas 1981 (hereinafter VGR), for a recent and very useful compilation] and supplemented by several of the blue standards from Table II of Landolt (1973). Each night about twenty observations were made of stars from the standard list. The standards were chosen to comfortably, though not excessively, bracket the color distribution of the program stars. A few faint standards were observed each night to verify the linearity of the detector. Bright standards were avoided and coincidence corrections were negligible. The secant of the zenith distance was computed for the mid-time of each observation and used as airmass.* All program stars were observed near the meridian at airmasses ≤ 1.3. Standard stars were observed largely at similar airmasses and in the same general part of the sky as the survey fields whenever possible. Each night a small number of observations of standard stars was carried out at slightly higher airmasses (typically $1.4 \lesssim \sec z \lesssim 2.0$) to give

---

* See appendix for a discussion regarding this procedure.

some weight to the extinction solution. In all, 253 photometric observations of 234 program stars were made during times of excellent photometric conditions.

(b) Reductions

A least squares solution was employed to solve for the nightly extinction and color terms using a procedure similar in philosophy, though not in detail, to that described by Harris, Fitzgerald and Reed (1981). An iterative process was employed to derive mean extinction coefficients for each of the two observing seasons and then a final solution was made employing the mean coefficients and solving for nightly zero points only. Table III presents a summary of each night's photometric observations. Included are the numbers of standard and program unknown observations made and the rms residuals in the final adopted fits to the standards. The last line shows the unweighted means of the residuals.

Although the size of the residuals of the standards provides a means for estimating internal errors, a more realistic measure of the probable errors can be derived from (1) the results of repeated observations of the same objects on different nights and from (2) a comparison with observations of the same stars made by other observers. Seventeen stars were observed twice and one star three times in the present program yielding twenty pairs of observations for comparison. Fourteen of the stars in the southern polar cap region have published UBV photometry by Eggen. His photometry for most of the stars from

Table 2 of Philip and Sanduleak (1968) was published by Rodgers (1971) and eleven of them are in common with the present work. They are those stars designated with "PS" numbers in Table VI below. Three of the stars from Table 3 of Eggen's (1968) photometry (CS22882-3, CS22882-31, and CS22942-31) are also in common. Figures 1(a) through (c) show the results of the comparisons where the differences in V, B-V and U-B respectively are plotted against B-V. Figures 1(d) through (f) show the differences plotted versus V. The diamond symbols indicate differences in pairs of observations of the same stars in the present work; the "+" symbols represent the differences between this work and that of Eggen (in Rodgers 1971); and the "X" symbol the differences between this work and Eggen (1968). No correlation seems to exist between the size of the differences and either color or magnitude. A similar plot of differences versus U-B (not included here) likewise shows no correlation.

A summary of the comparisons made is given in table IV where first is shown the standard error for a single observation determined from multiple observations of the same stars in the present work. A comparison of these errors with the residuals shown in Table III shows excellent agreement. Comparison with Eggen's published photometry is, regrettably, less satisfactory. The last four lines of Table IV show the mean differences [in the sense (this work)-(Eggen)] and the variances of the differences.

(c) Discrepant U-B Standards

Five of the E-region stars chosen as standards had consistently high residuals relative to the values given in VGR. The high residuals are independent of color and airmass. Table V shows the U-B colors derived by treating the five stars as unknowns. Also shown are the mean values and the rms for the observations. These stars are identified by their E region and their Cape "Q" numbers (Cousins and Stoy 1962). Also shown are the standard values quoted from VGR. The observed mean values were adopted as standard values for the present work and the stars were then used as U-B standards. (See Note Added in Proof at bottom of Table V).

IV. RESULTS

(a) Description of Table VI

The results of UBV observations for 234 stars are presented in Table VI as follows:

Column 1--The Curtis Schmidt plate number and the star number assigned by Preston as he scanned the plates.

Columns 2 and 3--Equatorial coordinates for epoch 1950.0.

Columns 4 and 5--Galactic longitude and latitude (System II).

Column 6--Spectral and brightness classification assigned by Preston. (b ==> bright, f ==> faint, m ==> medium, v ==> very).

Columns 7, 8 and 9--Reduced magnitude and colors. No corrections for reddening have been applied.

Column 10--The number of photometric observations obtained in the present work.

Column 11--Previous designations when known. PHL numbers are from Haro and Luyten (1962), PS from Table 2 of Philip and Sanduleak (1968), SB numbers from Slettebak and Brundage (1971), and TS numbers from the southern Tonantzintla list of Chavira (1958).

(b) The Two-Color Diagram

The (U-B)-(B-V) two-color diagram for 231 of the stars in the sample is shown in Figure 2. No reddening corrections have been applied to the reduced colors. Three stars (CS22936-267, CS22964-104 and CS22964-124) were omitted because their red colors make it clear that they are not AB stars. Misidentification at the telescope or possible misclassification on the objective-prism plates (due to overlapping images for example) are possible explanations. The two fields in which these stars lie (CS 22936 and CS 22964) are the most crowded of all the fields in the sample.

The smoothed curve labelled "V" in Figure 2 is a least-squares polynomial fit to the combined main sequence data of Johnson (1966) and Fitzgerald (1970). The curves labelled "III" and "I" are fits to luminosity classes III and Iab from Fitzgerald (1970). The black body

relation, labelled "BB", is a fit to combined data from Arp (1961) and Matthews and Sandage (1963). A representative 2σ error bar of ± 0.015 mag in each color is plotted in the upper right-hand corner of the diagram.

The part of the two-color diagram occupied by late B and early A stars is one where gravity and metallicity effects are difficult to disentangle. If these sample stars are evolved metal poor stars, as was expected *a priori*, then their surface gravities would be somewhat lower than main sequence gravities and their consequently larger Balmer discontinuity would contribute towards an ultraviolet deficiency. Barring other effects, such stars should lie below the main sequence relation. However, the relative absence of metallic line blanketing would normally be expected to act in the opposite sense (see Newell 1970 for a more complete discussion of these effects). For the hotter stars, however, Wolff (1967) showed that in some cases the deblanketing vectors act in the sense of increased ultraviolet deficiency.

A large majority of the stars in the color range $-0.10 \leq (B-V) \leq 0.15$ do lie well below the main sequence locus. For these relatively hot stars, the deblanketing vectors are largely oriented along B-V and have little negative (and perhaps even a positive) U-B effect while gravity effects tend to move the stars below the main sequence relation (increased U-B). The distribution of these stars in the (U-B, B-V) plane is very similar to the distribution of blue horizontal-branch (BHB) stars in the field and in globular clusters. For the purpose of comparison, Figure 3 shows the two-color diagram for a selection of previously published photoelectric UBV

photometry of BHB stars in the globular clusters M3, M13, M15 and M92 (Sandage 1969), NGC 6397 and ω Centauri (Newell, Rodgers and Searle 1969a,b), and NGC 6752 (Cannon and Stobie 1973). Also plotted are stars in the galactic polar regions classified as field horizontal-branch by Philip (1968; 1974). Additionally, those stars suspected of being globular cluster blue stragglers in M3 and M15 (Sandage 1970) and in M71 (Arp and Hartwick 1971) are plotted as plus symbols. All globular cluster star colors plotted in Figure 3 have been corrected for reddening using the E(B-V) values given for each cluster by Harris and Racine (1979) and adopting E(U-B) = 0.72E(B-V). No reddening corrections have been applied to the field horizontal-branch star colors due to their high galactic latitudes. The main sequence relation is again shown for reference. The similarity between the distribution of colors in Figures 2 and 3 is readily apparent.

For the cooler stars [(B-V) $\geq$ 0.25], line blanketing becomes increasingly important and those cooler stars lying well above the main sequence relation are likely to be unevolved and metal poor. Six of the coolest stars (CS22171-9, CS22882-8 and -27, CS22946-11, CS22949-1 and -7) lie in the region of the (U-B, B-V) plane occupied by the extreme subdwarfs [cf Figure 6 of Eggen and Greenstein (1965)]. These six stars are plotted as plus symbols in Figure 2. Comparison with Figure 3 shows that some of the globular cluster blue stragglers also lie in this region of the two-color diagram. Spectra have not been obtained for these stars and so no further discrimination can be attempted at present.

Three of the stars, plotted as open circles, lie in the region well above the main sequence and near the black body relation. In this domain reside high luminosity stars, white dwarfs, and composite systems [cf Figure 15 of Greenstein and Sargent (1974); Figure 6 of Eggen and Greenstein (1965)]. Spectra for two of these stars were obtained and from them it is clear that neither is a white dwarf. The spectrum of CS22875-25 shows weak Balmer absorption lines, He I λ4026 and λ4471 plus a broad, diffuse Ca II K (λ3934) line with an equivalent width of ~ 0.8 Å, far greater than what could easily be attributed to an interstellar origin. It is likely that this object is an unresolved composite with a hot star (sdO for example) plus a cooler star which makes a non-negligible contribution to the blue light. CS22875-27 also shows Balmer lines that are much too weak and narrow for a normal BHB or main sequence star and it has a K line of normal profile with equivalent width ~ 2.7 Å, unusually large for its color. This star is judged to be a high luminosity A star. No spectrum was obtained for the third star in this region, CS22949-5.

CS22941-24, plotted as an open square, lies in a region of the (U-B, B-V) plane unoccupied by any other star in the homogeneous data file which Nicolet (1978, 1980) selected from the published UBV photometry of over 5000 stars assembled in the Mermilliod-Nicolet catalogue (1977). Since this star is the faintest one observed one may well suspect large errors in the photometry. Unfortunately, there is only one photometric observation and no spectroscopic observation was obtained for this star. Further observations of CS22941-24 are planned.

V. PROSPECTS AND ACKNOWLEDGEMENTS

Moderate dispersion Reticon spectra have been obtained for about 200 of the stars in the sample. Radial velocities, Balmer line profiles and metallic line indices are being determined from the spectra. Discussion of the spectroscopic observations and reductions as well as a study of the population characteristics (kinematics and metallicities) derived from the combined photometric and spectroscopic data will be published in subsequent papers in this series.

It is a pleasure to thank Sr. Oscar Duhalde for his professional and friendly assistance at the telescope. Timely modifications by Bob Brucato considerably improved the photometer and are much appreciated. Jesse Greenstein's comments on spectra were very helpful and instructive. George Preston has been very generous and helpful with his time and critical comments. An anonymous referee is thanked for helpful suggestions which clarified the presentation. This research was support in part by the National Science Foundation under grants AST 77-22615 and AST 81-17754.

Finally, much gratitude is due the late Henrietta Swope who provided the funds for the telescope (subsequently named in her honor) used for this project. Her generosity paved the way for the installation of a fine instrument on a remote mountaintop and in doing so planted the decisive seed which has sprouted into a major and

beautiful southern hemisphere observatory.

APPENDIX

The practice of using the secant of the zenith distance (sec Z) in place of the more correct airmass (X) to determine extinction effects is in common practice and, for most purposes, introduces negligible ill effects (see, for example, Hardie 1962, where it is shown that sec Z departs from a more rigorously computed airmass by less than 2% for airmasses $\lesssim 3.0$).

Given the assumption that sec Z is an appropriate quantity to use one must decide the best way to define sec Z for an observation. One common practice, employed by the present author for example, is to calculate sec Z for the midpoint of the observation: sec Z($\langle h \rangle$). Another common practice is to compute sec Z for the beginning and ending hour angles of the observation and then average them. Both of these procedures are rough approximations at best. An illustrative way to see the errors introduced thereby is to consider the observation of an object which passes through the meridian halfway through the integration. The first method would give the minimum sec Z of the observation whereas the second would give the maximum. The obviously correct way is to compute mean sec Z:

$$\langle \sec Z(h) \rangle = \int (\sec Z)\,dh / \int dh \qquad (1)$$

where the limits of the integrations are the beginning and ending hour angles (h) of the observation. Since

$$\sec Z = [\sin(\phi)\sin(\delta)+\cos(\phi)\cos(\delta)\cos(h)]^{-1} \quad (2)$$

where ϕ is the latitude of the observatory and δ and h are the declination and hour angle of the object respectively, the integral is in the analytically soluble form

$$\langle \sec Z \rangle = (\Delta h)^{-1}\int[a+b\cos(h)]^{-1}dh \quad (3)$$

$$\text{with } a = \sin\phi\sin\delta$$

$$\text{and } b = \cos\phi\cos\delta.$$

In order to evaluate the differences between $\langle \sec Z \rangle$ and $\sec Z(\langle h \rangle)$ the two quantities were calculated for various declinations and beginning hour angles employing a latitude of 30^{o} and using various integration times. For each computation the percentage difference between them

$$\%\text{Diff} \equiv 100(\text{SecZ}(\langle h \rangle)-\langle \text{SecZ} \rangle)/\langle \text{SecZ} \rangle \quad (4)$$

was tabulated. Figures 4(a) through (d) show the results of the calculations for integration times of 60, 120, 180 and 240 minutes. The absolute value of the quantity %Diff is plotted versus $\langle \sec Z \rangle$. The result is an envelope outlining the maximum percentage error one makes in $\langle \sec Z \rangle$ from using $\sec Z(\langle h \rangle)$. For relatively short integrations carried out at reasonably small zenith distances, as is the case for the present work, the difference is small. When one considers that the airmass so derived is then multiplied by an

extinction coefficient typically ~ 0.1 to 0.2 for first order terms the overall effect on magnitudes and colors is negligible.

Note, however, that for long integrations the errors introduced can become quite significant. Although such long integrations are not usually the case in photoelectric stellar photometry, they are not infrequent in spectrophotometric work. It should be emphasized that a careless employment of sec Z(⟨h⟩) could result in significant errors in such cases.

TABLE I. Selected Survey Fields

Curtis-Schmidt Plate Number	R.A. (1950)	Dec.	l	b	# of AB stars with UBV Photometry
CS 22936	18 50	-35 00	1	-16	50
CS 22964	19 56	-40 00	0	-29	39
CS 22875	22 32	-40 00	0	-59	28
CS 22881	22 06	-40 00	2	-54	4
CS 22941	23 36	-35 00	2	-73	7
CS 22882	00 28	-30 00	2	-85	17
CS 22942	00 54	-25 00	148	-87	17
CS 22946	01 18	-20 00	166	-80	10
CS 22171	02 00	-10 00	170	-66	6
CS 22184	02 40	-10 00	185	-59	10
CS 22963	03 00	-05 00	183	-52	15
CS 22172	03 20	-10 00	194	-51	6
CS 22949	23 20	-05 00	76	-59	10
CS 22894	23 40	00 00	89	-58	5
CS 22968	03 10	-55 00	270	-52	10

TABLE II. UBV Filters Used

U	3 mm Corning 9863 + 2.5 mm 80% saturated $CuSO_4$
B	2 mm GG385 + 1 mm BG12 + 2.5 mm 80% saturated $CuSO_4$
V	2 mm GG495 + 2 mm BG18

TABLE III. UBV Observation Summary

Night	No. of Unknowns	No. of Standards	Rms Residuals of Standards σ(V)	σ(B-V)	σ(U-B)
Aug 4/5, 1980	9	10	.013	.021	.018
Aug 5/6, 1980	11	13	.012	.019	.023
Aug 8/9, 1980	21	17	.017	.013	.014
Aug 9/10,1980	19	15	.016	.015	.016
Aug 10/11,1980	22	19	.016	.012	.022
Aug 12/13,1980	26	17	.014	.013	.022
Sep 7/8, 1980	18	19	.008	.009	.010
Sep 8/9, 1980	24	20	.012	.009	.011
Sep 9/10,1980	19	23	.012	.006	.012
Sep 10/11,1980	20	23	.013	.006	.008
Sep 11/12,1980	13	23	.008	.009	.010
Aug 24/25,1981	18	18	.006	.010	.011
Aug 26/27,1981	14	21	.009	.011	.011
Aug 27/28,1981	19	24	.011	.013	.012
Mean Residuals			<.012>	<.012>	<.014>

Table IV. Comparison of Photometry

	ΔV $\pm\sigma$(rms)	$\Delta(B-V)$ $\pm\sigma$(rms)	$\Delta(U-B)$ $\pm\sigma$(rms)	# Pairs
Present Work	--- $\pm$(.012)	--- $\pm$(.009)	--- $\pm$(.018)	20
Eggen, in Rodgers(1971)	-.033 $\pm$(.041)	.006 $\pm$(.018)	-.030 $\pm$(.032)	11
Eggen (1968)	-.040 $\pm$(.037)	-.017 $\pm$(.022)	.047 $\pm$(.054)	3

Table V. Discrepant E-Region U-B Standards

Star	Night	Observed (U-B)	⟨U-B⟩ ±σ(rms)	Cousins' (U-B) from VGR
E 1,Q 52 (=HD 8024)	Aug 4/5, 1980	.008	.007 ±(.008)	-.038
	Aug 5/6, 1980	.013		
	Aug 8/9, 1980	.020		
	Aug 10/11,1980	.012		
	Aug 12/13,1980	.008		
	Aug 26/27,1981	-.005		
	Aug 27/28,1981	.000		
	Aug 27/28,1981	-.002		
E 6,Q 20	Aug 9/10,1980	.286	.278 ±(.014)	.208
	Aug 10/11,1980	.284		
	Aug 12/13,1980	.297		
	Aug 24/25,1981	.264		
	Aug 26/27,1981	.272		
	Aug 27/28,1981	.262		
E 7,Q 2	Aug 4/5, 1980	-.542	-.579 ±(.017)	-.554
	Aug 5/6, 1980	-.583		
	Aug 8/9, 1980	-.599		
	Aug 10/11,1980	-.603		
	Sep 7/8, 1980	-.571		
	Sep 8/9, 1980	-.589		
	Sep 10/11,1980	-.579		
	Aug 26/27,1981	-.569		
	Aug 26/27,1981	-.583		
	Aug 27/28,1981	-.573		
E 7,Q 23	Aug 5/6, 1980	.533	.539 ±(.010)	.422
	Aug 26/27,1981	.548		
	Aug 26/27,1981	.528		
	Aug 27/28,1981	.545		
E 8,Q 15	Aug 8/9, 1980	.023	.028 ±(.004)	.002
	Aug 24/25,1981	.026		
	Aug 24/25,1981	.030		
	Aug 27/28,1981	.033		

NOTE ADDED IN PROOF. Cousins has kindly made available his most recent U-B values (1982, S.A.A.O. Circ., in press). For E6,Q20 he gives 0.253, for E7,Q2 -0.574, for E7,Q23 0.533, and for E8,Q15 0.019. For E1,Q52 he states that the U-B give by VGR '...is an old value from R.Obs.Annals No. 7 and not good. There is nothing new.'

TABLE VI. UBV Photometry

Star (1)	R.A. (1950) (2)	Dec. (3)	l (4)	b (5)	Class (6)	V (7)	B-V (8)	U-B (9)	n (10)	Other Designations (11)
CS 22171- 1	01 50 36	-12 35.4	170.3	-69.3	A5 b	9.34	0.31	0.08	1	
2	01 53 31	-12 42.9	172.0	-68.9	A2 m	13.35	0.19	0.15	1	
4	01 55 53	-12 12.7	172.2	-68.2	AB m	14.29	0.08	0.11	1	
9	01 55 23	-09 01.1	166.6	-65.8	AB m	13.37	0.42	-0.16	1	
13	01 58 37	-10 15.9	170.1	-66.3	AB m	13.76	0.20	-0.03	2	
CS 22171- 23	02 02 39	-08 01.8	168.4	-63.9	AB f	15.34	0.00	0.12	1	
CS 22172- 7	03 13 49	-08 44.3	191.3	-51.1	AB mf	14.47	0.19	0.14	1	
9	03 15 13	-08 44.9	191.6	-50.8	A1 m	13.91	0.24	0.10	1	
10	03 17 18	-09 22.5	192.9	-50.7	AB mf	14.38	0.08	0.20	1	
12	03 17 32	-10 22.4	194.3	-51.2	A1 m	13.74	0.28	0.16	1	
17	03 20 41	-12 10.7	197.4	-51.4	AB m	13.38	0.34	-0.02	1	
CS 22172- 20	03 20 48	-10 08.5	194.6	-50.4	AB vf	15.19	0.22	0.01	1	
CS 22184- 6	02 32 28	-08 51.7	180.7	-59.3	AB mb	13.13	0.27	0.06	1	
9	02 35 13	-09 13.0	182.1	-59.1	AB mf	15.16	-0.06	0.11	1	
13	02 32 17	-11 13.7	184.3	-60.9	A m	13.07	0.25	0.08	1	
14	02 33 21	-11 15.9	184.7	-60.7	AB m	13.48	0.06	0.12	1	
28	02 38 10	-09 20.9	183.2	-58.6	AB m	13.70	0.20	0.10	1	
29	02 39 06	-10 22.7	185.0	-59.0	AB mb	13.20	0.03	0.11	1	
30	02 38 40	-11 28.2	186.6	-59.8	A m	12.99	0.21	0.14	1	
42	02 42 37	-09 00.9	184.0	-57.5	A mf	14.38	0.21	0.03	1	
45	02 46 52	-08 36.5	184.6	-56.4	AB mf	14.64	0.03	0.08	1	
CS 22184- 48	02 38 52	-08 10.9	181.7	-57.7	AB mf	15.06	0.08	-0.01	1	PHL 4260
CS 22875- 3	22 15 24	-41 33.0	358.5	-55.7	AB m	14.49	0.07	0.16	1	
5	22 18 41	-40 21.6	0.4	-56.5	AB f	15.32	0.09	0.05	1	
6	22 14 46	-39 40.5	1.9	-55.9	AB b	13.45	0.07	0.04	2	
7	22 16 55	-39 17.1	2.4	-56.4	A1 m	14.27	0.23	0.01	1	
11	22 23 59	-38 17.7	3.8	-57.9	AB f	14.86	0.32	-0.05	1	
13	22 22 35	-39 41.2	1.4	-57.4	AB f	14.83	0.23	0.06	1	
14	22 21 42	-40 30.3	359.9	-57.1	AB f	15.33	0.19	0.00	1	
15	22 24 40	-41 06.6	358.6	-57.5	AB m	14.12	0.10	0.19	1	
16	22 23 53	-41 16.8	358.4	-57.3	AB b	13.74	0.01	0.00	1	
18	22 25 37	-41 59.9	356.9	-57.4	AB mb	13.75	0.05	0.16	1	
19	22 24 30	-42 14.1	356.6	-57.2	A4 m	13.60	0.29	0.00	1	
20	22 27 48	-42 44.7	355.4	-57.6	AB m	14.14	0.06	0.15	2	
21	22 28 12	-42 29.2	355.8	-57.8	AB m	14.33	-0.06	-0.20	1	
22	22 28 09	-40 55.3	358.7	-58.2	A1 m	13.59	0.19	0.17	2	
23	22 29 49	-41 01.2	358.4	-58.4	AB f	15.50	-0.05	-0.02	1	
24	22 30 39	-40 30.2	359.2	-58.7	AB mf	14.80	-0.01	0.07	1	
25	22 30 16	-40 00.2	0.2	-58.8	AB mf	14.80	0.02	-0.91	1	
27	22 26 28	-40 05.3	0.4	-58.0	AB mf	14.47	0.09	-0.68	2	
30	22 25 20	-38 46.0	2.9	-58.1	AB f	15.45	-0.02	-0.02	1	
31	22 26 57	-38 38.5	3.0	-58.4	AB m	14.13	0.01	0.05	1	
34	22 34 09	-38 07.1	3.5	-59.9	AB mb	13.97	0.01	0.09	1	
35	22 34 05	-38 12.1	3.4	-59.9	AB m	14.90	-0.11	-0.44	1	
36	22 37 20	-38 07.0	3.3	-60.5	AB m	14.61	-0.05	-0.05	1	
37	22 39 27	-38 59.1	1.4	-60.7	AB m	14.32	0.02	0.10	1	
CS 22875- 40	22 36 16	-39 54.8	359.8	-59.9	A1 mb	14.29	0.13	0.17	1	

TABLE VI. (Continued)

Star (1)	R.A. (1950) (2)	Dec. (3)	l (4)	b (5)	Class (6)	V (7)	B-V (8)	U-B (9)	n (10)	Other Designations (11)
CS 22875- 41	22 35 8	-40 06.9	359.6	-59.6	AB mb	13.80	0.08	0.15	1	
42	22 40 11	-40 02.8	359.2	-60.6	Al b	12.80	0.20	0.12	1	
CS 22875- 44	22 35 49	-42 40.2	354.7	-59.0	AB m	14.68	0.05	0.12	1	
CS 22881- 20	21 55 58	-38 50.9	4.0	-52.4	AB m	14.09	-0.03	-0.04	1	
21	21 57 10	-38 40.4	4.3	-52.6	AB m	14.82	-0.02	-0.01	1	
34	22 05 22	-42 30.9	357.6	-53.7	AB f	15.27	-0.01	0.14	1	
CS 22881- 43	22 06 14	-38 36.3	4.1	-54.4	AB f	15.61	0.11	0.08	1	
CS 22882- 2	00 16 04	-30 53.8	5.1	-82.0	AB mb	12.75	0.14	0.18	1	CD-31°99=SB 122
3	00 16 46	-30 18.5	8.7	-82.4	AB m	14.53	0.01	0.08	1	SB 126=TS 150
7	00 17 47	-29 04.2	17.5	-82.9	AB m	14.49	0.04	0.10	3	PS 1=SB 133
8	00 18 56	-29 07.6	16.6	-83.2	AB m	13.97	0.38	-0.17	1	
11	00 21 23	-28 10.3	24.2	-83.8	AB f	15.63	0.00	0.03	1	
14	00 28 54	-28 14.1	21.2	-85.5	AB b	12.94	0.02	0.06	2	PS 13=SB 210
15	00 27 55	-28 25.6	19.4	-85.2	AB m	14.26	0.16	0.11	2	PS 10=SB 202
18	00 30 54	-28 51.0	12.0	-85.8	AB mb	14.26	0.10	0.14	2	PS 16=SB 225
19	00 31 36	-28 47.2	12.1	-85.9	AB b	13.19	-0.01	-0.03	2	PS 17=SB 231
20	00 36 10	-29 14.9	359.0	-86.6	A0 m	14.01	0.14	0.16	2	PS 20=SB 257
22	00 33 23	-30 16.7	352.0	-85.5	AB m	14.99	0.10	0.19	1	
25	00 33 54	-31 12.5	342.9	-85.0	AB m	14.91	0.03	0.12	1	
27	00 35 43	-32 04.4	333.9	-84.5	AB vf	15.11	0.42	-0.27	1	
31	00 26 38	-30 39.1	358.0	-84.1	AB mf	15.27	-0.16	-0.53	1	TS 159
32	00 26 45	-31 40.0	350.3	-83.6	AB f	15.41	0.08	0.22	1	
33	00 26 46	-31 42.3	350.0	-83.5	AB mb	14.20	0.06	0.13	2	PS 6=SB 192
CS 22882- 35	00 23 52	-32 13.9	349.9	-82.7	AB b	12.40	-0.02	0.00	1	CD-32°128=SB 172
CS 22894- 1	23 29 29	-02 09.3	82.6	-58.4	AB	13.97	0.16	0.11	1	
3	23 31 22	-01 28.8	84.1	-58.1	AB	14.64	0.14	0.11	1	
6	23 29 44	00 21.0	84.6	-56.9	AB	15.54	0.12	0.14	1	
8	23 31 07	00 27.0	85.9	-56.5	A3	13.12	0.33	0.10	1	
CS 22894- 13	23 33 56	01 31.0	88.0	-55.9	AB	15.17	0.12	0.22	1	
CS 22936-169	18 51 44	-32 27.8	3.8	-14.8	AB vb	11.52	0.23	0.14	1	
192	18 51 51	-36 13.9	0.2	-16.3	AB vb	11.98	0.14	0.30	1	
201	18 52 27	-35 21.3	1.1	-16.1	AB vb	12.59	-0.04	-0.32	1	
209	18 53 34	-36 12.0	0.4	-16.6	AB m	14.49	0.10	0.10	1	
211	18 53 29	-36 13.4	0.3	-16.6	AB f	15.11	0.12	0.10	1	
213	18 51 28	-36 18.3	0.1	-16.3	AB mf	14.90	0.19	0.16	1	
218	18 53 02	-36 56.6	359.6	-16.8	AB f	15.49	0.02	-0.03	1	
224	18 54 49	-36 07.7	0.5	-16.8	AB f	15.49	0.04	0.00	1	
225	18 54 47	-36 05.2	0.6	-16.8	AB f	14.93	0.26	0.14	1	
227	18 54 39	-35 46.6	0.8	-16.7	AB f	15.24	0.06	0.06	1	
229	18 55 12	-35 18.0	1.4	-16.6	AB mf	15.18	0.02	-0.23	1	
233	18 54 52	-34 43.3	1.9	-16.3	AB f	15.29	0.05	0.25	1	
235	18 55 15	-34 15.0	2.4	-16.2	AB f	15.73	0.02	0.00	1	
236	18 54 48	-34 13.2	2.4	-16.1	AB f	15.50	0.11	0.16	1	
237	18 53 45	-34 04.0	2.4	-15.8	AB mf	15.31	0.08	0.17	1	
238	18 53 21	-34 04.2	2.4	-15.8	AB m	14.23	0.43	0.12	1	
CS 22936-239	18 54 25	-33 57.6	2.6	-15.9	AB mb	13.40	-0.04	-0.04	1	

TABLE VI. (Continued)

Star (1)	R.A. (1950) (2)	Dec. (3)	l (4)	b (5)	Class (6)	V (7)	B-V (8)	U-B (9)	n (10)	Other Designations (11)
CS 22936-240	18 53 18	-33 56.2	2.5	-15.7	AB m	13.95	0.09	0.13	1	
243	18 55 00	-33 47.8	2.8	-16.0	AB mf	14.85	0.10	0.18	1	
244	18 55 20	-33 35.0	3.0	-16.0	AB mb	13.62	0.08	0.07	1	
246	18 55 12	-33 28.2	3.1	-15.9	AB mf	14.94	-0.02	-0.05	1	
247	18 54 51	-33 24.9	3.1	-15.8	AB m	14.71	0.01	0.02	1	
249	18 53 52	-33 14.2	3.2	-15.5	AB mf	15.25	0.03	0.18	1	
250	18 54 30	-33 10.8	3.3	-15.6	AB m	14.66	0.06	0.24	1	
252	18 54 55	-32 32.3	4.0	-15.5	AB mf	14.92	0.04	0.02	1	
255	18 56 54	-32 53.8	3.8	-16.0	AB mb	13.85	0.40	0.10	1	
256	18 55 35	-33 07.2	3.5	-15.8	A0 mb	13.15	0.29	0.11	1	
258	18 55 38	-33 18.2	3.3	-15.9	AB mf	15.11	0.07	0.12	1	
260	18 56 51	-33 21.8	3.4	-16.2	AB mb	12.86	0.39	0.16	1	
262	18 56 40	-33 24.1	3.3	-16.1	AB b	12.50	0.17	0.34	1	
263	18 56 19	-33 37.2	3.1	-16.2	AB mf	15.27	0.06	0.08	1	
264	18 57 16	-33 50.1	2.9	-16.4	AB mf	14.80	0.15	0.21	1	
267	18 56 14	-34 00.3	2.7	-16.3	AB m	12.11	1.15	1.01	1	
268	18 56 43	-33 60.0	2.7	-16.4	AB m	15.03	0.35	0.10	1	
270	18 57 30	-34 04.0	2.7	-16.6	AB mf	14.49	0.37	0.05	1	
274	18 57 36	-34 36.6	2.2	-16.8	AB mf	15.13	0.15	0.22	1	
275	18 56 09	-34 48.3	1.9	-16.6	AB mf	14.85	0.21	0.20	1	
278	18 57 38	-35 24.9	1.4	-17.1	AB m	14.16	0.11	0.21	1	
281	18 56 33	-35 53.6	0.9	-17.1	AB m	14.37	0.25	0.16	1	
282	18 56 37	-36 03.2	0.7	-17.1	AB m	14.87	0.02	-0.04	1	
283	18 57 27	-36 06.3	0.7	-17.3	AB m	14.50	0.11	0.14	1	
284	18 57 43	-36 06.6	0.8	-17.4	AB m	14.66	0.02	0.03	1	
285	18 56 44	-36 10.9	0.6	-17.2	AB m	14.58	0.11	0.15	1	
286	18 57 45	-36 12.9	0.7	-17.4	AB m	14.66	0.16	0.19	1	
287	18 57 30	-36 21.6	0.5	-17.4	AB m	14.72	0.09	0.04	1	
291	19 00 22	-35 44.1	1.3	-17.7	AB f	14.95	0.21	0.23	1	
294	18 58 19	-35 14.7	1.7	-17.2	AB f	15.36	0.17	0.14	1	
299	18 58 29	-34 29.4	2.4	-16.9	AB mf	14.65	0.19	0.23	1	
306	18 58 10	-33 28.0	3.4	-16.5	AB b	12.66	0.14	0.08	1	
CS 22936-341	19 00 45	-35 12.5	1.9	-17.6	AB vb	11.48	0.12	0.06	1	
CS 22941- 23	23 32 58	-35 58.0	0.3	-71.7	AB f	15.68	0.17	-0.03	1	
24	23 31 17	-36 20.2	359.6	-71.3	AB mf	15.86	-0.18	-0.23	1	
26	23 31 31	-37 16.5	356.9	-70.9	AB mf	15.45	0.10	0.13	1	
29	23 33 28	-37 08.1	356.8	-71.4	AB mf	15.05	0.07	0.11	1	
31	23 34 59	-36 40.9	357.7	-71.8	AB mf	15.03	-0.01	-0.05	1	
39	23 33 30	-33 34.8	7.6	-72.6	AB f	15.68	0.24	0.01	1	
CS 22941- 47	23 41 56	-36 03.5	357.5	-73.4	AB mf	14.68	0.15	0.12	1	
CS 22942- 4	00 43 46	-24 15.7	102.2	-86.6	AB m	14.61	0.17	0.06	1	
5	00 45 51	-23 47.9	111.7	-86.3	AB mf	15.53	0.11	0.28	1	
6	00 44 34	-23 36.5	108.0	-86.1	A b	12.90	0.18	0.08	2	PS 30=SB 322
8	00 49 15	-23 05.6	123.7	-85.7	AB mf	15.51	0.13	0.08	1	
9	00 47 26	-23 29.5	117.8	-86.1	A mf	14.76	0.29	-0.04	1	
13	00 50 13	-26 10.7	135.6	-88.7	AB m	14.61	0.19	0.17	1	SB 353
15	00 51 54	-27 11.9	195.8	-89.3	AB b	13.03	0.07	0.16	2	PHL 6850=PS 35=SB 362
CS 22942- 18	00 54 06	-26 15.9	168.4	-88.4	AB mf	15.23	0.23	-0.04	1	

TABLE VI. (Continued)

Star (1)	R.A. (1950) (2)	Dec. (3)	l (4)	b (5)	Class (6)	V (7)	B-V (8)	U-B (9)	n (10)	Other Designations (11)
CS 22942- 20	00 53 09	-23 44.7	137.6	-86.2	A b	12.26	0.21	0.06	2	PS 37=SB 366
21	00 53 40	-23 34.1	138.6	-86.0	AB f	14.34	0.37	0.08	1	
22	00 53 40	-23 09.5	137.2	-85.6	AB f	15.81	0.03	0.28	1	
25	00 55 49	-24 10.2	148.8	-86.4	AB b	12.35	-0.03	-0.09	1	CD-24°414=SB 388
26	00 55 57	-24 31.9	152.0	-86.7	AB m	14.38	0.18	0.06	1	SB 389
28	00 57 60	-25 33.9	171.2	-87.3	A m	13.54	0.32	0.08	1	SB 404
31	01 02 11	-26 47.8	202.1	-87.0	AB mf	14.98	0.08	0.14	1	PHL 7121=SB 432=TS 189
34	01 01 24	-24 17.2	165.6	-85.8	A b	12.77	0.09	0.14	1	CD-24°469=SB 420
CS 22942- 37	01 00 38	-23 34.6	158.1	-85.4	AB m	14.15	0.10	0.21	1	
CS 22946- 1	01 08 51	-21 54.8	163.5	-82.9	AB mb	13.04	0.01	0.03	1	PHL 7202=PS 53=SB 480
4	01 09 32	-20 42.0	159.1	-81.8	AB f	15.46	0.02	0.16	1	
8	01 23 10	-21 01.1	175.5	-79.9	A b	12.79	0.21	0.19	1	SB 573
9	01 25 27	-20 17.0	174.4	-79.0	AB mf	14.70	0.28	0.02	1	
10	01 21 44	-20 15.0	171.0	-79.7	AB f	15.60	0.22	0.16	1	
11	01 16 46	-19 39.7	163.9	-80.0	AB m	13.94	0.33	-0.14	1	
15	01 20 18	-17 41.7	161.3	-77.9	AB f	15.59	-0.04	0.13	1	
16	01 19 52	-17 27.5	160.2	-77.8	AB f	15.83	-0.08	-0.02	1	
19	01 10 31	-18 13.5	152.5	-79.6	AB mb	13.45	0.09	0.08	1	SB 490
CS 22946- 20	01 12 10	-18 46.7	155.9	-79.9	AB mf	14.88	0.13	0.18	1	
CS 22949- 1	23 12 27	-07 11.8	70.0	-59.5	AB f	14.38	0.42	-0.21	1	
3	23 11 01	-06 47.1	70.1	-58.9	AB mf	15.05	0.35	0.10	1	
4	23 09 49	-06 32.8	70.0	-58.6	AB m	13.09	0.24	0.16	1	
5	23 09 23	-05 19.6	71.5	-57.6	AB f	14.78	-0.05	-0.69	1	PHL 2115
6	23 13 37	-05 02.0	73.3	-58.1	AB mb	13.96	0.05	0.08	1	
7	23 13 22	-04 56.1	73.3	-58.0	AB m	13.67	0.43	-0.22	1	
9	23 12 52	-03 04.8	75.4	-56.6	AB vf	15.79	0.18	0.17	1	
12	23 16 37	-02 32.5	77.4	-56.7	AB m	14.14	0.03	0.06	1	PHL 5663
13	23 16 60	-02 35.0	77.5	-56.8	AB mf	14.80	0.11	0.16	2	
CS 22949- 41	23 23 54	-04 32.0	77.7	-59.4	AB b	13.50	-0.03	-0.05	1	PHL 5819
CS 22963- 11	02 56 29	-06 21.3	184.1	-53.2	AB mb	13.38	0.15	0.09	1	
12	02 55 43	-06 25.8	184.0	-53.4	AB m	14.36	0.18	0.21	1	
13	02 51 26	-06 54.5	183.5	-54.5	AB m	13.55	0.29	-0.11	1	
16	02 57 31	-07 13.7	185.5	-53.5	AB mb	13.64	0.15	0.19	1	
18	03 02 41	-06 43.9	186.1	-52.2	AB m	13.64	0.23	0.15	1	
19	03 09 15	-06 35.3	187.5	-50.8	AB f	15.21	0.08	0.14	1	
21	03 04 22	-05 02.3	184.4	-50.8	AB m	14.30	0.00	-0.11	1	
22	03 02 47	-04 59.5	183.9	-51.1	AB mf	15.23	-0.10	-0.51	1	
25	03 09 27	-03 59.7	184.3	-49.2	A mb	13.70	0.24	0.17	1	
30	03 06 37	-02 25.0	181.8	-48.7	A m	13.53	0.32	0.10	1	
31	03 05 19	-02 59.9	182.2	-49.3	AB m	14.34	0.13	0.20	1	
32	03 05 06	-02 55.3	182.0	-49.3	AB f	15.32	0.16	0.24	1	
33	03 03 33	-02 44.0	181.4	-49.5	AB:f	14.86	0.26	0.14	1	
35	02 59 53	-03 00.6	180.8	-50.4	AB mb	13.22	0.13	0.11	1	
CS 22963- 36	02 58 44	-02 52.1	180.3	-50.5	AB mb	13.84	-0.18	-0.88	1	
CS 22964- 1	19 45 52	-42 19.2	357.3	-28.1	AB m	14.68	0.08	0.10	1	
CS 22964- 2	19 42 42	-42 06.4	357.4	-27.5	AB mf	14.61	0.03	0.01	1	

TABLE VI. (Continued)

Star (1)	R.A. (1950) (2)	Dec. (3)	l (4)	b (5)	Class (6)	V (7)	B-V (8)	U-B (9)	n (10)	Other Designations (11)
CS 22964- 3	19 43 30	-41 52.0	357.7	-27.6	A mf	14.86	0.18	0.19	1	
4	19 45 03	-41 31.0	358.2	-27.8	AB mf	15.62	0.05	0.11	1	
5	19 44 33	-41 33.3	358.1	-27.7	AB mf	15.24	0.13	0.23	1	
7	19 41 60	-41 18.4	358.3	-27.2	AB m	14.54	0.19	0.20	1	
8	19 43 59	-41 04.7	358.6	-27.5	AB m	14.72	-0.06	0.10	1	
9	19 44 42	-41 00.8	358.7	-27.6	AB mf	15.07	0.24	0.18	1	
15	19 42 28	-40 05.2	359.6	-27.0	AB f	15.47	0.18	0.09	1	
16	19 40 58	-40 10.9	359.4	-26.7	AB b	12.48	0.08	0.11	1	
21	19 43 32	-39 47.0	0.0	-27.1	AB m	14.27	0.39	0.09	1	
23	19 44 51	-39 41.0	0.2	-27.3	AB f	15.58	0.03	0.00	1	
26	19 44 18	-39 21.6	0.5	-27.1	AB m	15.15	0.08	0.15	1	
29	19 41 16	-38 46.8	1.0	-26.4	AB vf	15.79	0.16	0.14	1	
31	19 41 09	-38 35.4	1.2	-26.3	AB vf	15.50	0.13	0.10	1	
32	19 44 32	-38 42.3	1.2	-27.0	AB mb	13.86	0.08	0.14	1	
39	19 44 13	-38 06.1	1.9	-26.8	AB mf	15.09	0.08	0.09	1	
58	19 45 53	-38 35.3	1.4	-27.2	AB mf	15.27	0.06	0.19	1	
66	19 45 51	-39 29.5	0.5	-27.4	AB mf	15.32	0.10	0.19	1	
67	19 46 59	-39 35.0	0.4	-27.7	AB f	15.89	-0.02	-0.01	1	
76	19 47 53	-40 07.4	359.9	-28.0	AB mb	14.34	-0.19	-0.93	1	
77	19 49 48	-40 06.9	360.0	-28.3	AB m	14.45	0.03	0.05	1	
78	19 50 32	-40 22.0	359.7	-28.5	AB mf	15.06	0.15	0.02	1	
81	19 50 46	-40 35.5	359.5	-28.6	A m	14.01	0.33	0.16	1	
83	19 48 35	-40 56.9	359.0	-28.3	AB m	14.69	0.21	0.17	1	
84	19 47 37	-40 55.8	359.0	-28.1	AB b	13.02	0.09	0.16	1	
85	19 46 05	-41 01.1	358.8	-27.8	AB m	15.14	-0.01	0.06	1	
87	19 47 46	-41 17.0	358.6	-28.2	AB mf	15.29	0.05	0.11	1	
102	19 53 03	-41 58.8	358.0	-29.3	AB mb	14.10	-0.12	-0.63	1	
103	19 51 55	-41 46.1	358.2	-29.1	AB m	14.67	0.19	0.10	1	
104	19 54 04	-41 29.0	358.6	-29.4	AB f	15.31	0.71	0.19	1	
105	19 56 12	-41 20.1	358.9	-29.8	AB m	14.72	0.07	0.14	2	
106	19 52 35	-41 23.0	358.7	-29.1	AB mf	15.06	0.37	0.08	1	
107	19 51 44	-41 23.8	358.6	-29.0	AB mb	14.11	0.19	0.16	1	
118	19 54 49	-39 57.0	0.4	-29.2	AB vb	11.89	0.09	0.05	1	
121	19 51 44	-39 29.2	0.8	-28.5	AB b	12.32	0.05	-0.10	1	
124	19 54 52	-39 05.9	1.4	-29.0	AB mf	14.33	0.95	-0.01	1	
125	19 53 57	-39 09.4	1.2	-28.9	AB mb	14.31	0.27	0.16	1	
CS 22964-126	19 50 54	-39 05.8	1.2	-28.3	AB mb	14.20	0.09	0.15	2	
CS 22968- 2	02 58 9	-56 29.6	273.7	-52.9	AB f	15.86	0.08	0.06	1	
6	02 53 47	-54 03.9	271.1	-54.9	AB mf	14.94	0.25	-0.13	1	
10	02 57 13	-53 38.6	270.0	-54.8	AB mf	15.30	0.19	0.03	1	
13	03 05 42	-54 38.3	270.2	-53.2	AB mb	13.72	0.17	0.12	1	
20	03 08 34	-56 54.3	272.8	-51.6	AB m	14.37	0.25	0.12	1	
28	03 20 03	-55 17.8	269.3	-51.1	AB m	14.48	0.11	0.14	1	
37	03 25 07	-53 09.3	265.7	-51.4	AB m	15.00	-0.09	-0.31	1	
45	03 09 47	-52 50.5	267.1	-53.6	AB mb	14.22	0.12	0.11	1	
46	03 09 11	-52 29.5	266.6	-53.9	AB f	15.79	0.14	0.13	1	
CS 22968- 48	03 22 03	-52 20.0	264.9	-52.2	AB m	13.17	0.06	0.11	1	

REFERENCES

Arp, H. C. (1961). Astrophys. J. 133, 874.

Arp, H. C., and Hartwick, F. D. A. (1971). Astrophys. J. 167, 499.

Cannon, R. D., and Stobie, R. S. (1973). Mon. Not. R. Astron. Soc. 162, 227.

Chavira, E. (1958). Bol. Obs. Tonantzintla y Tacubaya 2, No. 17, 15.

Cousins, A. W. J., and Stoy, R. H. (1962). R. Obs. Bull., No. 49.

Eggen, O. J. (1968). Astrophys. J. 153, 723.

Eggen, O. J., and Greenstein, J. L. (1965). Astrophys. J. 141, 83.

Fitzgerald, M. P. (1970). Astron. Astrophys. 4, 234.

Greenstein, J. L., and Sargent, A. I. (1974). Astrophys. J. Suppl. 28, No. 259, 157.

Hardie, R. H. (1962). "Photoelectric Reductions", in Astronomical Techniques, ed. by W. A. Hiltner, Vol. II of Stars and Stellar Systems, G. R. Kuiper, gen. ed. (University of Chicago, Chicago), Chap. 8.

Harris, W. E., Fitzgerald, M. P., and Reed, B. C. (1981). Publ. Astron. Soc. Pac. 93, 507.

Harris, W. E., and Racine, R. (1979). Annu. Rev. Astron. Astrophys. 17, 241.

Haro, G., and Luyten, W. J. (1962). Bol. Obs. Tonantzintla y Tacubaya 3, No. 22, 37.

Johnson, H. L. (1966). Annu. Rev. Astron. Astrophys. 4, 193.

Kinman, T. D., Mahaffey, C. T., and Wirtanen, C. A. (1982). Astron. J. 87, 314 (KMW).

Landolt, A. U. (1973). Astron. J. 78, 959.

Matthews, T. A., and Sandage, A. (1963). Astrophys. J. 138, 30.

Mermilliod, J.-C., and Nicolet, B. (1977). Astron. Astrophys. Suppl. 29, 259.

Mould, J. R. (1982). Annu. Rev. Astron. Astrophys. 20, in press.

Newell, E. B. (1970). Astrophys. J. 159, 443.

Newell, E. B., Rodgers, A. W., and Searle, L. (1969a). Astrophys. J. 156, 597.

Newell, E. B., Rodgers, A. W., and Searle, L. (1969b). Astrophys. J. 158, 699.

Nicolet, B. (1978). Astron. Astrophys. Suppl. 34, 1.

Nicolet, B. (1980). Astron. Astrophys. Suppl. 42, 283.

Philip, A. G. D. (1968). Astron. J. 73, 1000.

Philip, A. G. D. (1974). Astrophys. J. 190, 573.

Philip, A. G. D., and Sanduleak, N. (1968). Bol. Obs. Tonantzintla y Tacubaya 4, No. 30, 253.

Preston, G. W., and Shectman, S. A. (1979). Annual Report of the Director, Hale Observatories, (Carnegie Institution of Washington, Washington, D.C.)

Preston, G. W., Shectman, S. A., and Pier, J. R. (1982). In preparation.

Rodgers, A. W. (1971). Astrophys. J. 165, 581.

Sandage, A. (1969). Astrophys. J. 157, 515.

Sandage, A. (1970). Astrophys. J. 162, 841

Slettebak, A., and Brundage, R. K. (1971). Astron. J. 76, 338.

Vogt, N., Geisse, H. S., and Rojas, S. (1981). Astron. Astrophys. Suppl. 46, 7 (VGR).

Wolff, S. C. (1967). Astrophys. J. Suppl. 15, No. 134, 21.

FIGURE CAPTIONS

Figure 1 - Differences in observed magnitudes and colors. The diamond symbols represent the differences between pairs of observations of the same stars in the present work. Plus symbols are the differences [this work]-[Eggen (in Rodgers 1971)] and X's the differences [this work]-[Eggen 1968]. Figures 1(a) through (c) plot differences in V, B-V, and U-B respectively against B-V while 1(d) though (f) show them against V.

Figure 2 - The (U-B, B-V) two-color diagram for the program AB stars in Table VI. Smoothed curves are shown for luminosity classes I, III and V as well as for a black body. A 2σ error bar of ± 0.015 mag is shown in the upper right. Stars lying in the region of the extreme subdwarfs are shown as plus symbols; those suspected of being either high luminosity stars or composite systems are shown as open circles. The open square shows the unusual colors of CS22941-24.

Figure 3 - The (U-B, B-V) two-color diagram for field and globular cluster BHB stars (filled diamonds) and suspected globular cluster blue stragglers (plus symbols). All colors were taken from the literature. The colors of globular cluster stars have been corrected for foreground reddening. A smoothed luminosity class V curve is superposed.

Figure 4 - Percentage differences between $\langle \sec Z \rangle$ and $\sec Z(\langle h \rangle)$ computed for a latitude of 30°, declinations between -45° and $+85^{\circ}$, and beginning hour angles of from 0 hours to 6 hours. Figure 4(a) shows the results for 60 minute observations while (b), (c), and (d) are for

120, 180, and 240 minutes respectively.

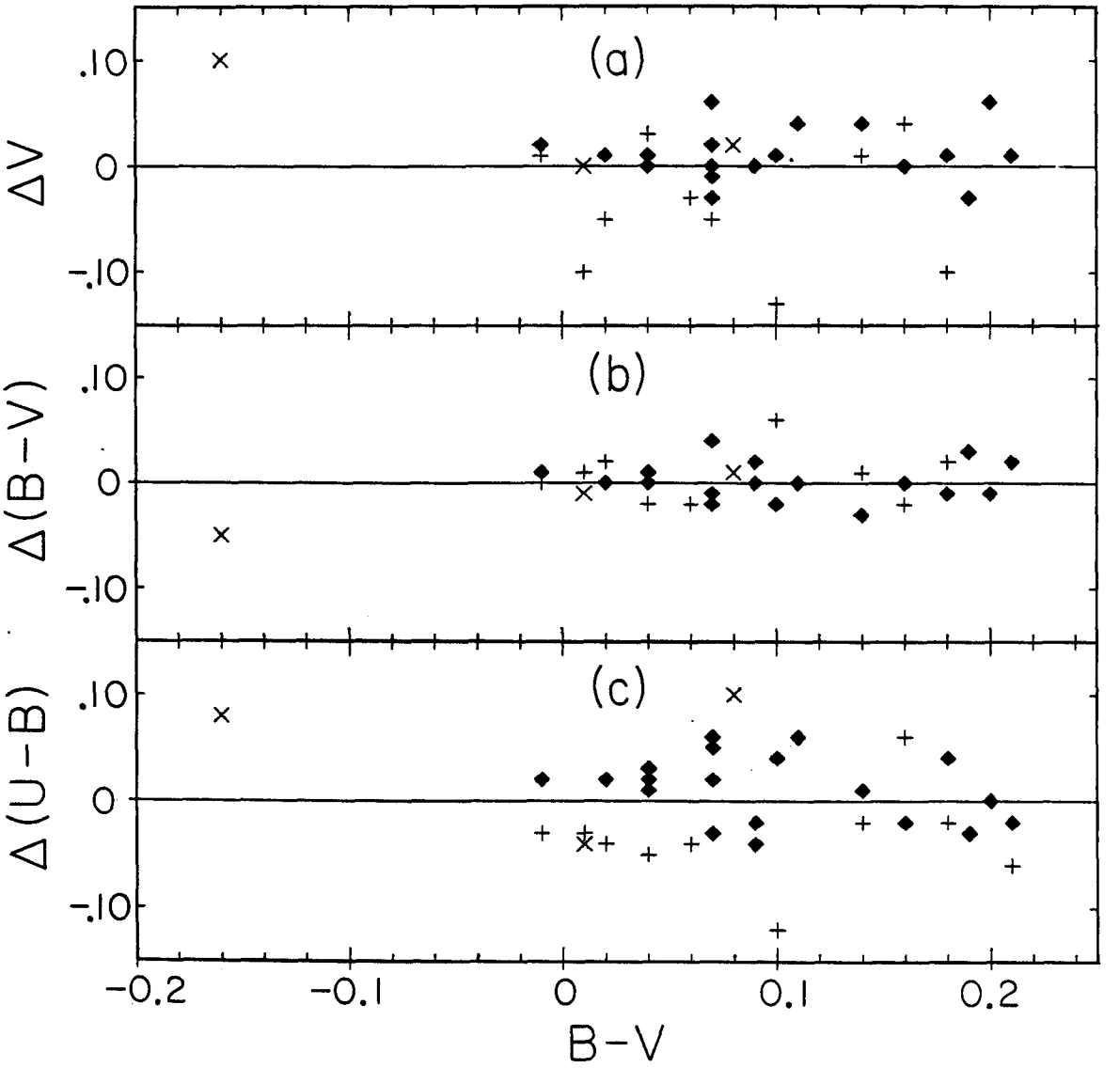

Figure 1(a,b,c)

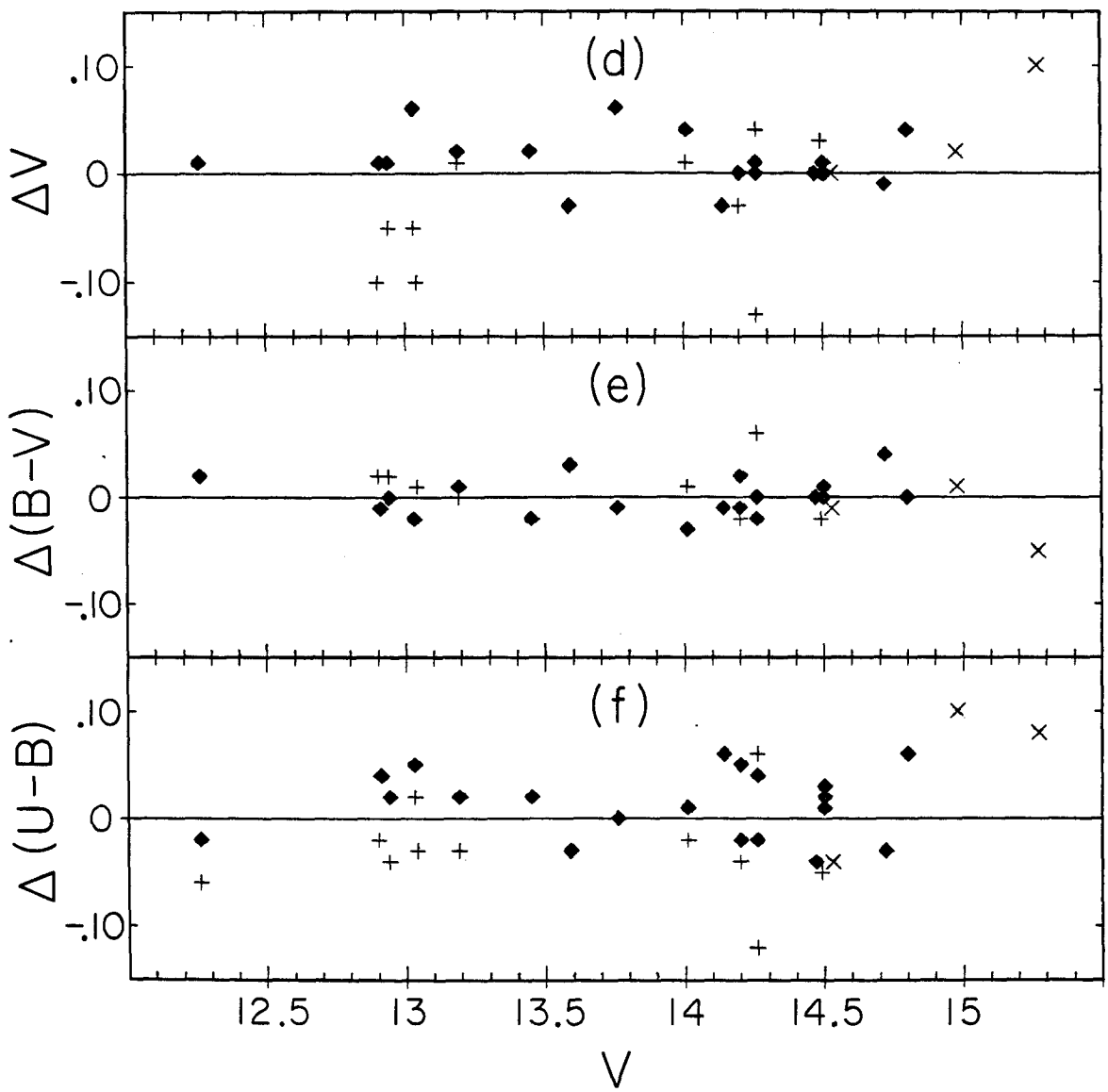

Figure 1(d,e,f)

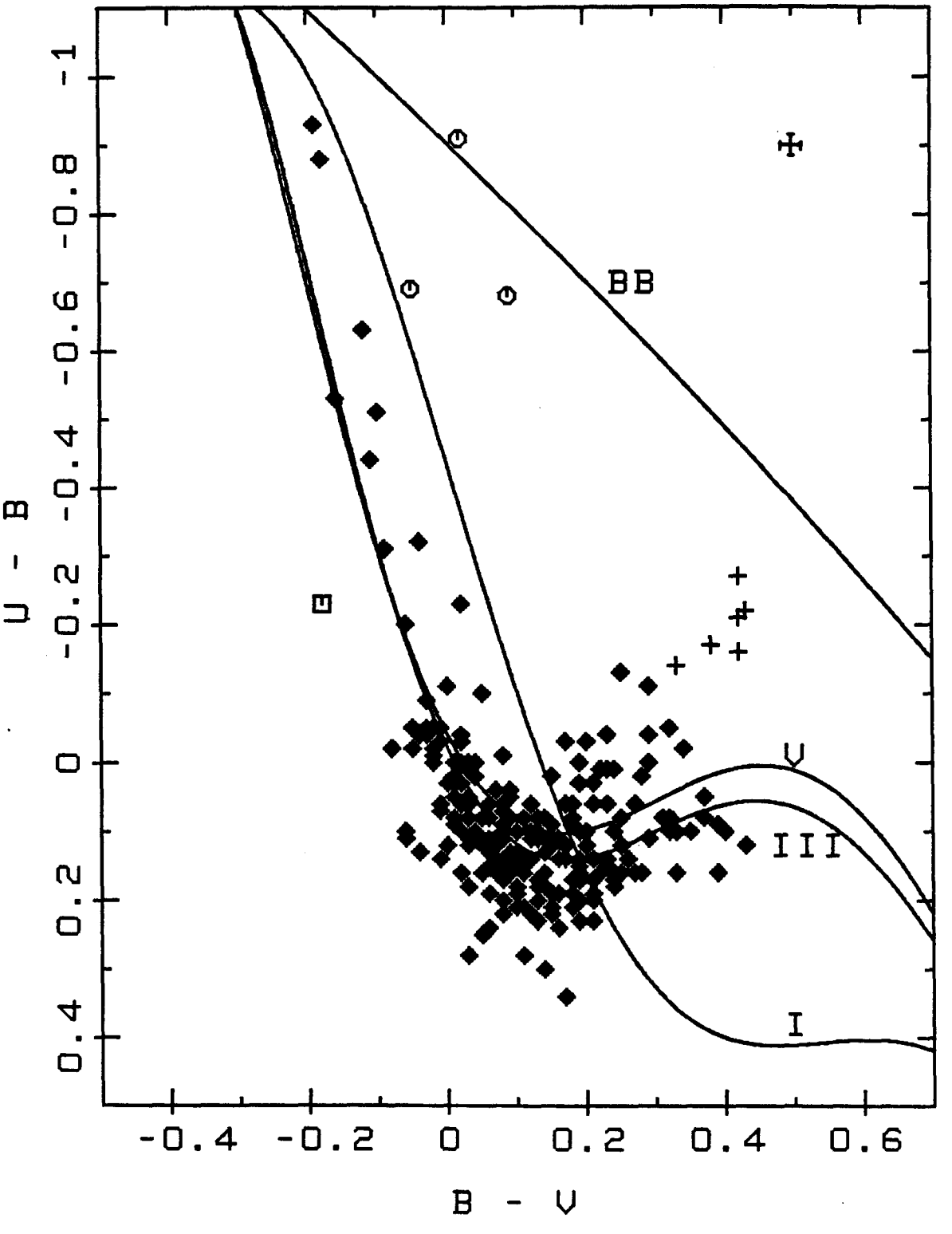

Figure 2

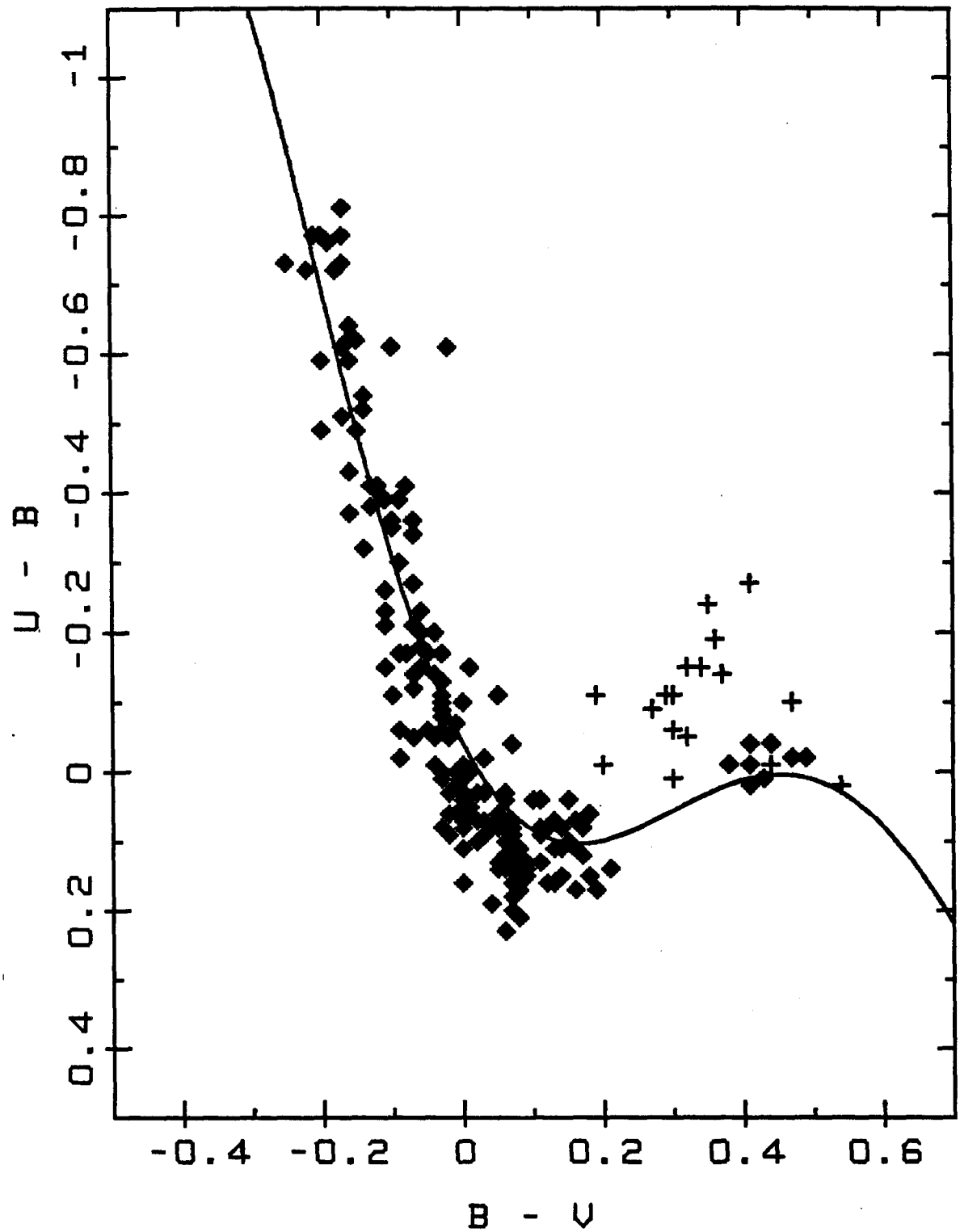

Figure 3

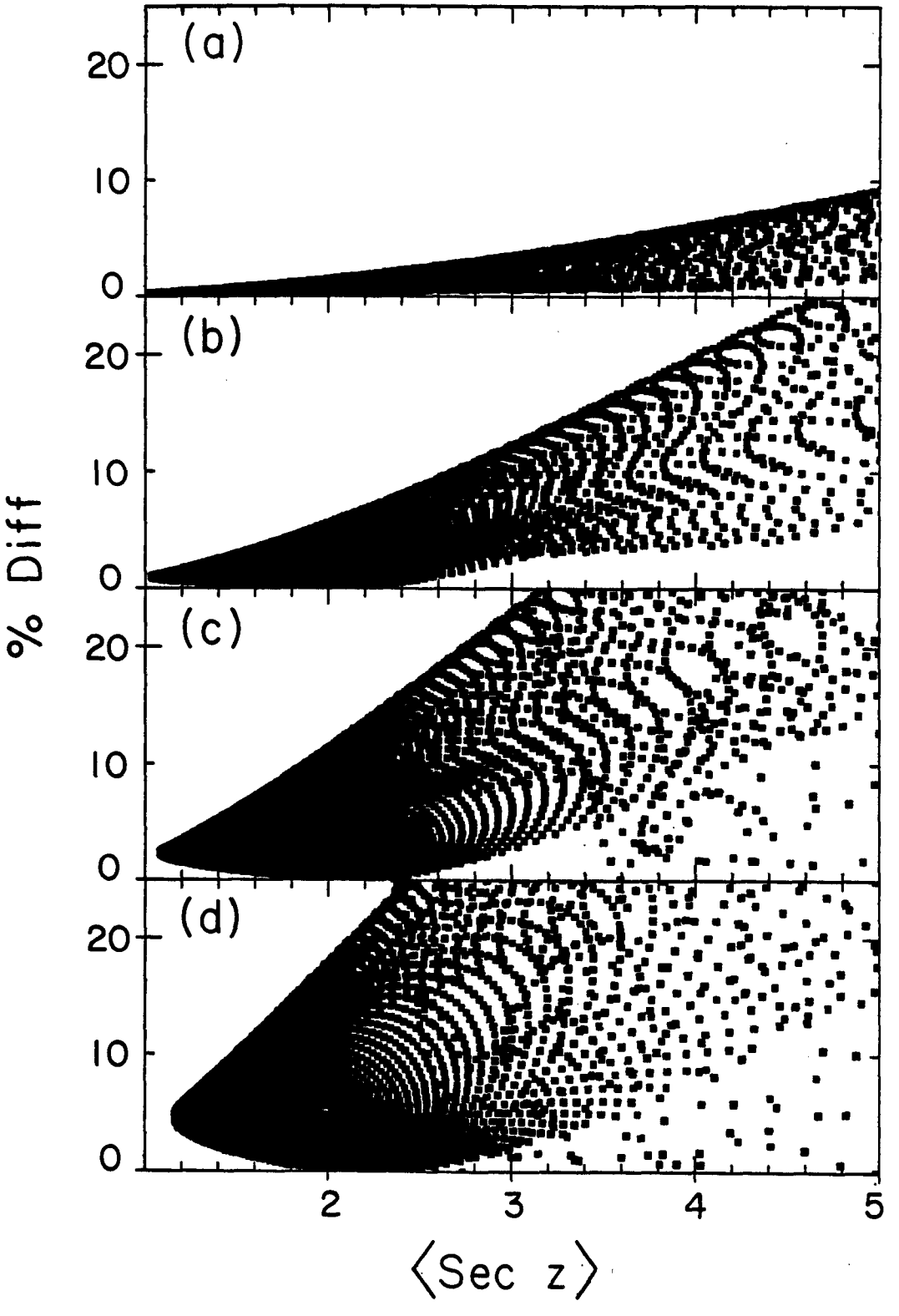

Figure 4

Chapter 2

RETICON SPECTROSCOPY OF HALO AB STARS

I. INTRODUCTION

Photometric and spectroscopic studies of faint early-type halo stars often pose more questions than they answer. The Galaxy does not, of course, fit the simple pictures we draw. Stars that don't belong in the halo are found there, with velocities, gravities and metallicities which are unnerving. Perhaps we have not looked far enough. There is growing evidence that the stars in the disk require more than a single exponential to characterize their vertical distribution. Burstein (1979) found that his surface photometry of external galaxies implied the presence of a 'thick disk'. Van der Kruit and Searle (1981a,b) find, from a careful photometric analysis of edge-on spirals, that galactic disks are indeed thicker than previously thought, however they believe the cause to be the flattening of the halo component by the gravitational potential of the disk. Recently, Gilmore and Reid (1982) have found, from photometry and counts of very faint stars towards the south galactic pole, that two exponential scale heights do indeed prevail in the Galaxy. One, of 300 pc, is applicable over the range $100 \leq |z| \leq 1000$ pc. The second, of ~ 1400 pc, then dominates and reaches up to several kpc.

In the present study, spectra were obtained for over 200 stars ranging from $|z| \sim 1 - 10$ kpc, two-thirds of which are at distances in excess of two thick disk scale heights. It will be seen that for this

sample complications still arise, but by-and-large a homogeneous population prevails, particularly beyond 3 kpc from the plane. The observations, reductions and radial velocity determinations are discussed in considerable detail in §§ II and III. Section IV presents a discussion of measurements of spectral features found in the halo AB stars. A comparison of observations of stars studied here which are in common with Rodgers (1971, hereinafter AWR) and Rodgers, Harding, and Sadler (1981, hereinafter RHS) comprises § V.

II. OBSERVATIONS AND REDUCTIONS

The observations were made with the Boller and Chivens Cassegrain spectrograph on the 100 inch du Pont telescope at Las Campanas Observatory using the Reticon spectrometer (Shectman 1981) as the detector. The observations were obtained on 15 nights in August and September of 1980 and 8 nights in September of 1981. All stars were observed through the apertures of both diode arrays for equal exposures. The same pair of 2 (direction of dispersion) by 4 arcsecond apertures was employed for all observations. A 1200 line mm^{-1} Bausch and Lomb grating blazed at 7500 Å was used in second order yielding a reciprocal dispersion of 30 Å mm^{-1} or ~ 0.28 Å $pixel^{-1}$. An order separation filter (either BG38 or an 80% saturated solution of $CuSO_4$) was used at all times. The spectral coverage extended from the Balmer limit to about 4500 Å. The spectra were widened ~ 150 microns along the Reticon diodes using the spectrograph's oscillating quartz widening

block. Typical FWHM of an unblended comparison arc line was 3.5 - 4.0 pixels (about 1 Å or 75 km s^{-1}) in the middle of the array to about 5.5 or 6.0 pixels near the ends.

All exposures of program AB stars were carried out to the point where 200 net (sky subtracted) counts per pixel had accumulated in the continuum in the center of the array. Hence, to first order, all observations were uniformly exposed to the same signal-to-noise ratio. Of course variations in the sky level (due principally to the moon) detracted somewhat from this uniformity. All objects were observed as near the meridian as was practicable.

Each night's observations were both preceded and followed by long exposures to the inside of the telescope dome illuminated by incandescent tungsten lighting. These "flat field" exposures provide a means of compensating for the response variations in adjacent pixels.

The Reticon spectrometer on the du Pont telescope uses an unshielded magnetically focused image tube ("Carnegie Tube") and, as a consequence, the mapping of the spectrum onto the Reticon diode array is affected by variations in the local magnetic field. In particular the spectrum is known to shift on the array as the telescope moves in declination, i.e. as the detector is moved through the variable magnetic field around the fork of the telescope (Shectman 1980, private communication). Furthermore, the detector is known to experience apparently random drifts of up to $\pm$ one pixel on time scales of the order of an hour (Young 1980, private communication). The spectrograph also suffers from flexure (Mould 1982). In an effort to thwart wavelength calibration difficulties due to such effects a comparison

Fe-Ar hollow cathode arc line spectrum was obtained at least once for every two stellar observations and at least once for every telescope position when adjacent observations were more than ~ 5^{o} apart on the sky during the 1980 observing run. In 1981 comparison spectra were taken before and after each stellar observation at the same telescope setting as the object.

Spectra were obtained for 207 of the 234 stars in Chapter 1. Most of the excluded stars[1] were either too bright for spectroscopic observations without introducing neutral density filtration or had UBV colors which were not typical of AB stars. Spectra were also obtained for an additional 17 stars for which, due to weather limitations, high quality UBV photometry had not been obtained. Table 1 identifies these stars by the Curtis Schmidt (CS) plate number and star numbers assigned by Preston as he scanned the plates. Also given are the 1950.0 equatorial and galactic coordinates. The last column gives Preston's spectral and brightness classifications (where b==> bright, f==> faint, m==> medium). Similar data for the remaining 207 stars , plus the results of UBV photometry, are given in Table VI of Chapter 1.

Along with the program AB star observations, spectra were also obtained of radial velocity standards, globular cluster blue horizontal-branch (BHB) and RR Lyrae stars, some of the A stars from Table II of Philip and Sanduleak (1968), and unevolved AB stars from a young open cluster. Additionally, one cloudy night was spent observing

---

[1]CS22171-1 and -9; CS22875-42; CS22881-20; CS22882-8 and -27; CS22936-201, -255, -260, -262, -267, -268, -270, 306, and 341; CS22941-24;CS22942-21; CS22949-1, -3, -5, and -7; CS22964-104, -106, -118, -121,-124, and -125.

bright early-type stars which had been assigned spectral classifications on the MK system and which were listed in the Yale Bright Star Catalogue (Hoffleit and Jaschek 1982, hereinafter YBSC).

The interactive general spectrum reduction package "LOLITA" (originally written by Peter Young) was installed with minor modifications on the Caltech astronomy VAX 11/780 computer ("PHOBOS") by the author. This set of routines was used to reduce all the Reticon data. Each night's data were reduced separately. The two flat field exposures taken at the beginning and end of the night were combined and normalized by a low order polynomial. All spectra were then divided by this normalized flat field to compensate for variations in the response of adjacent pixels.

Wavelength calibrations were established for each stellar object by using the approriate comparison spectrum/spectra. For each comparison spectrum, the pixel centroids of from 25 to 30 unblended arc lines were determined using the procedure outlined by Schneider and Young (1980). In this procedure the line is convolved with the derivative of a Gaussian function of similar width. The root, or zero crossing point, of the convolution defines the centroid of the line. The root is found by iteration using Newton's method.

A fifth order polynomial in wavelength vs. pixel number was fitted using least-squares techniques to establish the wavelength transformation. The typical rms residual in the fits was 0.08 Å (~ 6 km s^{-1} at 4000 Å). Since the wavelenth calibration outside the ends of the polynomial fit ($\lambda\lambda <$ 3700 Å and $\lambda\lambda >$ 4450 Å) rapidly becomes unreliable, no wavelength dependent analyses of such data were

conducted.

For the 1981 data, wavelength fits were made for each of the two diode arrays separately and then the data were shifted and similarly binned before combining and subtracting the sky contribution. The 1980 arc line spectra had fewer data numbers however, and it was necessary to first simply combine the data from the two arrays and then perform the calibration. Although the first method is obviously to be preferred, tests comparing the two different techniques showed that the resultant velocities differ by no more than a couple of km s^{-1}, demonstrating that the two diode arrays have a negligible difference in wavelength transformations.

Given an object's coordinates and the time and length of integration LOLITA computes the airmass and the observed velocity component due to the motion of the earth about the barycenter of the solar system. Of ~ 350 spectroscopic observations taken for which radial velocities have been determined, none was at an airmass $\geq$ 1.30 and only 10 had airmasses $\geq$ 1.20.

III. RADIAL VELOCITIES

a) Method and Results

Determination of the radial velocities of the program AB stars was one of the primary goals of the project. However, as mentioned in §II, the wavelength stability of the Reticon spectrometer on the du Pont

telescope was uncertain and consequently considerable care was exercised in taking the observations. If observational uncertainty could be held to one pixel or less (~ 20 km s^{-1} at 4000 Å), its contribution to the calculation of the velocity dispersion of these stars would be tolerable if, as was suspected *a priori*, they are high velocity halo stars.

The brightest stars which can safely be observed at the dispersion used here without possible damage to the image tube have apparent magnitudes of V ~ 12.0. A literature search for field A-type radial velocity standards fainter than V = 12 in the appropriate parts of the sky proved fruitless. Observing brighter radial velocity standards would have required the use of neutral density filters, which could well have introduced further complications. Instead, BHB stars from the metal-poor globular cluster NGC 6397 were chosen to serve as radial velocity standards. NGC 6397 has a well populated and well studied BHB (Searle and Rodgers 1966; Newell, Rodgers and Searle 1969) and these stars proved to be excellent spectral matches to the program stars. The cluster also has a well determined radial velocity and a small velocity dispersion (Da Costa *et al*. 1977; Webbink 1981).

Two BHB stars from the cluster (ROB #70 and #77 -- ROB star numbers in NGC 6397 are taken from Woolley *et al*. 1961) were observed at the beginning of each night's observations for a sufficient integration time to achieve a signal-to-noise ratio of two to three times that obtained for the program stars. Once the night's observations were begun, no alterations were made to the spectrograph (*i.e.*, no grating or grating setting changes, no slit/aperture movement

or adjustment, etc.) in order to avoid adding further uncertainties to the radial velocity determinations. As previously mentioned, all observations were made at small airmasses and comparison spectra were recorded frequently. One of the brighter program stars was observed several times to establish it as a secondary radial velocity standard in another part of the sky. Additionally, 32 stars were observed on two different nights.

Several schemes were tested for determining the radial velocities:

(1) Theoretical asymptotic Stark broadened profiles were fit to the Balmer lines H_γ through H_{12} (excepting H_ε λ 3970 Å which is contaminated by the H line of CaII λ 3968.5 Å) and the mean redshifts of the lines determined;

(2) The centroid of each of the Balmer lines was determined by using the Gaussian derivative method outlined above and mean redshifts determined;

(3) The spectra were cross-correlated with synthetic spectra;

(4) A model spectrum consisting of a flat continuum with delta function Balmer absorption lines widened to the resolution of the spectrograph was constructed. The spectra were then cross-correlated with this model; and

(5) The spectra were cross-correlated with radial velocity standards observed on the same night.

Although all of these methods produced essentially the same results,

the fifth method was adopted because it was the most consistent. Furthermore it has the great attraction that the velocity determination is made by using all of the available spectral information and correlating it with a spectrum taken with the same equipment on the same night so that it is therefore (theoretically at least) subject to fewer instrumental errors.

In preparation for cross-correlation analysis, the sky-subtracted, wavelength-calibrated spectra were "flattened" and normalized by fitting cubic splines through several pseudo-continuum points. Since with logarithmically binned spectra relative velocity is linearly related to relative bin position at all wavelengths, the spectra were rebinned so that:

$$\ln(\lambda) = a_0 + (a_1/n)b_i \qquad (1)$$

where a_0 and a_1 are constants and b_i is the ith of n bins. The binning employed was such that each bin corresponded to 1/2 of a spectral resolution element (~ 37 km s^{-1}). A small spectral region around the CaII K line (λ 3934 Å) was masked to prevent the frequent contamination by an interstellar component from biasing the determination. The "template" (radial velocity standard spectrum) was similarly prepared.

The flattened, masked and logarithmically binned spectra were next transformed to the Fourier domain using a Cooley-Tukey Fast Fourier Transform algorithm. In Fourier space the cross-correlation (convolution) becomes complex conjugation which is much more machine efficient. After performing the conjugation, the resultant power spectrum is transformed back to real space and the centroid of the

correlation function peak is located by using the Gaussian derivative method.

Figures 1(a) through (f) illustrate the procedure for a typical spectrum. The LOLITA processed spectrum of CS22882-7 is shown in Figure 1(a). The ordinate gives net accumulated counts per pixel for the total integration time of 1000 seconds. This star is located in the southern galactic polar region and, from Chapter I, it has V = 14.49, (B-V) = 0.04, and (U-B) = 0.10. The Balmer lines are, of course, dominant. The CaII K line λ 3934 Å is seen to have two components, one at a wavelength corresponding to the blue-shift of the Balmer lines (~ 115 km s^{-1}) and the other at a low velocity.

Taken on the same night (September 7, 1981) was an 800 second integration of ROB #70 in NGC 6397. The reduced spectrum of this radial velocity template is shown in Figure 1(b). Newell, Rodgers and Searle (1969) give V = 13.05, $(B-V)_0$ = 0.06, and $(U-B)_0$ = 0.16 for this star. The two spectra obviously match very well -- the only distinguishing features being the higher signal-to-noise ratio of the template and the lack of two distinct K lines (due to the low velocity of NGC 6397 which causes the interstellar component to be unresolved).

Figures 1(c) and (d) illustrate the object and template spectra after the (pseudo) continua have been flattened and normalized. Wavelength regions short of 3740 Å and longward of 4450 Å are set to unity due to lower signal-to-noise ratios and uncertain wavelength transformations on the ends of the detector array.

The correlation function resulting from the cross-correlation of these two spectra is shown in Figure 1(e). The ordinate is the normalized cross-correlation function (as defined, for example, by Tonry and Davis [1979]) in which an autocorrelation function would have a peak of unit height. In addition to the central peak of the correlation function, several other smaller local maxima can be seen. These result from the beatings of various Balmer lines of the two spectra against each other. Note the high degree of symmetry about the central peak; this reflects the fact that (1) the two spectra are closely matched (an autocorrelation function would be perfectly symmetrical) and (2) the signal-to-noise ratios in the spectra are reasonably high since there is no reason to expect that noise would enter into the two spectra similarly (see Tonry and Davis 1979 for an excellent and very helpful discussion of this and many other relevant cross-correlation technique details).

Figure 1(f) shows the enlarged central part of the correlation function. The striking aspects are the width and symmetry of the peak. The FWHM of the peak is on the order of 1400 km s^{-1} and one might initially suspect that only a modest accuracy (say a few %) could be attained in determining the centroid. The width of the peak is due to the great widths of the Balmer lines which it comprises. The great widths of the Balmer lines in A-type stars are due primarily to linear Stark broadening which is symmetric with respect to the line centers. Consequently the problem reduces to one of finding the center of symmetry of the correlation peak. An additional consideration is that the signal-to-noise ratios in the cores of the Balmer lines are very

low but have considerable weight in the correlation function peak. As a result, one does not want to rely primarily on using the maximum peak of the correlation function to define the velocity centroid. By choosing a proper weighting scheme which assigns little weight to the very peak of the line but weights the wings strongly and symmetrically the accuracy can be greatly improved. This is precisely the kind of weighting employed by the Gaussian derivative method which was used here.

Once the relatve bin shift (Δb) between the template and object spectra has been determined from the centroid of the cross-correlation peak, the heliocentric velocity of the objects follows via:

$$V_{h,*} = e^{a(\Delta b)}(c + V_{h,t} + V_{\oplus,t}) - (c + V_{\oplus,*}) \qquad (2)$$

where $V_{h,*}$ and $V_{h,t}$ are the heliocentric velocities of the star and the template respectively; $V_{\oplus,*}$ and $V_{\oplus,t}$ are the observed star and template velocity components due to the earth's movement about the barycenter of the solar system; c is the speed of light; Δb the relative bin shift and $a \equiv a_{1n}$ from equation (1).

The heliocentric radial velocities thus determined are presented in the third column of Table 2. The zero point of the radial velocity determinations is tied to the adoption of heliocentric velocities of 16 km s^{-1} for NGC 6397-70 and 22 km s^{-1} for NGC 6397-77. These two stars consistently showed a relative velocity of 6 km s^{-1} and their adpoted mean velocity of 19 km s^{-1} is that given for the weighted cluster mean by Webbink (1981) whose results depend largely upon the works of Da Costa *et al*. (1977) who give V = 20 $\pm$ 1 km s^{-1} and Kinman

(1959) who found V = 11 ± 6 km s^{-1}. (Hesser and Shawl [1982 private communication] have kindly made available preliminary radial velocity results from their Fabry-Perot interferometer scans of H_α. They find a velocity of 18 km s^{-1} for NGC 6397.)

Stars are identified in the first column of Table 2 by CS (Curtis Schmidt) plate and star numbers for the program AB stars; HR numbers for stars from YBSC; numbers assigned by Lee (1977) for BHB stars and by Sawyer-Hogg (1973) for RR Lyrae variables in NGC 6121 (M4); numbers from Eggen (1961) for stars in the young open cluster NGC 6383; ROB numbers for NGC 6397 BHB stars; and PS numbers are from Table II of Philip and Sanduleak (1968). Phases of mid-observations relative to ϕ = 0.00 at maximum light for the variables in M4 have been computed from the ephemerides of Sawyer-Hogg (1973) and are given in the notes to the table.

The second column of Table 2 shows the number of spectroscopic observations (Nsp) obtained. When Nsp > 1 and the different radial velocities were determined independently (e.g. secondary radial velocity standards for the night of the second observation were not bootstrapped from the night of the first observation) the fourth column shows the standard error in a single observation, i.e., the sample variance of the measurements:

$$\sigma = \left[\frac{1}{N-1} \sum (V_i - \langle V \rangle)^2 \right]^{1/2} \qquad (3)$$

where N is the number of observations. For N = 2 this becomes simply:

$$\sigma = 2^{-1/2} |V_1 - V_2| \qquad (4)$$

Lower case letters in parantheses refer to notes at the end of the table.

b) Error Analysis

Because of the high signal-to-noise ratios and the excellent spectral matches among object and template spectra the height of the normalized correlation peak was ≥ 0.90 for almost all of the program stars (none was < 0.80). Consequently there was never any ambiguity about which peak was the correct correlation peak. It is thought that errors arising in the process of determining the centroid of the peak are minimal. Some experiments were conducted using different methods of locating the centroid of the correlation peak, most notably that of fitting symmetric functions (Gaussians, parabolas, etc.) to the peak using least-squares techniques. Although all of these methods were felt to be inferior to the Gaussian derivative convolution method adopted, the velocity determination differences among such methods had a variance of only 3 km s^{-1}.

Errors due to the wavelength calibration of the comparison arc line spectra are also thought to be small. As mentioned in §II, the arc line polynomial fits were typically good to about 6 km s^{-1}. But this probably exaggerates the effect that wavelength calibrations make when two spectra which were calibrated in the same fashion are compared directly by cross-correlating.

In order to estimate the probable error contribution due to random detector drifts and variations in the local magnetic field the following experiment was conducted. Comparison arc spectra from six nights of the 1981 observing run were binned logarithmically. The binning covered the same range of pixels and was done at the same resolution used for the binning of the stellar spectra. These logarithmically binned comparison spectra were then cross-correlated with others taken the same night. The cross-correlation procedures employed were identical with those used for the stellar object and template computations. The results are presented in Table 3 for each of the six nights. The second column shows the number (N) of comparison spectra used in the analysis. In the third column are listed the variances of the relative "velocities" of the N-1 independent correlations. (All results have been converted to velocities for ease in comparison with the radial velocity measurements. To convert the pseudo-velocities back into pixels for use at other dispersions or spectral regions, divide them by 0.28Å pixel^{-1}c/4000Å ~ 21 km s^{-1}pixel^{-1}). A typical nightly instrumental dispersion is seen to be ~ 10 km s^{-1} (0.5 pixels).

In practice, wavelength calibrations were determined using comparison spectra taken immediately preceding and following the stellar observations and consequently a more relevant measure of the instrumental disperion is that which results from a comparison of the velocity shifts between pairs of consecutively taken comparison spectra. The results, given in Column 4, show that the dispersion is reduced to about 7 km s^{-1}. If the calculation is further restricted to

include only consecutive pairs between which telescope motion was $< 5^{o}$ the results (given in Column 5) are quite acceptable (~ 4 km s^{-1}). Column 6 lists the numbers of consecutive pairs used for this last calculation.

This experiment clearly demonstrates that the Reticon spectrometer suffers from drift and/or instability on the order of $\pm$ 1/2 pixel. But, by taking frequent comparison spectra at each telescope position, one can limit the instrumental contribution to the error to about 1/5 of a pixel.

The above error estimate, determined from very high signal-to-noise ratio comparison spectra containing many very narrow arc lines, sets a lower limit to the internal errors one can hope to achieve using the procedures and techniques employed here. An indication of the external errors can be obtained by comparing two or more independent radial velocity determinations of the same star.

As can be seen from Table 2, thirty-two program AB stars have two independent velocity measurements. Assume that (1) the errors in measurement are not correlated with velocity (no such relation has been found); (2) the stars in question do not have variable velocities; and further that (3) the errors are normally distributed with a variance of σ_{ε}. Define $x = V_1 - V_2$ to be the difference between two velocity measurements of the same star. Then for a sample of differences the variance is (see, for example, Hogg and Craig, 1970):

$$\sigma_x = 2^{1/2}\sigma_{\varepsilon}. \qquad (5)$$

Since $|x| = |V_1 - V_2|$ the mean or expectation value of the absolute value of the differences is:

$$\langle |V_1 - V_2| \rangle = \langle |x| \rangle =$$

$$= [\sigma_x (2\pi)^{1/2}]^{-1} \int_{-\infty}^{\infty} |x| e^{-0.5(x/\sigma_x)^2} dx$$

$$= \sigma_x (2/\pi)^{1/2} \qquad (6)$$

$$\text{and, by (5)} = 2^{1/2} \sigma_\varepsilon (2/\pi)^{1/2} \qquad (7)$$

$$\text{so that, finally } \langle |V_1 - V_2| \rangle = 2\pi^{-1/2} \sigma_\varepsilon \qquad (8)$$

Applying equation (8) to the thirty-two pairs of differences gives the standard error in a single observation of $\sigma_\varepsilon = 11$ km s^{-1}. No dependence of the size of the differences on declination or hour angle is seen in the data.

Additional insight into the accuracy can be gained by computing the observed velocity dispersion for the BHB stars in NGC 6397. Defining the observed velocity dispersion as:

$$\sigma_{obs} = \left[\frac{1}{N-1} \sum (V_i - \langle V \rangle)^2 \right]^{1/2} \qquad (9)$$

where N is the number of stars observed, the calculation gives $\sigma_{obs} = 9$ km s^{-1}. The observed dispersion comprises the intrinsic cluster velocity dispersion as well as that due to errors in the velocity determination σ_ε:

$$\sigma_{obs}^2 = \sigma^2 + \sigma_\varepsilon^2 \ .$$

(10)

Webbink (1981) gives a velocity dispersion of 4.4 km s^{-1} for NGC 6397 from which $\sigma_\varepsilon \sim 8$ km s^{-1}. Since the adopted radial velocity templates lie in the same cluster and all NGC 6397 observations were made at very similar telescope settings and were taken within a few minutes of each other this value for σ_ε must be considered a lower limit for the external errors.

A similar analysis for the BHB stars observed in M4 gives a mean cluster velocity of 68 and σ_{obs} of 12 km s^{-1}. Webbink gives V = 64 (Hesser and Shawl give a preliminary 72 km s^{-1}) and $\sigma = 4.8$ km s^{-1} which implies $\sigma_\varepsilon = 11$ km s^{-1}. The radial velocities of the c-type RR Lyrae stars in M4 were not included in this calculation because (1) the ephemerides used to determine the phase at mid-observation are quite old and the added contribution to the velocity dispersion from pulsation velocities would probably dominate over the other contributions; and (2) the spectral types are not as well matched by the template stars as are the program AB stars.

From these results the standard error in a single observation is judged to be 11 km s^{-1}.

Two velocity measurements of the A0 V star HD 213468 were made by introducing a neutral density filter in the optical path between the spectrograph slit and the collimator. Comparison arc-line spectra were taken with the same neutral density filter in place. The results were -181 and -174 km s^{-1}. Przybylski and Kennedy (1965) give a heliocentric velocity of -182.0 ± 0.2 km s^{-1} for this star. No

apparent ill effects were associated with the neutral density filter in place. One of the program AB stars, CS22875-6, was also observed on two different nights both through a neutral density filter and without the filter. The differences in the velocity determinations were well within the 11 km s^{-1} standard error.

IV. SPECTRAL LINE MEASUREMENTS

a) Interstellar K Lines

The possible existence of large amounts of absorbing material in the extended haloes of galaxies is commonly thought to give rise to the narrow absorption features seen in QSO's (see, e.g., Young, Sargent and Boksenberg 1982 and many references therein). Absorption due to interstellar origins in the spectra of high latitude objects within the Galaxy was noted over two decades ago (Munch and Zirin 1961). More recently, several studies of absorption of galactic origin in the spectra of extragalactic objects has been undertaken (especially by Blades, Songaila and coworkers. See Blades and Morton 1982 for references where a very nice and concise history of this topic appears).

It has often been suggested that the High Velocity Clouds (HVCs) that surround the Galaxy may be representative of the kind of material surrounding other galaxies which may give rise to QSO absorption lines. The distances to the HVCs are unknown and difficult to determine.

Perhaps by looking at a series of apparently fainter and fainter intrinsically luminous stars toward the direction of a HVC one could detect the onset of absorption and hence deduce its distance. HVCs are especially prevalent in the southern galactic hemisphere and typically have velocities relative to the Local Standard of Rest (LSR) of from -80 up to -400 km s^{-1}.

A search for absorption in the K line of CaII λ 3934 Å at high (especially negative) velocities in the spectra of the sample halo AB stars proved fruitless. Since the resolution employed and the signal-to-noise achieved in this study were, at best, only moderate, about all that can be concluded is that if HVCs do give rise to significant absorption (say, $\gtrsim$ 200 mÅ) then either none of the observed halo stars happens to lie on a line-of-sight to a HVC or else the HVCs are greater than ~ 10 kpc from the plane.

A look at the K lines in Figure 1(a) however, shows that there does exist low-velocity absorbing material between the sun and halo stars. In fact, of the thirty-six stars in Table 2 that have velocities in excess of 150 km s^{-1} (~ 2 Å or two resolution elements at K) relative to the sun, twenty-two of them show two distinct K lines. Another thirteen stars of lower velocity (typically 50 - 150 km s^{-1} relative to the sun) have an intrinisic K line small enough to allow the presence of an interstellar component to be resolved. Since (1) the resolution obtained for these spectra was ~ 1 Å (which corresponds to ~ 75 km s^{-1} at K), (2) many of the spectra have total K line widths of about 1 Å (see §IV<u>c</u>, below), and (3) many have velocities relative to the sun of $\lesssim$ 75 km s^{-1}, one cannot rule out the existence of an

interstellar component in a large fraction of the stars.

The equivalent widths and velocities of both components were determined by fitting a double Gaussian to the lines using a nonlinear least-squares technique after flattening the continuum as discussed in §III*a*. The fitting procedure is illustrated in Figure 2 for CS 22172-7, where the part of the flattened spectrum in the region of the K line is plotted with points and the smooth curve is the fit. The extended wings of the fitted Gaussian are constrained to match the normalization of the continuum. Considering the resolution and the signal-to-noise in the spectra the fit adequately represents the data. Note that, at least in this particular spectrum, the interstellar component is quite broad and may well result from several small absorption lines at slightly differing velocities. At this resolution one cannot discriminate further. The equivalent widths determined by this procedure are estimated to have a standard error of 150 milli-Ångstroms.

Table 4 lists the measured interstellar K line equivalent widths and velocities for the 35 stars. The equivalent widths are largely in the range $100 \leq W(K) \leq 500$ mÅ. This agrees with findings by several other authors (*c.f.* Greenstein 1968; Blades and Morton 1982). Note that no interstellar component has a velocity exceeding 42 km s^{-1}. The average velocity of all of the interstellar components in the table is just 7 with a variance of 23 km s^{-1}. The interstellar K line velocity was determined by applying the velocity difference between the intrinsic and interstellar components to the velocity of the star taken from Table 2. This measurement depends on fitting just one weak and

unresolved line and comparing that fit with the stellar velocity which has an uncertainly of ~ 11 km s^{-1}. It is therefore doubtful that the velocity of the interstellar K line is determined to better than the observed variance. Consequently, there is no compelling evidence that any of the interstellar components has a velocity significantly different from that of the sun.

Photometric parallaxes were used to find the distances to the stars (and hence, given galactic latitude, z -- the distance from the plane) using the photometry results given in Chapter 1 and employing a color-magnitude relation for Population II BHB stars drawn from the works of Sandage (1970) and Philip, Cullen and White (1976). All of the stars listed in Table 4 are far below the plane of the Galaxy (with $-10 \leq z \leq -1$ kpc). It therefore seems likely that all of the interstellar absorption occurs in the disk of the Galaxy, unless one adopts the view that halo material giving rise to the absorption has a low velocity relative to the sun.

Figure 3 shows the equivalent widths (in Angstroms) of the interstellar components plotted against z (in kpc). Note that those stars with the greatest amounts of absorption lie closest to the plane of the Galaxy. Since the sample is magnitude limited, those stars of low z have, on average, a line-of-sight which passes through more disk material. Figure 3 simply shows the result of a cosecant b effect and lends support to the hypothesis that the absorption takes place within 1 kpc of the disk. This same conclusion has also been reached by Blades and Morton (1982) who looked at extragalactic objects with higher resolution. Hence there is no evidence, from the present work,

of absorbing clouds of material in the halo of the Galaxy within 10 kpc of the solar position. If QSO absorption lines do arise in galaxies like the Milky Way, they must originate in the disk or in an extended halo. Furthermore, it appears that either the HVCs have a column density of Ca that is too low to be measured or else they are located far in the halo.

b) Weak Metallic Lines

The dominant metallic feature in the spectra of late-B and early-A stars is the Ca II K line, and its equivalent width is often used to gauge the overall metallicity of such stars (see, for example, AWR; RHS). In order to judge whether K line strengths do correlate with other elemental abundances, RHS obtained high resolution spectra of three halo A stars from which they concluded that the calcium abundances did faithfully represent [Fe/H] in all three stars.

No high resolution spectra of the CS AB stars have been obtained which would allow the kind of comparative analysis employed by RHS. A few bright field horizontal-branch A stars have been studied at high resolution (Danford and Lea 1981; Kodaira, Greenstein, and Oke 1969). Excepting the Ca II K line, both sets of authors find that the strongest metallic lines typically have equivalent widths of less than 150 mÅ. The detection and measurement of such weak features from the spectra obtained for the present work would be guesswork at best. Such unresolved lines would be largely indistinguishable from the noise. In order to extract a metallicity indicator from the spectra it was

necessary to improve the signal-to-noise ratio. The following scheme was adopted towards this goal.

A composite spectrum of all the sample CS AB stars was made by shifting each spectrum to zero velocity and adding the spectra together. This high signal-to-noise composite spectrum showed several absorption features and a list of the most prominent was made. Synthetic spectra, kindly made available by Armando Manduca, were also used to produce a list of metallic lines. Finally, the line lists in Danford and Lea (1981), Kodaira, Greenstein, and Oke (1969), and Philip (1981) were consulted. From these sources, ten metallic lines were selected which lie near the middle of the observed spectral region where detector stability and signal-to-noise ratios are highest. The selected lines were among those which consistently had the greatest equivalent widths in the above line lists. The ten lines are identified in Table 5.

For each observed spectrum, small spectral regions surrounding the ten lines were shifted to zero velocity and then added together. Since the signal in the superposed spectra increases linearly with N (=10, the number of regions added together) while the noise grows as $N^{1/2}$, the superposition increases the signal-to-noise ratio by a factor of slightly over 3. The depths of the absorption feature in the superposed spectra, taken as a positive value, was used as a metallicity index.

For comparison purposes, ten line-free spectral regions were also selected, each adjacent to one of the metal lines. These line-free spectral regions were also superposed. Additionally, for each of the

metallic line wavelengths λ_i, a nearby spectral region was chosen which had a central wavelength $\lambda_{r,i}$ selected using Monte Carlo techniques via:

$$\lambda_{r,i} = \lambda_i \pm (2.5 + 10\ R_i) \quad , \tag{11}$$

where R_i is a computer generated positive random number $0.0 \leq R_i < 1.0$ and the sign of the displacement is also determined randomly. In practice, the calculations for the randomly selected regions were carried out ten times for each star. From the resulting ten random indices the mean and variance were determined. As a result, for each star there were formed a metal index $\underline{M}$, metal-free continuum index $\underline{F}$, and an expected chance index $\langle \underline{C} \rangle$ along with its variance $\sigma_{\underline{C}}$. $\underline{M}$ itself is, of course, the primary metal indicator but, in addition, a measure of the significance, $\underline{S} \equiv (\underline{M} - \langle \underline{C} \rangle)/\sigma_{\underline{C}}$ was used to estimate the amount $\underline{M}$ deviated from the index one could expect to get by simply superposing randomly selected wavelength intervals of noise (perhaps contanimated by other weak spectral features). It should be noted that this analysis is similar to, and has benefitted from, the techniques of Wavelength Coincidence Statistics developted by Hartoog, Cowley, and Cowley (1973).

Figures (4a,b,c) illustrate the results for

(a) NGC 6397-70, a BHB star with $(B-V)_o = 0.06$ (Newell, Rodgers and Searle 1969) located in a metal-poor globular cluster ([Fe/H] ~ -1.5);

(b) NGC 6121-2415, a BHB star with $(B-V)_o = 0.07$ (the average value of four measurements taken from

Cacciari 1979, Lee 1977, Alcaino 1975, and Lloyd-Evans 1977 and corrected for E(B-V) = 0.36 from Cacciari). This star is a member of the moderately metal-poor ([Fe/H] ~ -1.0) globular cluster M4; and

(c) NGC 6383-13, a late-B or early-A star in a young metal-rich open cluster (Eggen 1961 gives $(B-V)_o = -0.07$, although the cluster is highly reddened and the spectrum indicates a spectral type near A1).

Each of the ten spectral regions surrounding the metallic features is displayed in the top part of the figures, where they have been shifted vertically by an arbitrary amount for clarity of presentation. All ten are plotted on the same vertical scale of relative net counts. The horizontal scale is in bins where 1 bin corresponds to 0.5 Å (so that two bins correspond to one resolution element). The bottom three lines show the superposition of (from top to bottom) the line-free regions (dash-dot), randomly selected regions (dashed) and selected metallic regions (solid). These three curves have been scaled vertically by dividing the sum of the superposition by $10^{1/2}$ (so that they are enhanced vertically by a factor of $10^{1/2}$ relative to the scale of the top ten lines).

Because the ten metallic line regions are aligned horizontally the eye can easily pick out the central features, at least for Figures 4(b) and (c). But note especially that in Figure 4(b) the individual lines are really indistinguishable from the noise. However, the superposed

curve clearly shows the presence of a coherent absorption feature centered in the chosen wavelength bands. The reality of the "lines" in the superposed curves can best be judged by comparing with the chance, or noise superposition immediately above them. Note also the clear progression of metallicity from Figures 4 (a) through (c), and bear in mind that although NGC 6383-13 is apparently hotter than the two BHB stars it nonetheless shows the presence of considerably more line absorption.

Although Figures 4(a-c) are not unrepresentative of the method, it must be stressed that the technique is really valid in a statistical context only. In particular the technique seems best suited for moderately metal-poor stars and becomes less sensitive for stars whose metallicities approach the solar value owing to the increasing number of absorption features which both contaminate the randomly-selected areas and depress the continuum, resulting in artificially low indices. This last complication is, of course, one that has always plagued equivalent width measurements. As a result it will be seen that the line index approaches an asymptotic limit as it begins to saturate. However, it is felt that the technique is well suited for application to the sample at hand. Figure 5 shows the relation between the significance indicator $\underline{S}$ and the line index for the CS AB Stars. The relation, though not tight, is reassuringly linear and shows that there are no cases of a large metal index with low significance. Application of equation (8) to the differences in line indices for the stars observed twice gives a standard error of 0.010.

Figure 6 shows the relation between the line index and the K line equivalent width for 44 synthetic spectra with effective temperatures $7000^{o} \leq T_{eff} \leq 12000^{o}$, gravities $3.0 \leq \log g \leq 4.5$, and metallicities $-2.0 \leq [A/H] \leq 0.0$. (The method employed and results of equivalent width determinations are discussed in §IV<u>c</u> below). The synthetic spectra were computed from model atmospheres by A. Manduca who generously made them available to the author (see Manduca and Bell 1978 and references therein for details on the construction of the synthetic spectra). The relation for the synthetic spectra is very tight, as one would expect for such data which contain essentially no noise. As anticipated above, the line-index -- W(K) relation reaches a limit for higher metallicities.

Figure 7 shows the same diagram for the sample AB stars. A comparison of Figures 6 and 7 reveals that the measurements of the observed spectra follow the relation for synthetic spectra for the large majority of stars, albeit with considerable scatter.

The five stars plotted as open circles in Figure 7 are clearly displaced above and to the left of the main locus of points. These stars (CS22172-12, CS22184-13, CS22936-192 and -256 and CS22942-34) have K lines which seem to be abnormally large for their metal indices. The spectrum of CS 22936-192 shows very sharp and narrow Balmer lines. This star does show metal lines along with its deep K line and is judged to be a low gravity high luminosity star. The spectra of the remaining four do indeed show metal lines which are weak for the stars' colors and for their K line strengths.

Six stars (CS22876-7, CS22882-15, CS22936-169, CS22946-8, CS22949-4 and CS22964-81) lie well below and to the right in Figure 7. As their position there would predict, the spectra of all six do show strong metallic absorption lines and a relatively weak K line. They exhibit the classic features of the metallic line ("Am") stars (see Conti 1970 for a review). Four other stars (CS22184-28, CS22881-43, CS22941-39, and CS22963-18) show the same characteristics as the Am stars, but to a lesser degree. These ten stars are plotted as open squares in Figure 7. It is not surprising that from a sample of over 200 AB stars a few percent turn out to be spectroscopically unusual. The A star population in the solar neighborhood is rich with such oddities as metallic line stars, magnetic stars, HgMn stars, He-weak stars and λ Boo stars (see Preston 1974 for a review where it is shown that chemically peculiar stars comprise one fourth to one fifth of main sequence stars with spectral types from B8 to F0).

The remainder of the scatter in Figure 7 is attributed to a combination of observational and intrinsic scatter along with imperfections in the technique. The method has demonstrated its ability to pick out the pathological stars which show abnormal K line strengths. Based on the present analysis the K line strengths of the CS AB stars are assumed to be representative of metallicity, excepting those cases cited in the previous two paragraphs which comprise about 7 % of the sample.

c) Ca II K Line Equivalent Widths

A single Gaussian function was fitted in nonlinear least-squares to the K lines in the same manner described in §IVa. The equivalent widths were then determined from the fitted parameters. The results are given in column 5 of Table 2. For those stars observed more than once, the standard error in a single observation is given in column 6 to the nearest tenth of an Ångstrom. As before, lower case letters in parentheses refer to notes at the end of the table.

Equivalent width measurements often vary appreciably from one author to another owing to the inherent dependence of the determination upon the resolution of the spectrograph used and the method of measurement employed. Consequently direct comparison with other published values must be rather loosely interpreted. Nonetheless such comparisons can be useful in pointing out gross systematic differences. Nineteen of the stars in the present work are in common with AWR and RHS and Figure 8 shows the values obtained there (along the ordinate) plotted against determinations made here (along the abscissa). When two measurements were made by the same author(s) the values are connected by a straight line. For several of the stars Rodgers and RHS give only an upper limit of 0.4 Å and such cases are plotted at at 0.4 on the ordinate. A line of unit slope and zero intercept is shown for orientation. All-in-all the agreement is satisfactory with the outstanding exception of CS22942-20 = PS37 which will be discussed in greater detail in §V below.

As a measure of the consistency of the measurements equation (8) was applied to the differences of the widths measured from the two spectra taken of 32 stars. The standard error in a single observation is found to be 0.12 Å.

A plot of the K line equivalent widths against B-V has often been used to roughly determine stellar metallicities (Searle and Rodgers 1966; Sargent 1968; AWR). K line widths were determined for the synthetic spectra in the same manner as for the program stars. UBV colors for the synthetic spectra were provided by A. Manduca. Figure 9 shows the regions in the W(K) -- B-V plane occupied by synthetic stars with metallicity parameters [A/H] = -0.5, -1.0, and -2.0. A mean relation derived from measurements of the observations taken of the main-sequence stars from YBSC lies virtually on top of the upper envelope relation for [A/H] = -0.5. It coincides very well with the main-sequence relation shown in AWR.

Figure 10 shows the same diagram for the CS AB stars for which UBV photometry is available. Eleven stars, plotted as open circles, show K line strengths which are close to that found for normal main-sequence stars. Four of these stars (CS22172-12, CS22184-13, CS22936-256, and CS22942-34) were found in §IV<u>b</u> to have K line strengths abnormally large for their metal indices. CS22875-27 was discussed in Chapter 1 in the context of its UBV colors. The photometry for CS22171-2 may be in error -- see §IV<u>d</u>. CS22936-192 is a high luminosity star and is discussed further in §§IV<u>b</u> and IV<u>d</u>. The remaining four stars -- CS22875-13, CS22936-250, CS22942-6, and CS22942-20 appear to be normal main sequence stars. They are further discussed in §§IV<u>d</u> and V.

Comparing Figures 9 and 10 clearly shows that the Ca abundances of the remaining stars (and hence, following §IVb the metal abundances) are well below that shown by Population I stars. While regarding Figure 10 one should bear in mind that the measured equivalent widths have not been corrected for the interstellar components (except for those stars listed in Table 4 which have mean K line interstellar component equivalent widths of 0.3 Å). Consequently, for many of these stars the intrinsic K line widths may be substantially less than the plotted values. This point is particularly significant for the bluest stars. Figure 10 shows that the sample CS AB stars comprise a homogeneous sample of halo Population II objects.

d) Hydrogen Lines

Owing to the great wings of the Balmer lines in A stars it is difficult to define the continuum and hence to determine equivalent widths. Instead it is customary to measure the full width of the lines at some depth (typically 20%) below the pseudo-continuum. This measure, D(.2), is closely related to the equivalent width through the Stark profile (Kodaira 1975) but more clearly defined operationally.

The wings of the Balmer lines were fitted by a simple $(\Delta\lambda)^{-5/2}$ power law -- the asymptotic limit for the Stark profile. Figure 11 illustrates the fit for the H_δ line of ROB 70 in NGC 6397. The fit is quite good, particularly near the point where the relative counts are 0.8 of the normalized pseudo-continuum.

As Kodaira (1975) discusses, the first few members of the Balmer series (H_α through ~ H_ε) are very similar in their responses to changes in physical parameters (specifically to effective temperature and gravity). H_δ falls nearly in the center of the observed spectral region where detector response and stability and the resulting signal-to-noise ratios were highest. Consequently D(.2) was calculated for the H_δ line of the stars by using the parameters determined from the fit. The results are given in column seven of Table 2 and, when more than one spectrum was obtained the standard error in a measurement is given to the nearest Ångstrom in column eight. The error in a single measurement, determined through application of equation (8), is 1.4 Å.

Kurucz (1979) published detailed Balmer line profiles and UBV colors along with a grid of model stellar atmospheres for a wide range of temperatures, gravities and abundances. He has kindly made all of the tabular material available on magnetic tape. Using the same procedures as those used for the observed spectra, D(.2) was measured for the H_δ profiles for those models in the temperature range $6500^o \leq T_{eff} \leq 12000$, gravities $2.0 \leq \log g \leq 4.5$, and abundances $-2.0 \leq [A/H] \leq 0.0$. The measurements showed little dependence upon metallicity since the dominant source of free electrons in this temperature range is hydrogen.

Figure 12 shows D(.2) for H_δ plotted against B-V for the Kurucz models with [A/H] = -1.0 and gravities ranging from log g = 4.5 (top set of connected points) to 2.0. Figure 13 is the same diagram for the observed stars. Note that although some curvature is present in the

distribution of points in Figure 13, it is apparent from a comparison with Figure 12 that the observed stars are of varying gravities. For those stars bluer than B-V = 0.10, the cooler stars have lower gravities and the hotter stars higher gravities (c.f. Figure 5 of Searle and Rodgers 1966). Since a star's luminosity (L), radius (r) and effective temperature (T_e) are related by $L \propto r^2T_e^4$ while the mass (M), gravity (g), and radius obey $g \propto M/r^2$ it follows that $M/L \propto g/T_e^4$. Since for BHB stars M/L is fairly constant (Newell 1970; Greenstein and Sargent 1974), the behavior shown in Figure 13 is just what one would expect. This behavior is seen to break down at the red end of the BHB as is also observed in globular cluster BHB stars (Searle and Rodgers 1966).

The five stars plotted as open squares (CS22936-192 and -229, CS22171-2, CS22875-25 and -27) lie well below the others in Figure 13. In §IVb it was argued that that CS22936-192 was a high luminosity star as CS22936-229 also appears to be. The spectra of the CS22171-2 shows sharp Balmer lines, a strong K line and many metal lines. In other words, the spectrum is like that of a normal late A or early F star so that one is led to suspect the photometry (although it is quite bright). The other two stars were discussed in Chapter 1 owing to their location in the UBV two-color diagram.

Twenty-one stars in Figure 13 lie above the main locus -- i.e., they have broad H_δ lines characteristic of high gravity. They are plotted as open circles (only 20 are apparent because the values for two of the stars coincide). Five of these stars (CS22876-7, CS22882-15, CS22936-169, CS22946-8, and CS22963-18) were discussed in

•IVb as having Am-type spectra. Of the remaining sixteen stars in this group two of the brightest (CS22942-20 with V = 12.26 and -6 with V = 12.90) appear to be normal main-sequence A stars, although the latter has a high velocity (65 km s^{-1}).

The remaining thirteen stars present a problem. They range from moderately to substantially metal-poor, from V = 13.45 to 15.33 and include a few high velocity stars. Two of them (CS22942-26 and CS22946-19) show mild Am features. The rest, however, appear to be weak-lined, normal-gravity A stars. It is tempting to suggest that these stars are akin to λ Boo stars. However, all known λ Boo stars have low velocities and velocity is frequently used as a classification criterion for them (e.g. Slettebak, Wright, and Graham 1968). Sargent (1965) argued that λ Boo stars were Population I stars passing through an evolutionary state wherein their atmospheres are depleted of heavy elements, perhaps enroute to becoming Ap stars. It seems stretching the point unreasonably to classify these halo stars as λ Boo stars.

There remains the possibility that at least some of these weak-lined normal-gravity A stars are field Population II Blue Stragglers. Several globular cluster color-magnitude diagrams contain a few such objects located well above the turn-off along the projected main-sequence. Due to their faintness ($V \gtrsim 15$) little is known about their spectroscopic properties, although a few of the brighter field Population II Blue Stragglers have been studied (Carney and Peterson 1981). The evolutionary status of these stars remains a mystery (see Wheeler 1979 for a recent summary of possibilities).

e) Notes on Reddening, Deblanketing, and Stellar Rotation

At the dispersion employed here no quantitative measurements of rotational broadening of absorption lines would be meaningful. About the most that can be said is that none of the sample stars shows any evidence of extremely rapid rotation. Values for V sin(i) are given for some of the stars observed from YBSC and even for those stars rotating at V sin(i) ~ 120 km s^{-1} the spectra do not differ appreciably in appearance from normal. However, when V sin(i) approaches ~ 150 km s^{-1} the effects upon the spectrum become noticeable. One of the stars (HR8419) has a catalogue value of V sin(i) of 360 km s^{-1} and the effect is readily evident in its spectrum. A typical main-sequence A star is rotating ~ 130 km s^{-1} and about 35% have V sin(i) in excess of 150 (Jaschek, 1970). None have been found in the CS sample.

The effects of reddening have been ignored in this work. Most of the stars lie at high galactic latitude where $E(B-V) \lesssim 0.03$ (Burstein and Heiles 1982). Such small reddening corrections would not appreciably affect the results obtained here. Two of the fields lie at lower galactic latitudes. Chosen by Preston and Shectman specifically as a low-latitude field with little reddening, CS22936 lies at $b = -16^{o}$ below the bulge in the direction of the globular cluster NGC 6723 which has a reddening of $E(B-V) = 0.03$ (Harris and Racine 1979). CS22964, at $b = -29^{o}$ lies in the regions where $0.03 \leq E(B-V) \leq 0.09$ according to the recent findings of Burstein and Heiles.

It is apparent from the distribution of colors in the UBV two-color diagram presented as Figure 2 in Chapter 1 that the sample stars are not heavily reddened. Plotting the low latitude fields separately shows the same distribution. There is, nonetheless, a great deal of scatter in the UBV plane -- particularly below the main sequence in the color range $-0.10 \leq B-V \leq 0.20$. Wolff (1967) pointed out that for early A and late B stars the opacity in the U passband is dominated by the continuous and line absorption of hydrogen and hence line blanketing would have rather little effect in U relative to B. In such cases the deblanketing vectors (as drawn in the traditional two-color diagram) will point to the left and <u>down</u> (unlike the behavior to which one is accustomed for F and G subdwarfs where the absence of line opacity in the U pass band is so significant that the deblanketing vectors point <u>up</u> and to the left). An examination of the UBV colors computed from the Kurucz (1979) model atmospheres confirms Wolff's hypothesis. Figure 14 illustrates the results of the combined effects of lowering both metallicity and surface gravity. Straight lines are drawn through points connecting the colors for model atmospheres with effective temperatures from 6500° to 12000° for (1) solar metallicity, log g=4.5 and (2) [A/H] = -2.0, log g = 3.0. Figure 14 shows the kind of color changes one expects from main-sequence stars to BHB stars. Because of the difficulty of sorting out gravity effects and deblanketing vectors for AB stars, and further because no evidence for heavy reddening is apparent in the data, no reddening determinations have been attempted.

V. THE METAL-RICH HALO A STAR POPULATION

AWR obtained spectra for 62 "PS" stars classified as A stars in the objective prism survey taken of the southern galactic polar region by Philip and Sanduleak (1968). Photometry obtained by Eggen was published by Rodgers who found that a surprisingly large fraction of stars with $12.0 \leq V \leq 14.5$ had metallicities which were near the solar value, or at most were deficient by a factor of only a few. Their distances below the plane ranged up to 4 kpc and their velocities were representative of the kinematics of the halo. Greenstein and Sargent (1974) similarly found that a substantial fraction of faint high latitude B stars have normal spectra and apparently large z distances. Other workers have reached similar findings (e.g. Tobin and Kilkenny 1981; see Stetson 1981 for a recent summary).

Although a few apparently normal stars have been found from one to three kpc from the plane in the present work, the number is far less than expected on the basis of Rodgers' findings. Before jumping to conclusions it must be noted that the classification procedure used by Preston (outlined in Chapter 1) may well result in a bias against the selection of stars of normal metallicities.

The three CS plates which either partially or wholly overlie the field of Philip and Sanduleak's objective-prism search should contain 18 stars from the list of 62 PS stars. Eleven of them were rediscovered (they are those identified by their PS numbers in the last column of Table VI in Chapter 1). Of the remaining seven stars, three (PS9, 44, and 57) were brighter than V = 12.5 (from Eggen's photometry)

and one has V = 12.97. Reinvestigation of the CS plates has shown these stars to be too bright for reliable classification. A second examination of the appropriate CS plate revealed that PS11 was unaccountably overlooked and is an AB star. PS4 is classified as late A to early F by Preston (Eggen's B-V = 0.31). PS38 is somewhat of a mystery and could not be located on a second look at the CS plate. Presumably an error exists in the coordinates.

Five of the seven stars not classified as AB by Preston fall into Rodgers' metal-rich category -- all five are, however, brighter than V = 13.5. In summary, of the 18 stars lying in CS fields only one star fainter than V = 13.5 was overlooked and Rodgers did not classify that star as one of the strong-lined stars.

Table 6 compares measurements of the 11 CS stars in common plus those of an additional 8 PS stars observed for the purpose of comparison with Rodgers' work. The table is largely self-explanatory. The values for Rodgers' measurements are taken from his 1971 paper unless a different, more recent value appeared in RHS. The K line equivalent width comparisons were illustrated in Figure 8. They are in reasonable agreement and show no systematic differences. The W(K) measurements for CS22942-20 = PS37 strongly disagree, as do the measurements of the H_δ D(.2). Presumably a misidentification has occurred. Curiously the photometry agrees very well, at least in V and B-V. There is no other nearby star of similar brightness and spectral class seen on the objective prism plate. RHS list this star as an example of the weak-lined stars. The values given there for W(K), $D(.2)_\delta$, and velocity are identical with the 1971 paper. The spectrum

obtained in the present work shows it to be a normal main-sequence A star as suggested in §IV*d*.

The D(.2) measurement of H_δ are generally in acceptable agreement with five exceptions: CS22942-6 = PS30, a normal A star (see preceding section) and PS33, a late B. The values of D(.2) were remeasured on plots of the spectra of these two stars by simply drawing in the continuua with a straight edge and then measuring with a ruler. The results were consistent with those obtained in the fitting procedure. PS3, 4, and 31 (of normal metallicity) are the coolest stars involved (B-V $>$ 0.30) and it is likely that the fitting procedure adopted here fails due to the presence of many absortion lines which probably results in an unreliable estimate of the continuum by the algorithm.

The agreement between the velocity determinations is not so good. The mean difference is $\langle V_R - V_P \rangle = -10 \pm 52$ km s^{-1} (rms). Applying equation (8) to the mean of the absolute value of the differences yields $\sigma_{tot} = 36$ km s^{-1}. Adopting $\sigma_P = 11$ km s^{-1} and employing $\sigma^2_{tot} = \sigma^2_P + \sigma^2_R$ gives $\sigma_R = 34$ km s^{-1}. AWR suggests a <u>probable</u> error (p.e.) of 20 km s^{-1} for his velocity measurements from which it follows that the standard error is σ_R = p.e./0.6745 ~ 30 km s^{-1} in reasonable agreement with the result just reached. RHS apparently did not redetermine the velocities since the values given there are identical with those in the 1971 paper. The largest radial velocity disagreement is with CS22882-18 = PS16, one of the stars Rodgers classified as a strong-line star. Rodgers found a velocity of -215 km s^{-1} from which RHS predicted that this star attains a maximum z distance below the plane on the order of 8 kpc. The two spectra obtained here give -45 ± 20 km s^{-1}.

Three of the CS stars were among those classified by Rodgers as having near solar metallicities. CS22942-6 = PS30 was discussed in §IVd where it was judged a normal A star. CS22882-15 = PS10 was classified as an Am star. The third star, CS22882-15 = PS16 was not found to be either high gravity nor metal rich by any of the methods employed here. Its W(K) was measured here twice at 0.44 and 0.60 Å (RHS give 0.66) which may, of course, include an interstellar component. The B-V of 0.10 given in Chapter 1 resulted from the average of two measures on two different nights of 0.11 and 0.09. A solar abundance star of this color would be more likely to have a W(K) of 1.5 - 2.0 Å (see Figure 9). Rodgers used a B-V of 0.04 for this star which apparently led him to conclude that the width of the K line was normal for a near solar metal abundance star.

The spectra of five PS stars from the strong-line list of RHS stars do appear to be those of normal main-sequence stars. But it is perhaps significant that only two stars classified herein from the CS survey as normal main-sequence stars have been found fainter than V ~ 13.5 (both of which, due to their relatively low galactic latitudes, are less than ~ 3 kpc from the plane). RHS list seven such stars, all bluer than B-V = 0.20, three of which are fainter than V = 14.0. Of these three there is PS16 just discussed and here judged not to show evidence of being metal-rich; PS10, judged an Am star; and PS60 -- a star with B-V = 0.00 (Eggen) and W(K) = 0.43 (Rodgers). Based on the discussion regarding interstellar K line in §IVa, the evidence for normal metal abundance in this star seems less than compelling.

None of the foregoing changes Rodgers' results in a substantive way. There clearly do exist early-type stars with near normal metallicities and moderately high radial velocities at distances of 2-3 kpc from the plane of the Galaxy. In particular, many of the stars found here with Am-type spectra are quite faint and have appreciable radial velocities. Similarly, the stars classified as normal main-sequence A stars, though brighter than V = 13.0, have substantial radial velocities. But there seems to be evidence here that these stars drop off substantially in number beyond 2 - 3 kpc. It is felt that the kind of objects that comprise Rodgers' strong-line A stars are members of an old disk population with the scale height found by Gilmore and Reid (1982), discussed in §I.

VI. CONCLUDING NOTE

The foregoing has demonstrated that the AB stars found at high galactic latitude by Preston and Shectman are, with several interesting exceptions, largely BHB stars. When the normal main-sequence stars and metallic line stars are culled from the sample, the remainder represents a homogeneous sample of metal-poor, evolved Population II stars. Reports of more detailed analyses of the spectra of the metallic line stars and possible blue stragglers will be relegated to future work. The task at hand is to try to make some sense of the kinematics of the halo stuff, the subject of Chapter 3.

TABLE 1. AB STARS NOT IN PAPER I

Star	R.A. (1950)	Dec.	l	b	Class
CS 22184- 3	02 30 11	-09 09.2	180.4	-60.0	AB f
CS 22184- 23	02 36 04	-11 03.9	185.2	-60.0	AB f
CS 22876- 4	23 50 06	-36 31.6	353.1	-74.6	AB f
CS 22876- 5	23 49 55	-36 19.9	353.8	-74.6	AB f
CS 22876- 7	23 50 39	-36 11.0	354.0	-74.8	AB mf
CS 22881- 44	22 04 49	-38 20.2	4.6	-54.2	AB m
CS 22881- 54	22 07 49	-38 33.0	4.1	-54.7	AB mf
CS 22881- 56	22 08 25	-39 55.0	1.8	-54.7	AB mf
CS 22942- 32	01 02 33	-25 58.2	188.5	-86.7	AB m
CS 22964- 30	19 40 02	-38 38.4	1.1	-26.1	AB f
CS 22964- 36	19 43 23	-38 17.2	1.6	-26.7	AB mf
CS 22964- 45	19 47 42	-37 32.8	2.7	-27.3	AB mf
CS 22964- 62	19 50 10	-39 18.0	0.9	-28.2	AB mf
CS 22968- 22	03 19 59	-57 06.4	271.8	-50.1	AB mf
CS 22968- 25	03 21 27	-56 00.9	270.1	-50.5	AB f
CS 22968- 27	03 17 45	-55 27.8	269.8	-51.3	AB f
CS 22968- 34	03 22 23	-54 18.9	267.7	-51.3	AB mb

TABLE 2. SPECTROSCOPIC MEASUREMENTS

Star	Nsp	Helio Vel	σ_V	W(K)	σ_K	H_δ	σ_δ
		<- km/sec ->		<-------- Angstroms --------			
CS 22171- 2	1	68	-	3.4	-	12	-
CS 22171- 4	2	-56	12	0.5	0.1	28	1
CS 22171- 13	2	31	4	1.4	0.2	25	0
CS 22171- 23	2	-62	8	0.2	0.1	24	2
CS 22172- 7	1	-190	-	1.1	-	22	-
CS 22172- 9	1	168	-	1.2	-	31	-
CS 22172- 10	1	-41	-	1.1	-	27	-
CS 22172- 12	1	80	-	4.5	-	22	-
CS 22172- 17	1	332	-	1.3	-	16	-
CS 22172- 20	1	64	-	1.9	-	26	-
CS 22184- 3	1	223	-	1.4	-	23	-
CS 22184- 6	1	39	-	3.0	-	27	-
CS 22184- 9	1	3	-	0.3	-	27	-
CS 22184- 13	1	2	-	4.6	-	23	-
CS 22184- 14	1	32	-	0.7	-	26	-
CS 22184- 23	1	72	-	0.6	-	30	-
CS 22184- 28	1	136	-	1.7	-	28	-
CS 22184- 29	1	117	-	0.3	-	26	-
CS 22184- 30	1	3	-	2.5	-	27	-
CS 22184- 42	1	-50	-	2.0	-	32	-
CS 22184- 45	1	4	-	0.5	-	26	-
CS 22184- 48	2	39	4	0.5	0.1	37	3
CS 22875- 3	1	64	-	1.0	-	28	-
CS 22875- 5	1	-57	-	0.4	-	28	-
CS 22875- 6	8	-27	15	0.8	0.2	39	2
CS 22875- 7	1	-124	-	2.4	-	23	-
CS 22875- 11	1	5	-	2.4	-	20	-
CS 22875- 13	1	-133	-	3.1	-	22	-
CS 22875- 14	1	-11	-	1.2	-	31	-
CS 22875- 15	1	62	-	0.2	-	28	-
CS 22875- 16	1	-111	-	0.7	-	24	-
CS 22875- 18	1	24	-	0.3	-	29	-
CS 22875- 19	1	-29	-	3.3	-	15	-
CS 22875- 20	1	-116	-	0.6	-	28	-
CS 22875- 21	1	78	-	0.3	-	20	-
CS 22875- 22	1	7	-	2.3	-	21	-
CS 22875- 23	1	108	-	0.4	-	27	-
CS 22875- 24	2	155	6	0.5	0.2	25	0
CS 22875- 25	1	-12	-	0.8	-	9	-
CS 22875- 27	1	7	-	2.7	-	13	-

TABLE 2. (Continued)

Star	Nsp	Helio Vel	σ_V	W(K)	σ_K	H_δ	σ_δ
		<- km/sec ->		<------- Angstroms --------->			
CS 22875- 30	1	23	-	0.4	-	24	-
CS 22875- 31	1	105	-	0.1	-	26	-
CS 22875- 34	1	45	-	0.3	-	28	-
CS 22875- 35	1	43	-	0.5	-	13	-
CS 22875- 36	2	-127	0	(a)	-	22	2
CS 22875- 37	1	-47	-	0.6	-	27	-
CS 22875- 40	1	-24	-	1.2	-	27	-
CS 22875- 41	2	16	7	0.7	0.1	29	1
CS 22875- 44	1	39	-	1.0	-	26	-
CS 22876- 4	1	-34	-	2.7	-	24	-
CS 22876- 5	1	-36	-	0.4	-	27	-
CS 22876- 7	1	-12	-	1.5	-	34	-
CS 22881- 21	1	-85	-	0.3	-	25	-
CS 22881- 34	1	-66	-	0.9	-	27	-
CS 22881- 43	1	43	-	1.3	-	28	-
CS 22881- 44	1	-31	-	0.3	-	26	-
CS 22881- 54	1	-8	-	0.5	-	25	-
CS 22881- 56	1	248	-	0.8	-	26	-
CS 22882- 2	1	18	-	1.0	-	27	-
CS 22882- 3	1	32	-	0.3	-	28	-
CS 22882- 7	2	-115	16	0.5	0.1	27	0
CS 22882- 11	1	-36	-	0.4	-	26	-
CS 22882- 14	2	22	26	0.5	0.0	26	0
CS 22882- 15	2	76	14	1.5	0.1	31	2
CS 22882- 18	2	-45	20	0.5	0.1	27	1
CS 22882- 19	2	-50	8	0.5	0.2	23	0
CS 22882- 20	2	15	3	1.5	0.0	26	1
CS 22882- 22	1	92	-	0.5	-	29	-
CS 22882- 25	1	19	-	0.5	-	30	-
CS 22882- 31	2	12	(b)	0.3	0.3	13	0
CS 22882- 32	1	98	-	0.2	-	25	-
CS 22882- 33	2	0	(b)	0.7	0.0	28	2
CS 22882- 35	1	-13	-	0.2	-	25	-
CS 22894- 1	1	-245	-	0.8	-	26	-
CS 22894- 3	1	-184	-	1.3	-	26	-
CS 22894- 6	1	-230	-	0.3	-	27	-
CS 22894- 8	1	-10	-	3.7	-	17	-
CS 22894- 13	1	-42	-	1.2	-	27	-
CS 22936-169	1	-58	-	1.7	-	31	-
CS 22936-192	1	5	-	2.7	-	13	-

TABLE 2. (Continued)

Star	Nsp	Helio Vel (- km/sec ->)	σ_V	W(K) (<------- Angstroms)	σ_K	H_δ (----------> Angstroms)	σ_δ
CS 22936-209	1	-186	-	0.4	-	27	-
CS 22936-211	1	73	-	1.0	-	28	-
CS 22936-213	1	185	-	1.7	-	24	-
CS 22936-218	1	107	-	0.3	-	23	-
CS 22936-224	1	-90	-	0.6	-	27	-
CS 22936-225	1	6	-	0.8	-	22	-
CS 22936-227	1	-47	-	0.6	-	24	-
CS 22936-229	1	111	-	0.6	-	12	-
CS 22936-233	1	61	-	1.1	-	27	-
CS 22936-235	1	-164	-	0.2	-	26	-
CS 22936-236	1	-94	-	0.6	-	29	-
CS 22936-237	1	19	-	1.1	-	29	-
CS 22936-238	1	-75	-	1.6	-	28	-
CS 22936-239	1	55	-	0.9	-	28	-
CS 22936-240	1	-103	-	1.1	-	30	-
CS 22936-243	1	98	-	0.8	-	30	-
CS 22936-244	1	35	-	0.4	-	28	-
CS 22936-246	1	-121	-	0.3	-	25	-
CS 22936-247	2	154	12	0.3	0.1	23	1
CS 22936-249	1	-77	-	0.9	-	31	-
CS 22936-250	1	32	-	1.7	-	29	-
CS 22936-252	1	0	-	0.6	-	23	-
CS 22936-256	1	-130	-	4.5	-	22	-
CS 22936-258	2	-314	5	0.4	0.1	26	2
CS 22936-263	1	-32	-	0.5	-	23	-
CS 22936-264	1	-50	-	1.5	-	26	-
CS 22936-274	1	-65	-	1.3	-	28	-
CS 22936-275	1	1	-	1.3	-	35	-
CS 22936-278	1	228	-	0.8	-	26	-
CS 22936-281	1	-111	-	1.8	-	22	-
CS 22936-282	1	73	-	0.6	-	24	-
CS 22936-283	1	-62	-	0.8	-	30	-
CS 22936-284	1	-67	-	0.9	-	23	-
CS 22936-285	2	201	(b)	0.6	0.0	27	0
CS 22936-286	1	-98	-	0.7	-	26	-
CS 22936-287	1	-60	-	0.7	-	26	-
CS 22936-291	1	-58	-	2.2	-	23	-
CS 22936-294	1	-49	-	0.8	-	25	-
CS 22936-299	1	55	-	0.9	-	26	-
CS 22941- 23	1	-21	-	1.0	-	32	-

TABLE 2. (Continued)

Star	Nsp	Helio Vel	σ_V	W(K)	σ_K	H_δ	σ_δ
		<- km/sec ->		<------- Angstroms --------->			
CS 22941- 26	1	-172	-	0.5	-	28	-
CS 22941- 29	1	98	-	0.6	-	28	-
CS 22941- 31	1	73	-	0.5	-	21	-
CS 22941- 39	1	41	-	1.1	-	28	-
CS 22941- 47	1	-1	-	0.9	-	26	-
CS 22942- 4	1	95	-	1.0	-	37	-
CS 22942- 5	1	-20	-	0.5	-	28	-
CS 22942- 6	1	65	-	3.1	-	32	-
CS 22942- 8	2	18	9	0.8	0.1	31	2
CS 22942- 9	1	-5	-	1.6	-	21	-
CS 22942- 13	1	31	-	0.6	-	24	-
CS 22942- 15	1	-32	-	0.5	-	28	-
CS 22942- 18	1	-33	-	1.5	-	21	-
CS 22942- 20	1	0	-	2.9	-	30	-
CS 22942- 22	2	5	11	1.2	0.2	26	2
CS 22942- 25	1	94	-	(a)	-	21	-
CS 22942- 26	1	-28	-	1.1	-	38	-
CS 22942- 28	1	34	-	3.2	-	19	-
CS 22942- 31	1	2	-	0.4	-	28	-
CS 22942- 32	1	72	-	1.5	-	17	-
CS 22942- 34	1	192	-	2.7	-	34	-
CS 22942- 37	1	-98	-	1.4	-	29	-
CS 22946- 1	1	85	-	0.1	-	27	-
CS 22946- 4	1	153	-	0.2	-	27	-
CS 22946- 8	1	32	-	1.6	-	33	-
CS 22946- 9	1	-17	-	2.3	-	21	-
CS 22946- 10	1	26	-	0.5	-	37	-
CS 22946- 11	1	-20	-	1.2	-	14	-
CS 22946- 15	1	-139	-	0.5	-	28	-
CS 22946- 16	1	-51	-	0.3	-	21	-
CS 22946- 19	1	25	-	1.4	-	34	-
CS 22946- 20	1	189	-	0.8	-	29	-
CS 22949- 4	1	-24	-	1.8	-	25	-
CS 22949- 6	1	-177	-	0.5	-	27	-
CS 22949- 9	1	-99	-	1.7	-	24	-
CS 22949- 12	1	-196	-	0.2	-	25	-
CS 22949- 13	1	-189	-	0.5	-	29	-
CS 22949- 41	1	-345	-	0.2	-	17	-
CS 22963- 11	1	66	-	1.1	-	36	-
CS 22963- 12	1	133	-	0.8	-	27	-

TABLE 2. (Continued)

Star	Nsp	Helio Vel	σ_V	W(K)	σ_K	H_δ	σ_δ
		<- km/sec ->		<------- Angstroms --------->			
CS 22963- 13	1	-123	-	1.1	-	18	-
CS 22963- 16	1	-9	-	0.9	-	28	-
CS 22963- 18	1	-34	-	1.3	-	33	-
CS 22963- 19	1	181	-	0.2	-	25	-
CS 22963- 21	1	-25	-	0.3	-	24	-
CS 22963- 22	1	136	-	0.3	-	16	-
CS 22963- 25	1	-175	-	0.9	-	20	-
CS 22963- 30	1	-59	-	3.3	-	16	-
CS 22963- 31	1	207	-	1.1	-	27	-
CS 22963- 32	1	88	-	1.1	-	26	-
CS 22963- 33	1	-3	-	2.3	-	26	-
CS 22963- 35	1	29	-	1.5	-	29	-
CS 22963- 36	1	59	-	0.1	-	17	-
CS 22964- 1	1	51	-	0.8	-	26	-
CS 22964- 2	2	165	11	0.5	(c)	24	1
CS 22964- 3	1	-28	-	1.5	-	27	-
CS 22964- 4	1	24	-	0.5	-	26	-
CS 22964- 5	1	-16	-	0.8	-	24	-
CS 22964- 7	1	-33	-	2.0	-	24	-
CS 22964- 8	1	86	-	0.4	-	29	-
CS 22964- 9	2	205	8	1.0	(c)	24	1
CS 22964- 15	1	-18	-	1.0	-	28	-
CS 22964- 16	2	-145	4	1.1	0.0	27	3
CS 22964- 21	1	57	-	4.0	-	15	-
CS 22964- 23	2	-13	2	0.6	0.0	24	3
CS 22964- 26	1	-19	-	0.7	-	26	-
CS 22964- 29	1	68	-	0.6	-	26	-
CS 22964- 30	1	-135	-	0.3	-	29	-
CS 22964- 31	1	83	-	1.4	-	29	-
CS 22964- 32	2	186	4	0.2	0.0	26	1
CS 22964- 36	1	-180	-	0.3	-	26	-
CS 22964- 39	1	94	-	0.3	-	26	-
CS 22964- 45	1	-377	-	0.3	-	27	-
CS 22964- 58	1	65	-	1.3	-	26	-
CS 22964- 62	1	-84	-	0.9	-	25	-
CS 22964- 66	1	-35	-	0.7	-	29	-
CS 22964- 67	1	-86	-	0.1	-	23	-
CS 22964- 76	1	-33	-	0.3	-	14	-
CS 22964- 77	1	-14	-	0.3	-	26	-
CS 22964- 78	2	-45	17	0.5	0.1	28	1

TABLE 2. (Continued)

Star	Nsp	Helio Vel	σ_V	W(K)	σ_K	H_δ	σ_δ
		<- km/sec ->		<------- Angstroms --------->			
CS 22964- 81	1	-42	-	2.0	-	15	-
CS 22964- 83	2	49	2	1.5	0.0	24	1
CS 22964- 84	2	12	5	0.8	0.1	27	1
CS 22964- 85	1	42	-	0.6	-	27	-
CS 22964- 87	1	-21	-	0.8	-	26	-
CS 22964-102	1	-66	-	0.3	-	13	-
CS 22964-103	1	45	-	1.2	-	23	-
CS 22964-105	1	-41	-	0.8	-	28	-
CS 22964-107	2	330	(b)	1.2	0.0	24	1
CS 22964-126	1	3	-	0.5	-	29	-
CS 22968- 2	1	335	-	-	-	25	-
CS 22968- 6	1	68	-	0.5	-	18	-
CS 22968- 10	1	84	-	1.2	-	31	-
CS 22968- 13	2	42	9	1.2	0.0	23	1
CS 22968- 20	1	133	-	1.5	-	22	-
CS 22968- 22	2	103	2	0.2	(c)	18	0
CS 22968- 25	1	213	-	1.2	-	29	-
CS 22968- 27	1	4	-	0.5	-	27	-
CS 22968- 28	1	226	-	0.9	-	26	-
CS 22968- 34	1	-19	-	0.2	-	23	-
CS 22968- 37	1	116	-	0.2	-	17	-
CS 22968- 45	1	72	-	0.5	-	27	-
CS 22968- 46	1	97	-	0.7	-	25	-
CS 22968- 48	2	117	3	0.8	0.0	26	0
HD 213 468	2	-179	3	0.5	0.0	27	1
HR 6843	1	-	-	4.9	-	22	-
HR 7086	1	-	-	1.5	-	33	-
HR 7088	1	-	-	6.4	-	10	-
HR 7286	1	-	-	2.3	-	22	-
HR 7558	1	-	-	3.5	-	30	-
HR 7630	1	-	-	5.7	-	16	-
HR 7710	1	-	-	0.3	-	23	-
HR 7773	1	-	-	0.5	-	25	-
HR 7848	1	-	-	4.7	-	16	-
HR 7981	1	-	-	1.4	-	32	-
HR 8114	1	-	-	2.9	-	25	-
HR 8140	1	-	-	3.9	-	30	-
HR 8230	1	-	-	2.3	-	29	-
HR 8264	1	-	-	4.6	-	23	-
HR 8358	1	-	-	0.7	-	35	-

TABLE 2. (Continued)

Star	Nsp	Helio Vel	σ_V	W(K)	σ_K	H_δ	σ_δ
		<- km/sec ->		<------- Angstroms --------->			
HR 8404	1	-	-	0.4	-	19	-
HR 8419	1	-	-	0.8	-	24	-
HR 8459	1	-	-	2.8	-	29	-
HR 8880	1	-	-	3.5	-	28	-
HR 8891	1	-	-	0.7	-	24	-
NGC 6121-1103	1	83	-	0.8	-	27	-
NGC 6121-1207	1	78	-	1.9	-	26	-
NGC 6121-1520	1	75	-	1.7	-	27	-
NGC 6121-2104	1	64	-	1.8	-	28	-
NGC 6121-2415	1	58	-	1.4	-	27	-
NGC 6121-3408	1	46	-	1.6	-	28	-
NGC 6121-4315	1	69	-	1.2	-	28	-
NGC 6121-4316	1	72	-	1.0	-	30	-
[d]NGC 6121-V1	1	64	-	3.7	-	14	-
[d]NGC 6121-V6	1	43	-	2.7	-	19	-
[d]NGC 6121-V20	1	27	-	2.3	-	22	-
[d]NGC 6121-V23	1	34	-	2.2	-	21	-
[d]NGC 6121-V30	1	69	-	1.9	-	25	-
[d]NGC 6121-V37	1	37	-	2.2	-	24	-
[d]NGC 6121-V42	1	24	-	3.6	-	15	-
[d]NGC 6121-V43	1	55	-	2.5	-	18	-
NGC 6383- 7	2	14	6	0.9	0.0	33	1
NGC 6383- 13	2	-56	3	1.7	0.1	31	0
NGC 6383-13A	2	-1	20	3.1	0.1	26	0
NGC 6383- 22	1	-58	-	3.0	-	27	-
NGC 6383- 25	1	15	-	0.6	-	31	-
NGC 6397- 26	1	18	-	0.6	-	25	-
NGC 6397- 44	1	11	-	0.6	-	24	-
NGC 6397- 48	1	29	-	0.7	-	26	-
NGC 6397- 70	17	16	(e)	0.9	0.0	26	1
NGC 6397- 77	18	22	(e)	0.6	0.1	25	1
NGC 6397-438	1	-4	-	0.3	-	18	-
NGC 6397-544	1	14	-	0.4	-	21	-
NGC 6397-584	1	17	-	0.7	-	25	-
NGC 6397-679	1	19	-	0.6	-	22	-
PS 3	1	39	-	5.5	-	12	-
PS 4	1	-94	-	4.0	-	15	-
PS 7	1	-23	-	2.4	-	27	-
PS 31	1	41	-	1.6	-	16	-
PS 32	1	-50	-	1.4	-	34	-

TABLE 2. (Continued)

Star	Nsp	Helio Vel	σ_V	W(K)	σ_K	H_δ	σ_δ
		<- km/sec ->		<------- Angstroms --------->			
PS 33	1	68	-	0.2	-	19	-
PS 39	1	-15	-	3.7	-	28	-
PS 45	1	-41	-	0.3	-	25	-

NOTES TO TABLE 2

[a]K-line too small to measure.

[b]The radial velocity determinations are not independent.

[c]Only one K-line measurement obtained.

[d]Phases at mid-observation for variables in NGC 6121:

V1	0.57	V6	0.68	V20	0.47	V23	0.40
V30	0.65	V37	0.55	V42	0.46	V43	0.51

[e]Adopted radial velocities for template stars.

TABLE 3. DISPERSIONS OF COMPARISON SPECTRA PSUEDO-VELOCITIES

Night	N All Arcs	Nightly σ (km/sec)			N Close Pairs
		All Arcs	Consec Pairs	Close Pairs	
Sept. 3/4, 1981	23	8	8	6	10
Sept. 4/5, 1981	27	11	10	6	11
Sept. 5/6, 1981	28	13	8	4	15
Sept. 6/7, 1981	34	14	6	3	21
Sept. 7/8, 1981	32	9	5	4	15
Sept. 10/11, 1981	38	7	4	3	24

TABLE 4. INTERSTELLAR K LINES

Star	W(K) (Å)	Vel (km/sec)	Star	W(K) (Å)	Vel (km/sec)
CS 22172- 7	0.42	27	CS 22942- 37	0.25	-34
CS 22172- 9	0.62	-1	CS 22946- 1	0.19	2
CS 22172- 17	0.46	2	CS 22946- 20	0.12	15
CS 22875- 15	0.15	-7	CS 22949- 12	0.38	-35
CS 22875- 24	0.13	-4	CS 22949- 13	0.22	-18
CS 22875- 31	0.24	-32	CS 22963- 19	0.30	39
CS 22881- 56	0.11	-18	CS 22963- 25	0.13	38
CS 22882- 3	0.15	-42	CS 22963- 31	0.42	10
CS 22882- 7	0.12	-4	CS 22964- 9	0.41	2
CS 22882- 32	0.18	3	CS 22964- 30	0.45	20
CS 22894- 1	0.42	-2	CS 22964- 32	0.32	15
CS 22894- 6	0.11	-11	CS 22964- 36	0.48	40
CS 22936-209	0.32	-4	CS 22964- 39	0.28	10
CS 22936-236	0.46	35	CS 22964- 45	0.48	21
CS 22936-247	0.25	10	CS 22964- 67	0.48	33
CS 22936-258	0.37	18	CS 22964-107	0.29	31
CS 22968- 22	0.22	27	CS 22936-278	0.38	21
CS 22936-285	0.44	38			

TABLE 5. WEAK METALLIC LINES

Element	Wavelength(Å)	Element	Wavelength (Å)
Fe I	4005.3	Sr II	4215.5
Ti II	4012.5	Ca I	4226.7
Fe I	4045.8	Fe II	4233.2
Fe I	4063.6	Fe I	4271.8
Sr II	4077.7	Ti II	4290.2

TABLE 6. COMPARISON WITH RODGERS

CS22+ #	PS#	$W(K)_R$	$W(K)_P$	$H_{\delta R}$	$H_{\delta P}$	Vel_R	Vel_P
		<---------- Angstroms ---------->				<-- km/sec -->	
882- 7	1	<0.4	0.5	25.6	27	-64	-115
882- 14	13	<0.4	0.5	25.8	26	-	22
882- 15	10	2.02	1.5	31.0	31	105	76
882- 18	16	0.66	0.5	23.5	27	-215	-45
882- 19	17	<0.4	0.5	23.8	23	-35	-50
882- 20	20	2.5	1.5	28.0	26	45	15
882- 33	6	<0.4	0.7	28.9	28	-51	0
942- 6	30	2.50	3.1	40.8	32	25	65
942- 15	35	0.6	0.5	28.9	28	-51	-32
942- 20	37	1.0	2.9	17.0	30	-35	0
946- 1	53	<0.4	0.1	25.5	27	82	85
	3	5.15	5.5	17.1	12	-	39
	4	4.60	4.0	22.1	15	-34	-94
	7	2.60	2.4	29.2	27	-31	-23
	31	1.0	1.6	21.6	16	-61	+41
	32	1.57	1.4	34.0	34	-60	-50
	33	<0.4	0.2	12.8	19	52	68
	39	4.03	3.7	32.1	28	-33	-15
	45	<0.4	0.3	24.6	25	-2	-41

REFERENCES

Alcaino, G. 1975, Astr. Ap. Suppl., 21, 5.

Blades, J. C., and Morton, D. C. 1982, M.N.R.A.S., submitted.

Burstein, D. 1979, Ap. J., 234, 829.

Burstein, D., and Heiles, C. 1982, A. J., 87, 1165.

Cacciari, C. 1979, A. J., 84, 1542.

Carney, B. W., and Peterson, R. C. 1981, Ap. J., 251, 190.

Conti, P. S. 1970, Pub. A. S. P., 82, 781.

Da Costa, G. S., Freeman, K. C., Kalnajs, A. J., Rodgers, A. W., and Stapinski, T. E. 1977, A. J., 82, 810.

Danford, S. C., and Lea, S. M. 1981, A. J., 86, 1909.

Eggen, O. J. 1961, R. Obs. Bull., No. 27.

Gilmore, G., and Reid, N. 1982, M.N.R.A.S., in press.

Greenstein, J. L. 1968, Ap. J., 152, 431.

Greenstein, J. L., and Sargent, A. I. 1974, Ap. J. Suppl., 28, 157.

Harris, W. E., and Racine, R. 1979, Ann. Rev. Astr. Ap., 17, 241.

Hartoog, M. R., Cowley, C. R., and Cowley, A. P. 1973, Ap. J., 182, 847.

Hoffleit, D. and Jaschek, C. 1982, The Bright Star Catalogue, (4th ed.;New Haven:Yale University Observatory) (YBSC).

Hogg, R. V., and Craig, A. T. 1970, Introduction to Mathematical Statistics, (New York:Macmillan), p. 168.

Jaschek, C. 1970, in Stellar Rotation, ed. A. Slettebak, (Dordrecht:Reidel), p. 219.

Kinman, T. D. 1959, M.N.R.A.S., 119, 157.

Kodaira, K. 1975, in Problems in Stellar Atmospheres and Envelopes, ed. B. Baschek, W. H. Kegel, and G. Traving (New York:Springer-Verlag), p. 149.

Kodaira, K., Greenstein, J. L., and Oke, J. B. 1969, Ap. J., 155, 525.

Kurucz, R. L. 1979 Ap. J. Suppl., 40, 1.

Lee, S. W. 1977, Astr. Ap. Suppl., 27, 367.

Lloyd-Evans, T. 1977, M.N.R.A.S., 178, 353.

Manduca, A., and Bell, R. A. 1978, Ap. J., 225, 908.

Mould, J. R. 1982, preprint.

Munch, G., and Zirin, H. 1961, Ap. J., 133, 11.

Newell, E. B. 1970, Ap. J., 159, 443.

Newell, E. B., Rodgers, A. W., and Searle, L. 1969, Ap. J., 156, 597.

Philip, A. G. D. 1981, Newsl. Astr. Soc. N. Y., 1, No. 8, 5.

Philip, A. G. D., Cullen, M. F., and White, R. E. 1976, Dudley Obs. Rpt., No. 11.

Philip, A. G. D., and Sanduleak, N. 1968, Bol. Obs. Tonantzintla y Tacubaya, 4, No. 30, 253.

Pier, J. R. 1982, A. J., 87, in press (Chapter 1).

Preston, G. W. 1974, Ann. Rev. Astr. Ap., 12, 257.

Przybylski, A. and Kennedy, P.M. 1965, M.N.R.A.S., 129, 63.

Rodgers, A. W. 1971, Ap. J., 165, 581 (AWR).

Rodgers, A. W., Harding, P., and Sadler, E. 1981, Ap. J., 244, 912 (RHS).

Sandage, A. 1970, Ap. J., 162, 841.

Sargent, W. L. W. 1965, Ap. J., 142, 787.

--------1968, Ap. J., 152, 885.

Sawyer-Hogg, H. 1973, Publ. David Dunlap Obs., 3, No. 6.

Schneider, D. P. and Young, P. 1980, Ap. J., 238, 946.

Searle, L. and Rodgers, A. W. 1966, Ap. J., 143, 809.

Shectman, S. A. 1981, in Annual Report of the Director, the Mount Wilson and Las Campanas Observatories (Washington:Carnegie Institution of Washington), p. 586.

Slettebak, A., Wright, R. R. and Graham, J. A. 1968, A. J., 73, 152.

Stetson, P. B. 1981, A. J., 86, 1337.

Tobin, W., and Kilkenny, D. 1981, M.N.R.A.S., 194, 937.

Tonry, J. and Davis, M. 1979, A. J., 84, 1511.

van der Kruit, P. C., and Searle, L. 1981, Astr. Ap., 95, 105.

--------1981b, Astr. Ap., 95, 116.

Webbink, R. F. 1981, Ap. J. Suppl., 45, 259.

Wheeler, J. C. 1979, Ap. J., 234, 569.

Wolff, S. C. 1967, Ap. J. Suppl., 15, 21.

Woolley, R., Alexander, J. B., Mather, L. and Epps, E. 1961, R. Obs. Bull., No. 43.

Young, P., Sargent, W. L. W., and Boksenberg, A. 1982, Ap. J. Suppl., 48, 455.

FIGURE CAPTIONS

Fig. 1. - An illustration of the cross-correlation procedure. 1(a) shows the reduced spectrum of the object CS22882-7 whose radial velocity is determined by cross-correlating with the template, ROB#70 in NGC 6397, a spectrum of which is shown in 1(b). The results of flattening the continuua by fitting cubic splines is shown for the object and template in 1(c) and (d) respectively. The normalized cross-correlation function is plotted in 1(e) where one bin along the abscissa corresponds to 37 km s^{-1} or one-half of a resolution element. The central peak dominates and the several other smaller peaks result from the beating of the Balmer lines against each other. An enlarged view of the central peak is shown in 1(f).

Fig. 2. - The spectral region surrounding the Ca II K line of CS22172-7, a star with a heliocentric velocity of -190 km s^{-1}. A double Gaussian function (smooth curve) is fitted in least-squares to the data. The small absorption line near λ 3934 Å is of interstellar origin.

Fig. 3. - The equivalent widths (in Ångstroms) of interstellar K line components of high velocity stars shown against the stars' distances from the plane of the Galaxy. Absorption is seen to take place primarily within the disk.

Fig. 4. - The metallic line index calculation illustrated for three

stars of similar temperatures located in clusters of increasing metallicity. The top ten lines in each panel show the individual spectral regions that comprise the index. The dashed-dotted line shows the sum of ten line-free regions, the dashed line shows the sum of ten regions chosen at random from regions adjacent to the metallic lines. The final, continuous, line is the sum of the ten metallic lines. The three summed curves have been divided by $10^{1/2}$.

Fig. 5 - The metallic line index for the sample stars plotted against the significance of the measurement. The significance is a measure of the number of standard deviations by which the line index exceeds the mean index of the randomly selected regions.

Fig. 6 - The relation between the equivalent width (Å) of the Ca II K line and the metallic line index computed from synthetic spectra.

Fig. 7 - Same as Fig. 6 only for the sample stars. Points plotted with open circles are those of stars with unusually large K line widths for their respective metallic indices. Open squares show stars with rather larger metallic line indices. Their spectra show them to be metallic line stars.

Fig. 8 - The equivalent width measurements of the Ca II K line as determined by Rodgers (1971) (along the ordinate) and the present work (abscissa). A line of unit slope and zero intercept is also shown.

Fig. 9 - K line equivalent widths for synthetic spectra. Those spectra constructed from models with metallicity parameter [A/H] = -0.5 (of varying temperatures and gravities) have K line widths which fall in the upper region between the two continuous lines. Those with [A/H] = -1.0 fall between the two dashed lines and those with [A/H] = -2.0

between the two lower continuous lines. K line widths of normal main-sequence stars fall along the upper continuous line.

Fig. 10 - Same as Fig. 9 for the sample AB stars. Those points plotted with open circles show K line strengths similar to those for normal main-sequence stars.

Fig. 11 - The H_δ Balmer line of NGC 6397-70 is shown along with the fit to an asymptotic Stark profile of $(\Delta\lambda)^{-5/2}$.

Fig. 12 - The widths of the H_δ line at 20% below the pseudo-continuum (determined by fitting asymptotic Stark profiles) plotted against B-V colors of the model atmospheres computed by Kurucz (1979). The effective temperatures range from 6500° to 12000° and gravities from log g = 2.0 to 4.5.

Fig. 13 - Same as Fig. 12 but for the sample AB stars. Open squares show results for those stars with narrow Balmer lines, including high-luminosity stars and one with a probable photometric error. Open circles show stars with Balmer line profiles typical of main-sequence gravities.

Fig. 14 - The UBV two-color diagram for model atmosphere colors given by Kurucz (1979). The combined effects in the UBV plane of decreased metallicity and decreased surface gravity are illustrated by the two series of connected points.

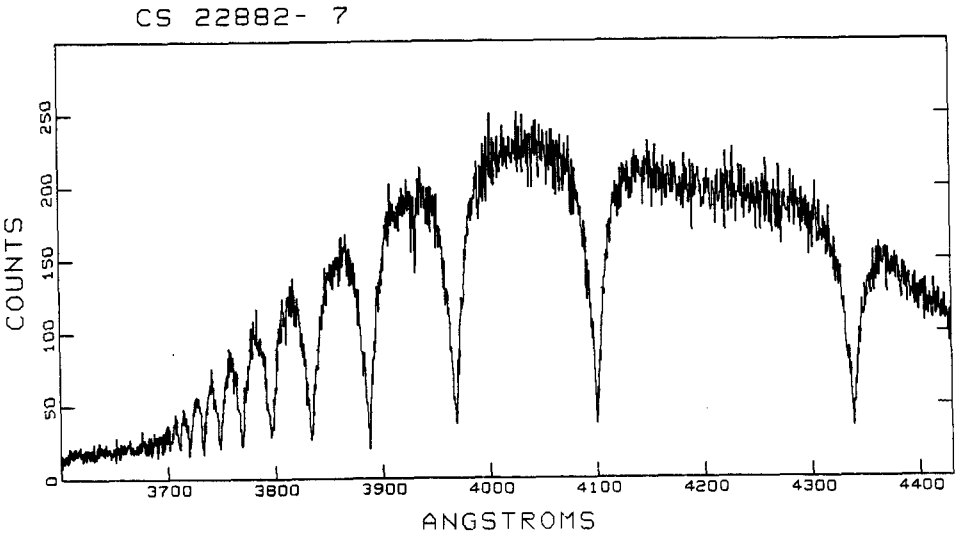

(a)

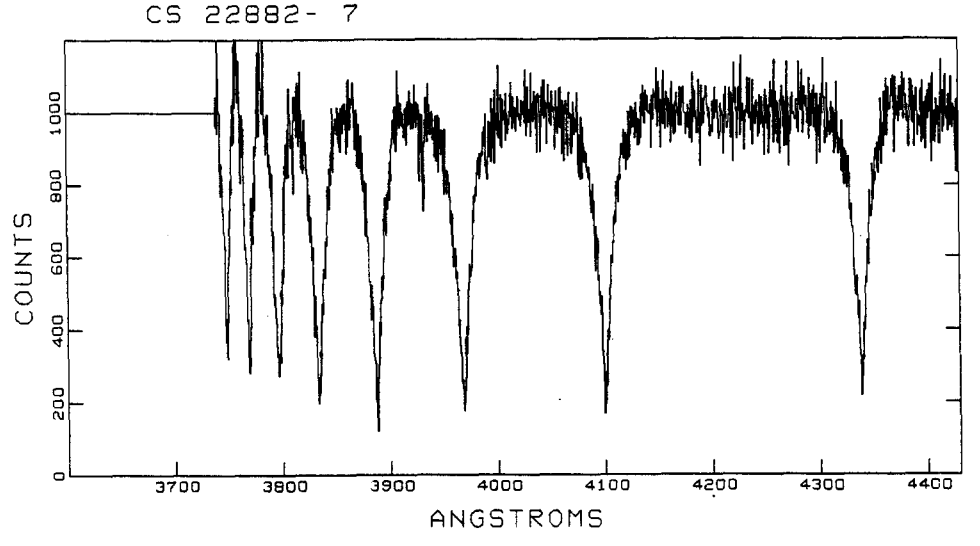

(c)

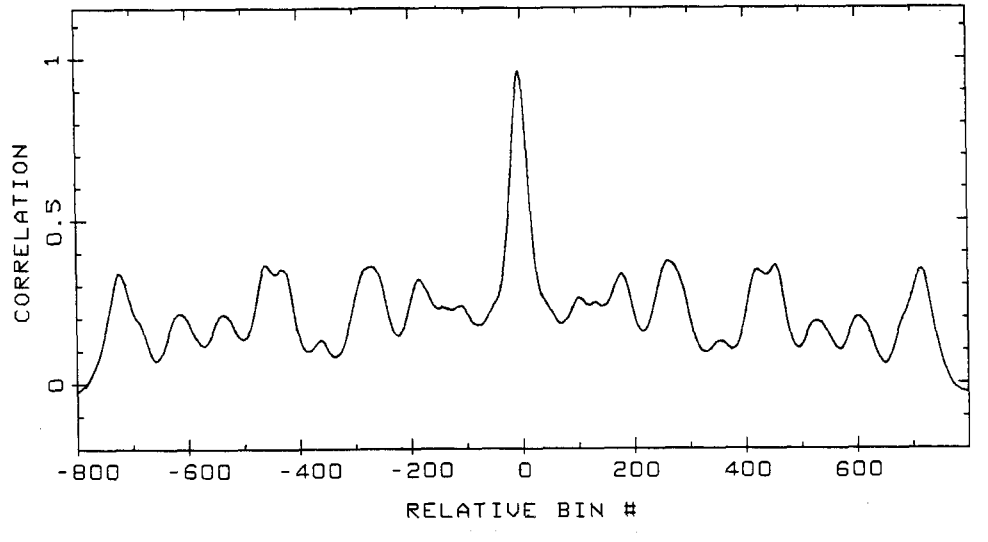

(e)

Figure 1(a,c,e)

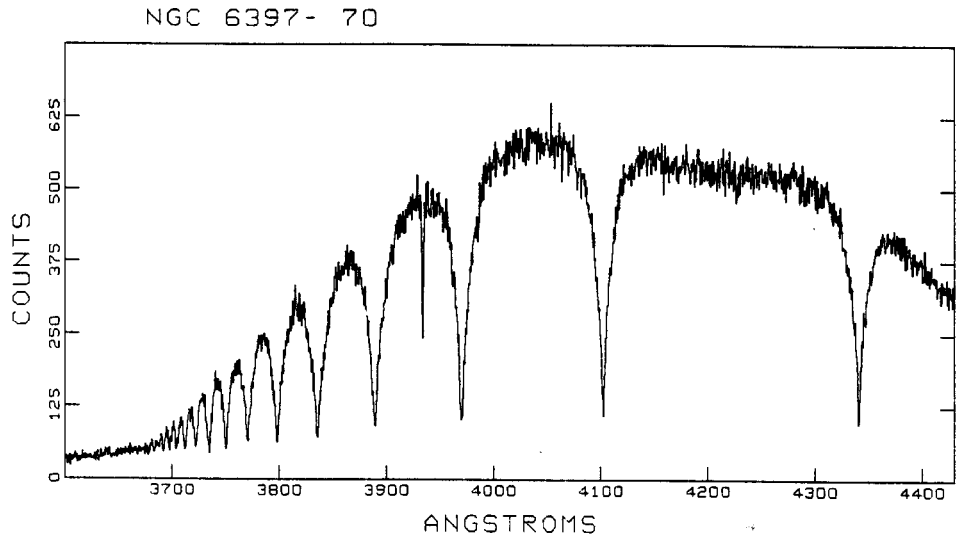

(b)

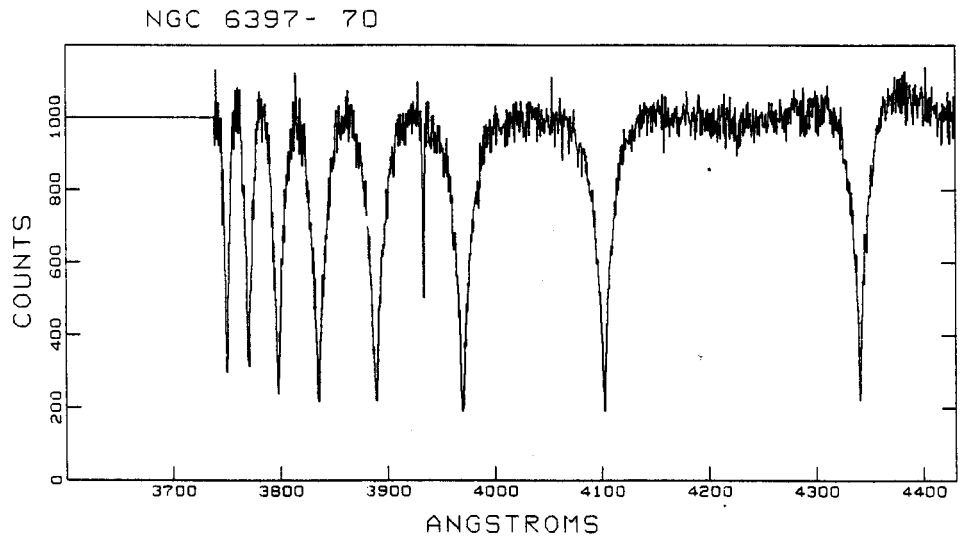

(d)

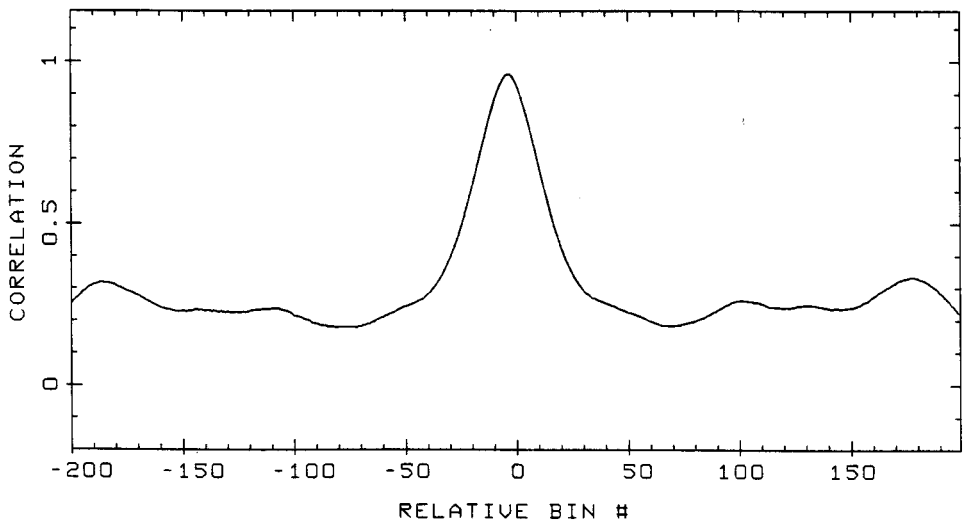

(f)

Figure 1(b,d,f)

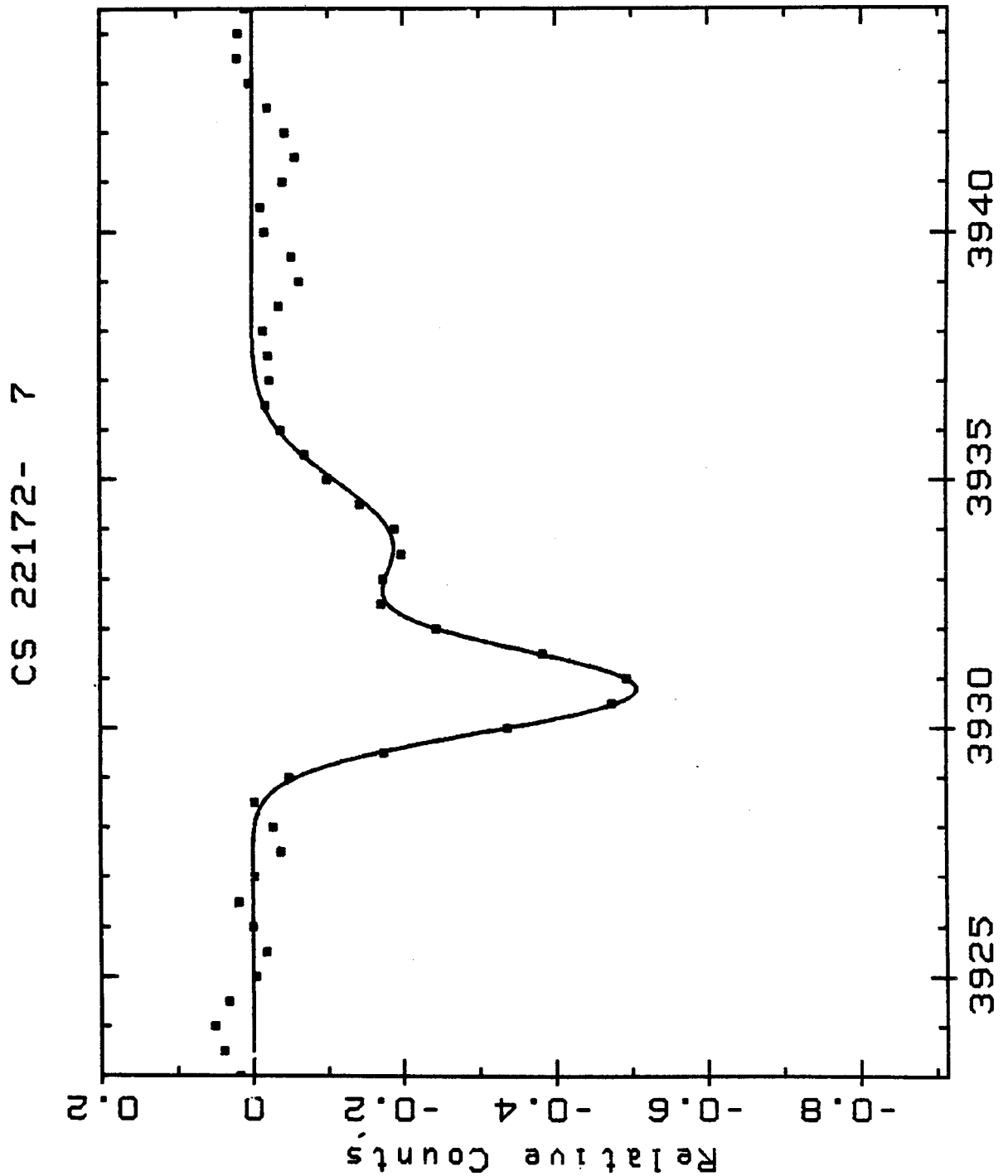
CS 22172- 7
Relative Counts
0.2
0
-0.2
-0.4
-0.6
-0.8
3925
3930
3935
3940
Wavelength (A)

Figure 2

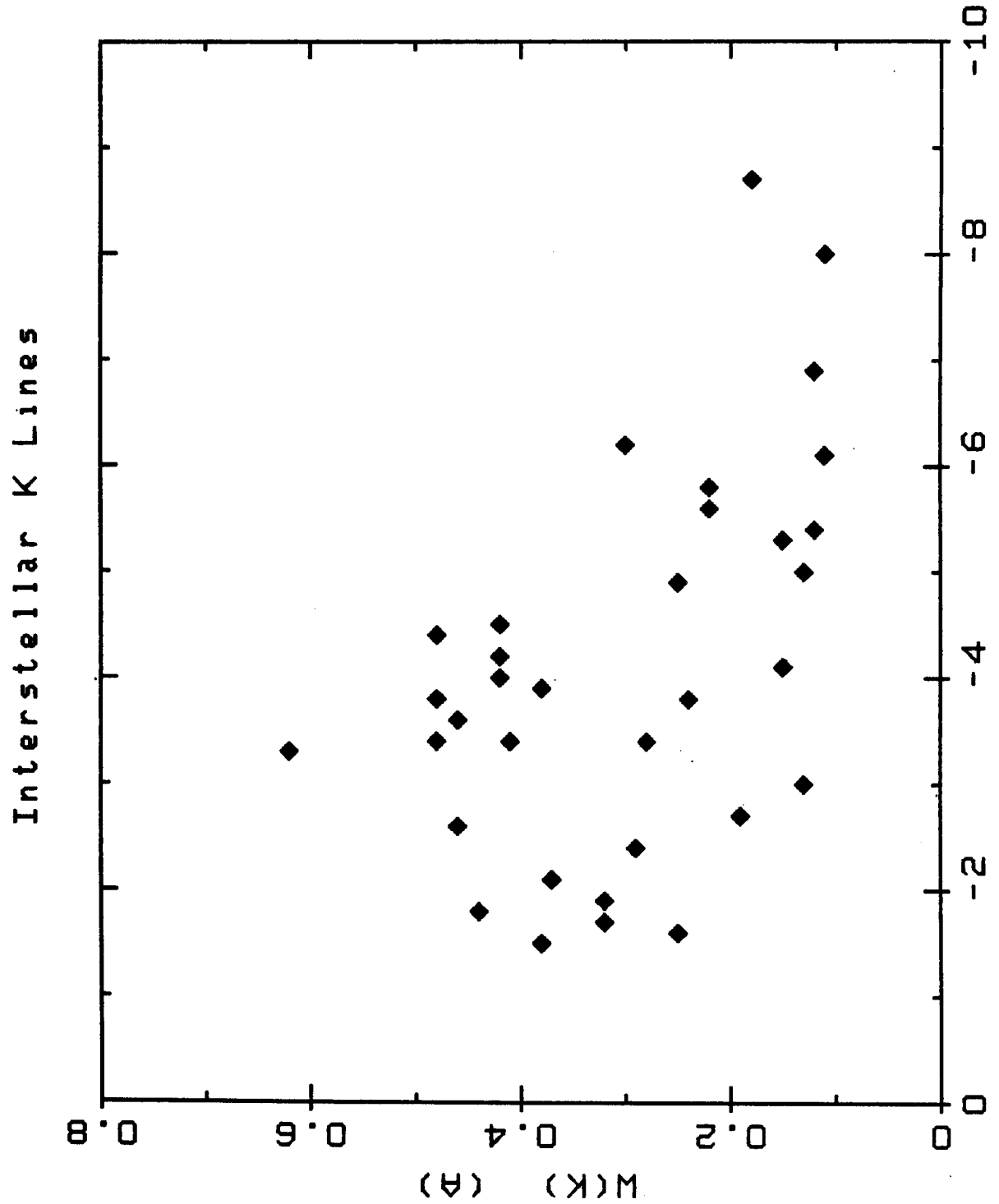

Figure 3

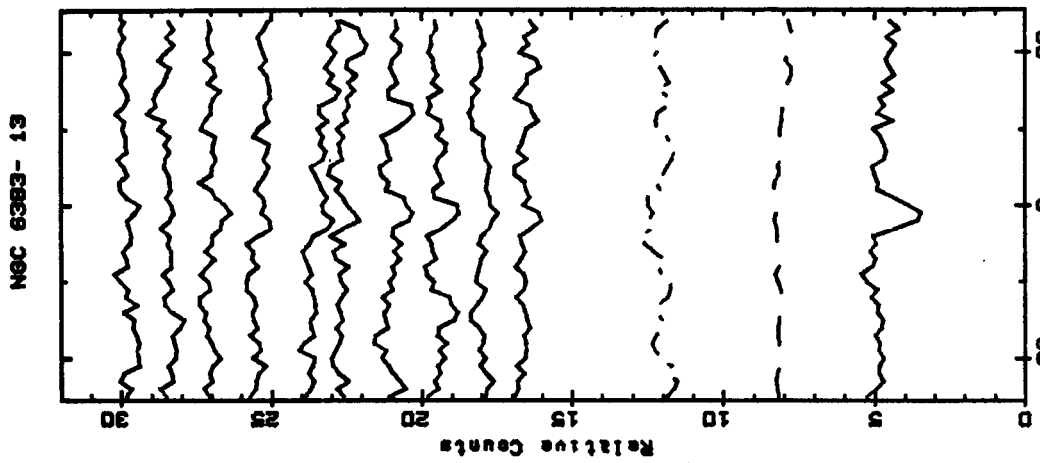

Figure 4c

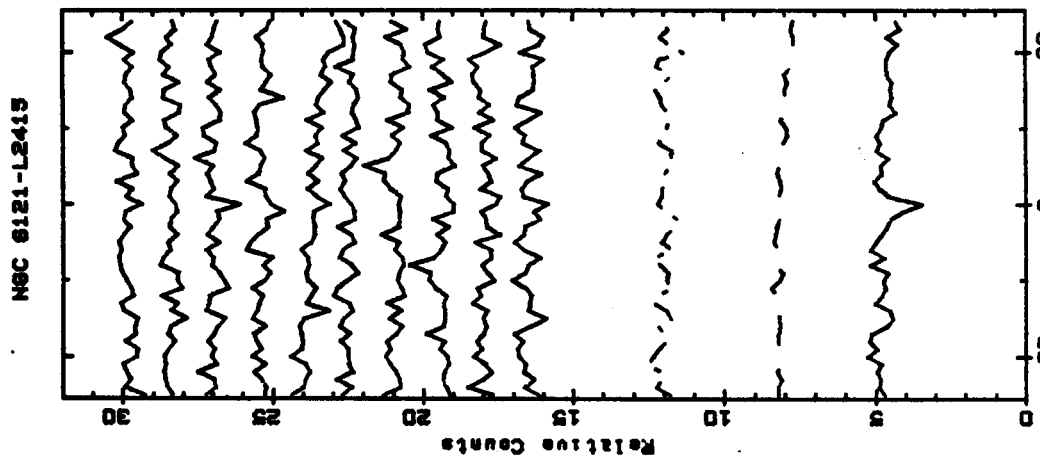

Figure 4b

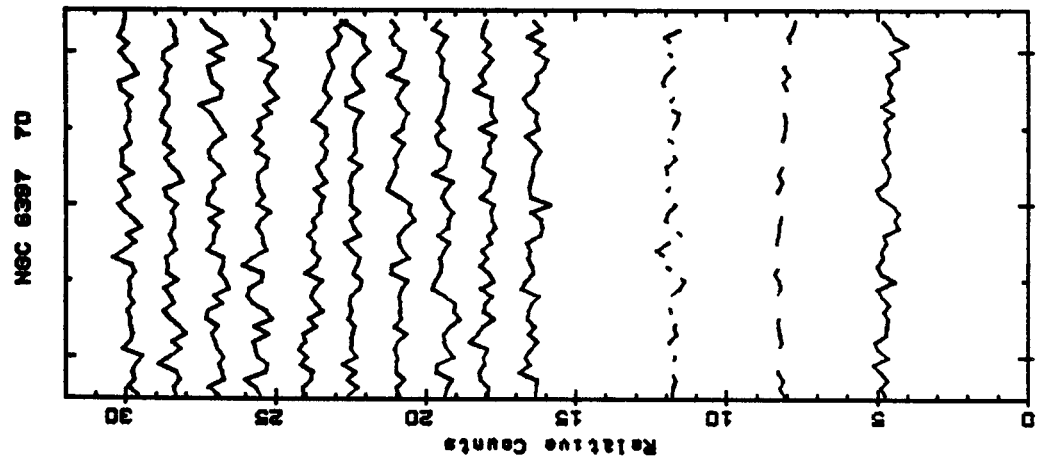

Figure 4a

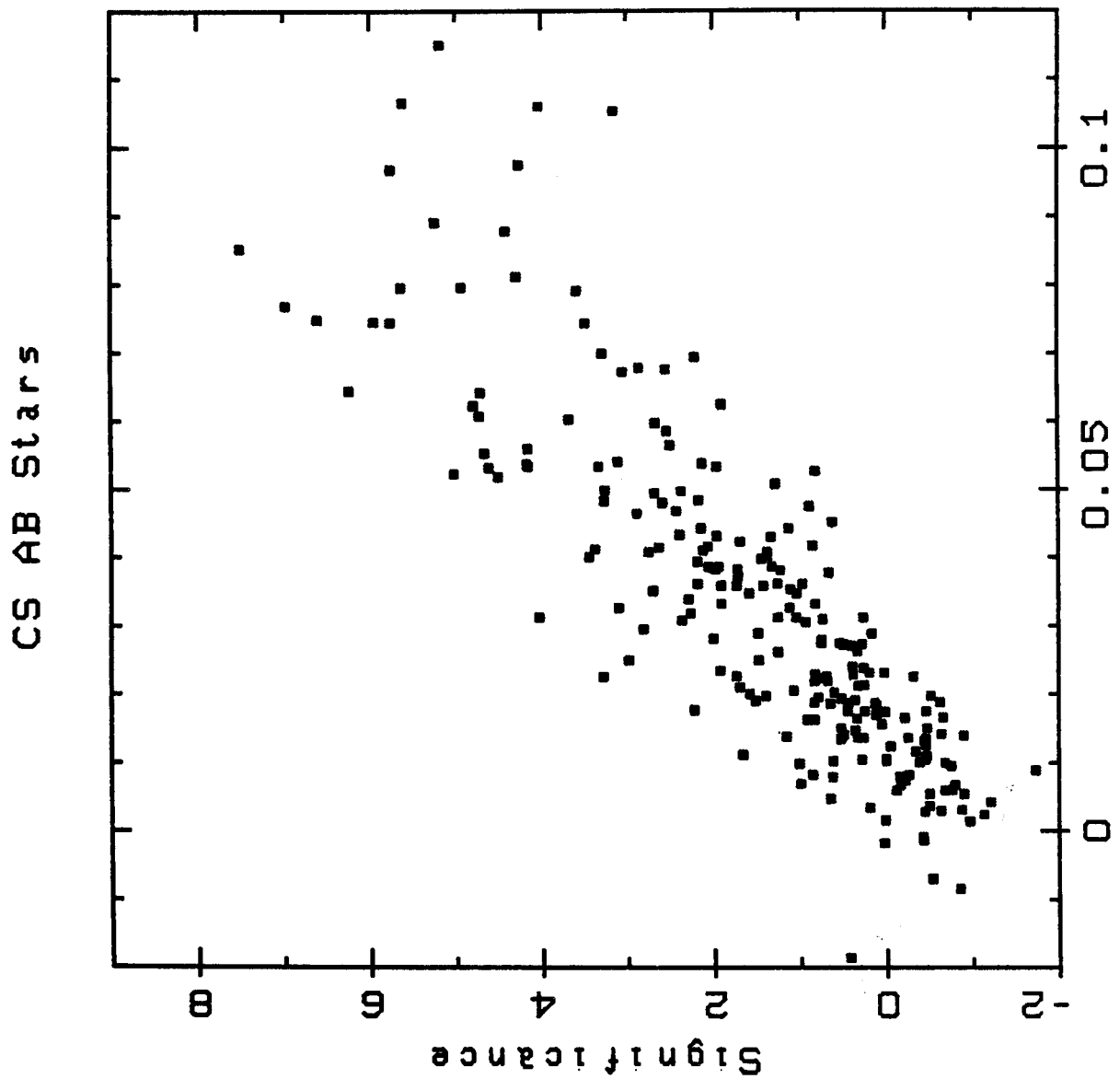
CS AB Stars
Signi ficance
8
6
4
2
0
-2
0
0.05
0.1
Metallic Line Index

Figure 5

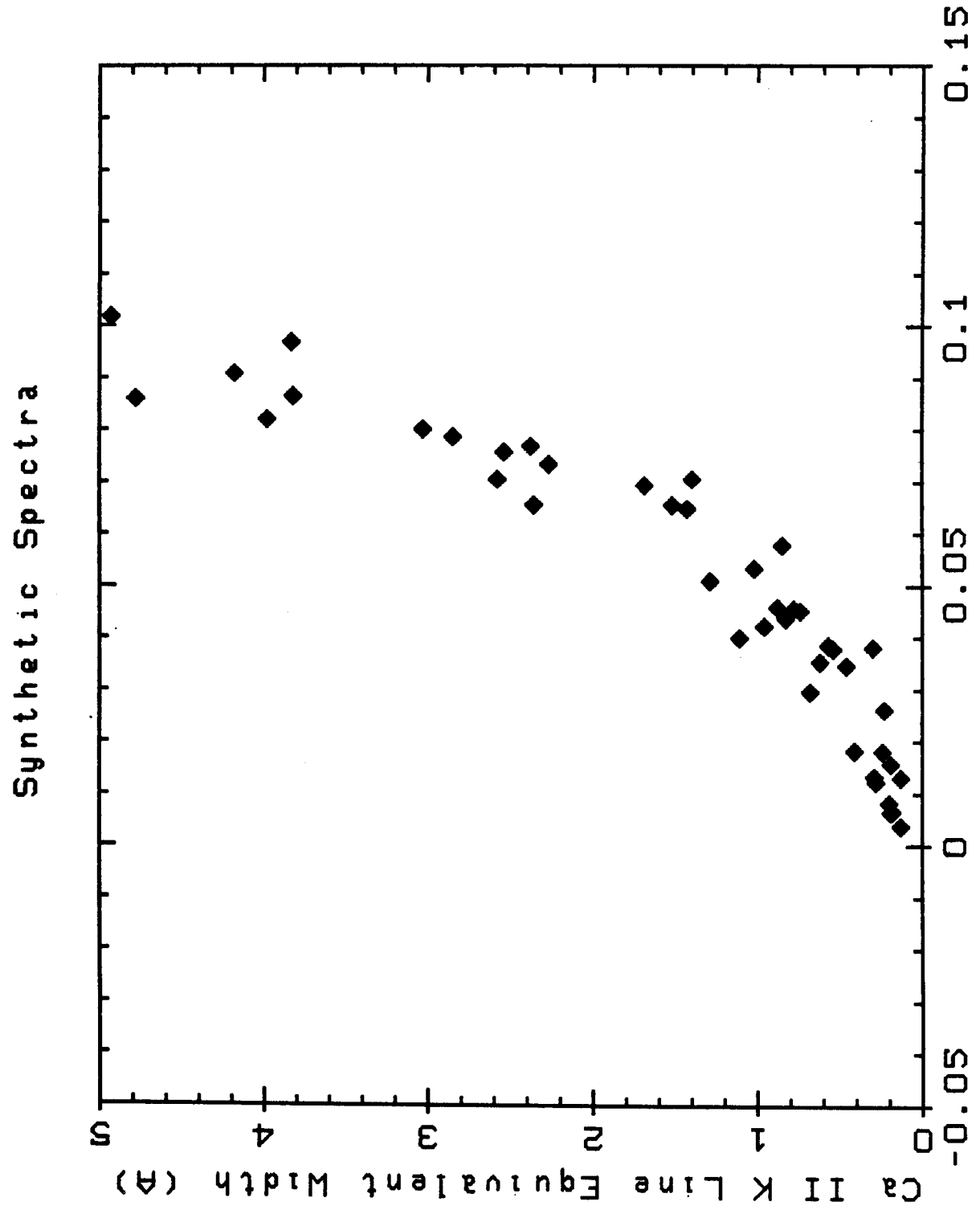
Synthetic Spectra
Ca II K Line Equivalent Width (A)
0
1
2
3
4
5
-0.05
0
0.05
0.1
0.15
Metallic Line Index

Figure 6

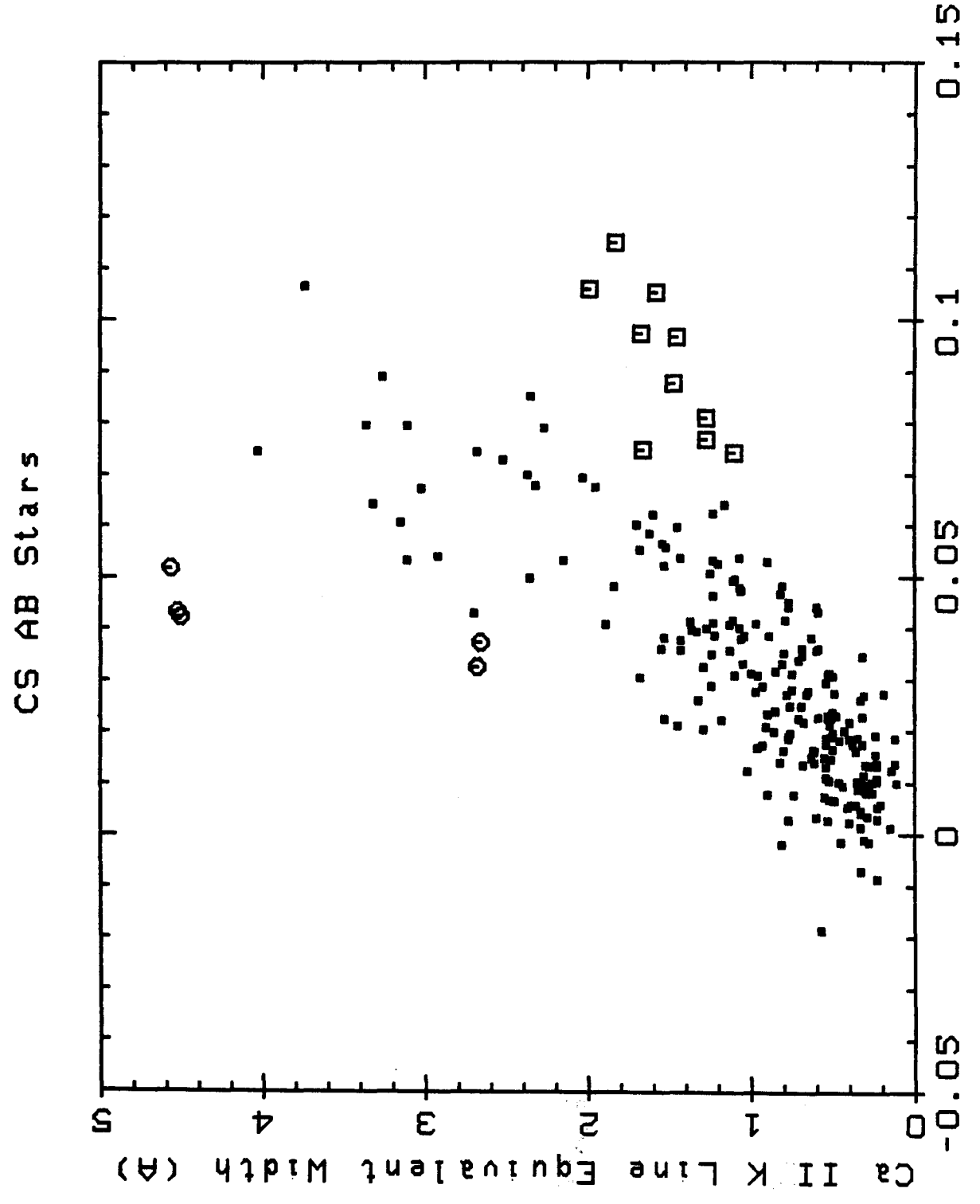
CS AB Stars
Ca II K Line Equivalent Width (A)
Metallic Line Index
0
1
2
3
4
5
-0.05
0
0.05
0.1
0.15

Figure 7

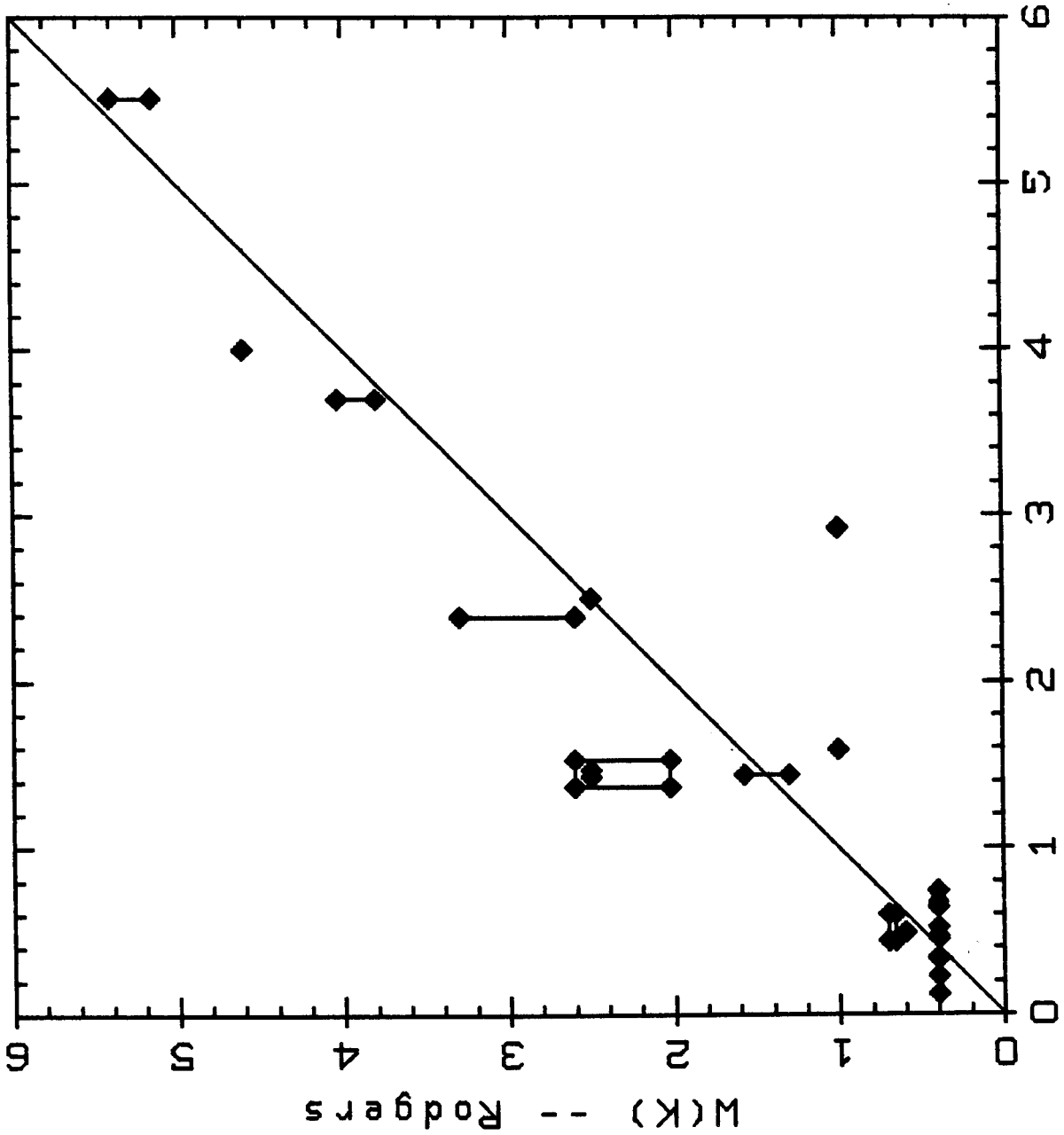

Figure 8

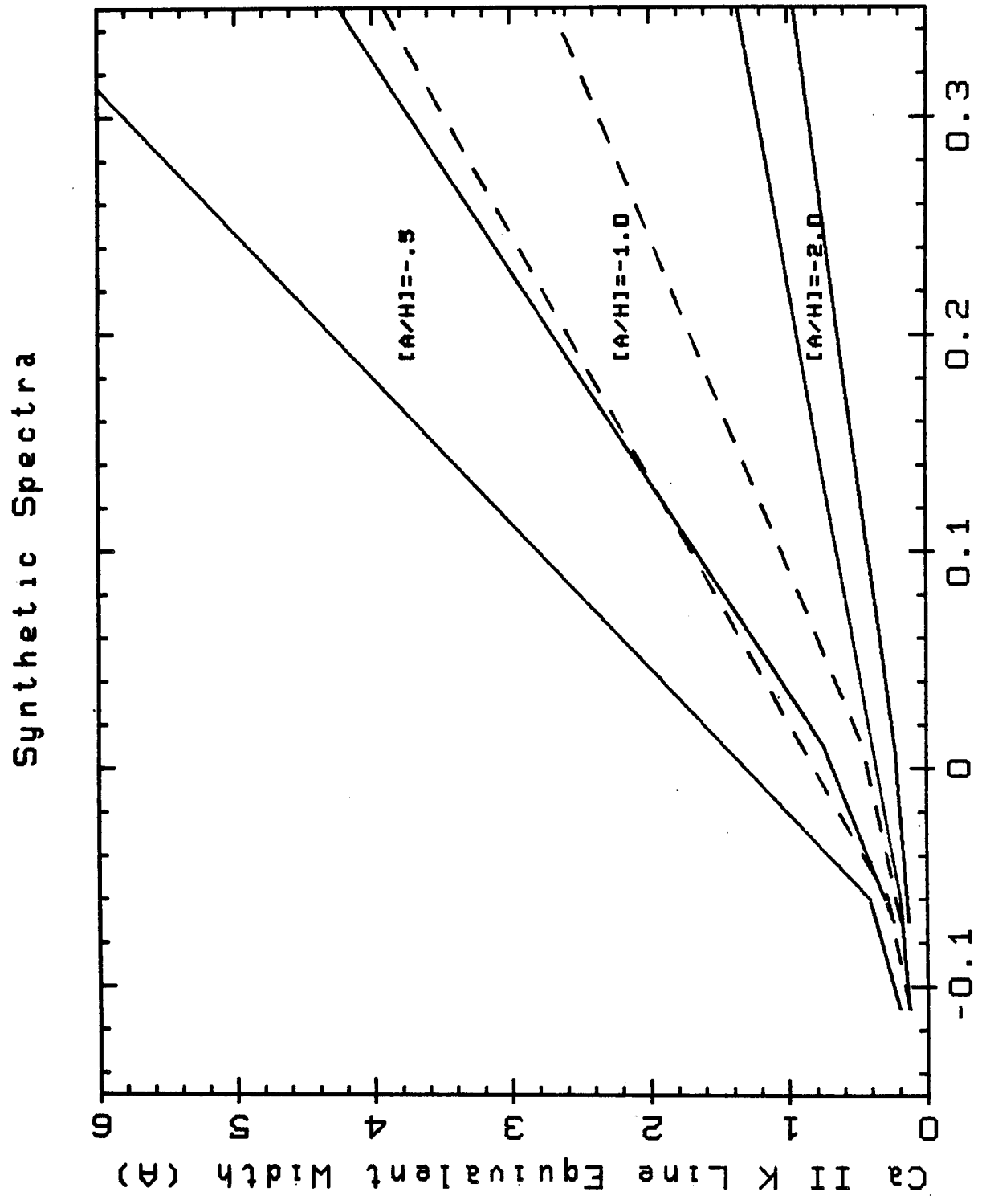
Synthetic Spectra
Ca II K Line Equivalent Width (A)
B-V
[A/H]=-.5
[A/H]=-1.0
[A/H]=-2.0
0
1
2
3
4
5
6
-0.1
0
0.1
0.2
0.3

Figure 9

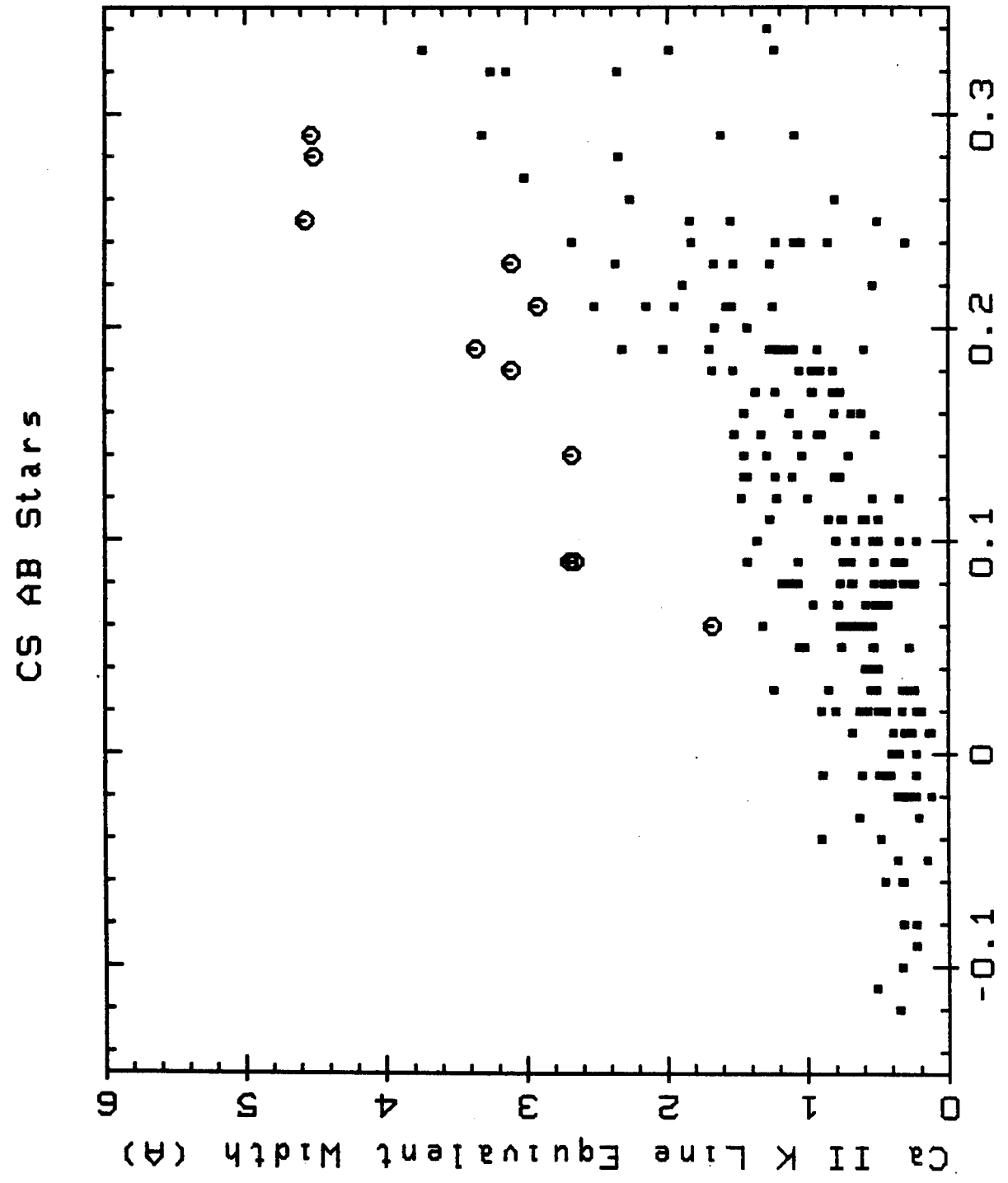
CS AB Stars
Ca II K Line Equivalent Width (A)
B-V
0
1
2
3
4
5
6
-0.1
0
0.1
0.2
0.3

Figure 10

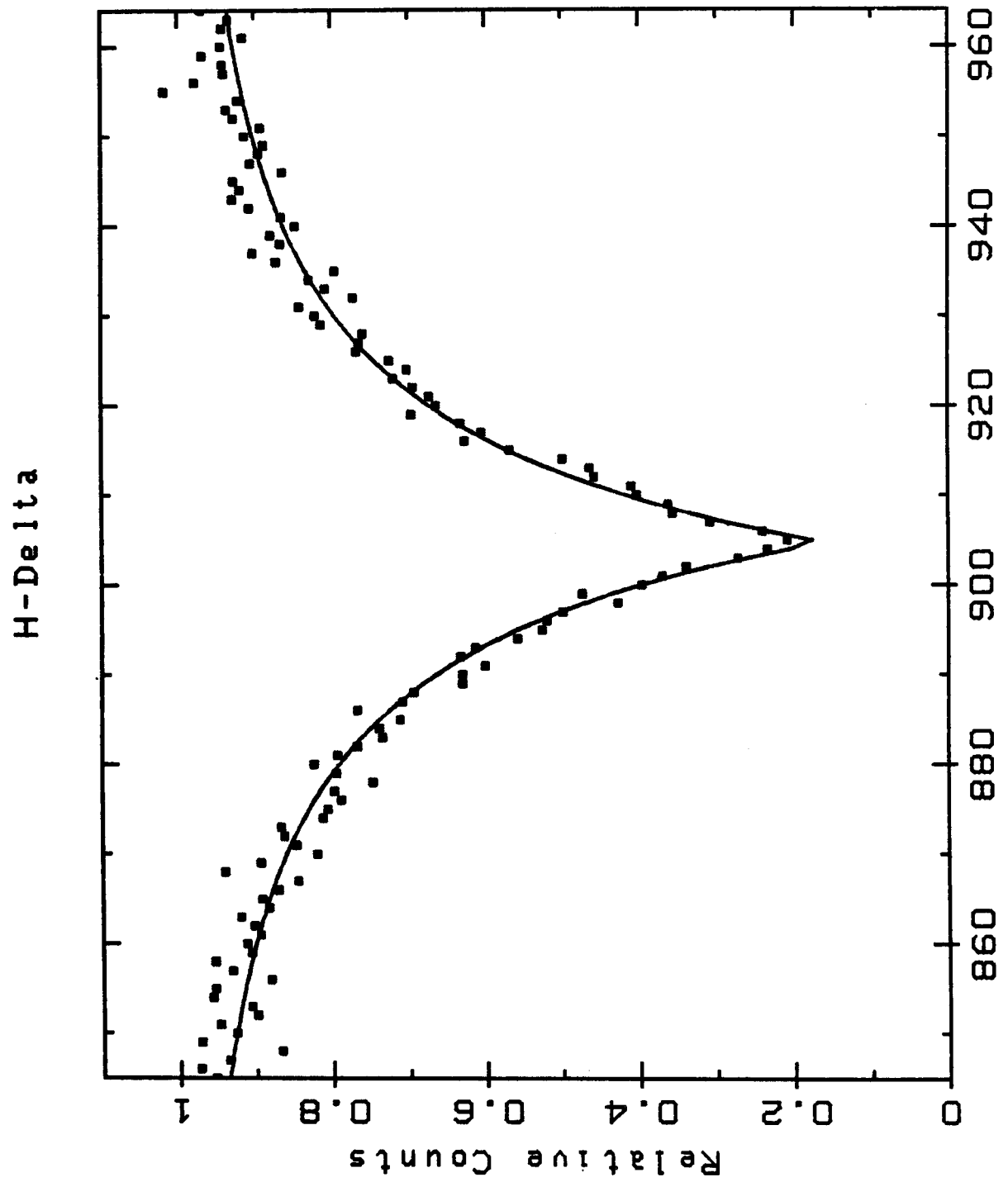
H-Delta
Relative Counts
0
0.2
0.4
0.6
0.8
1
860
880
900
920
940
960
Bin Number

Figure 11

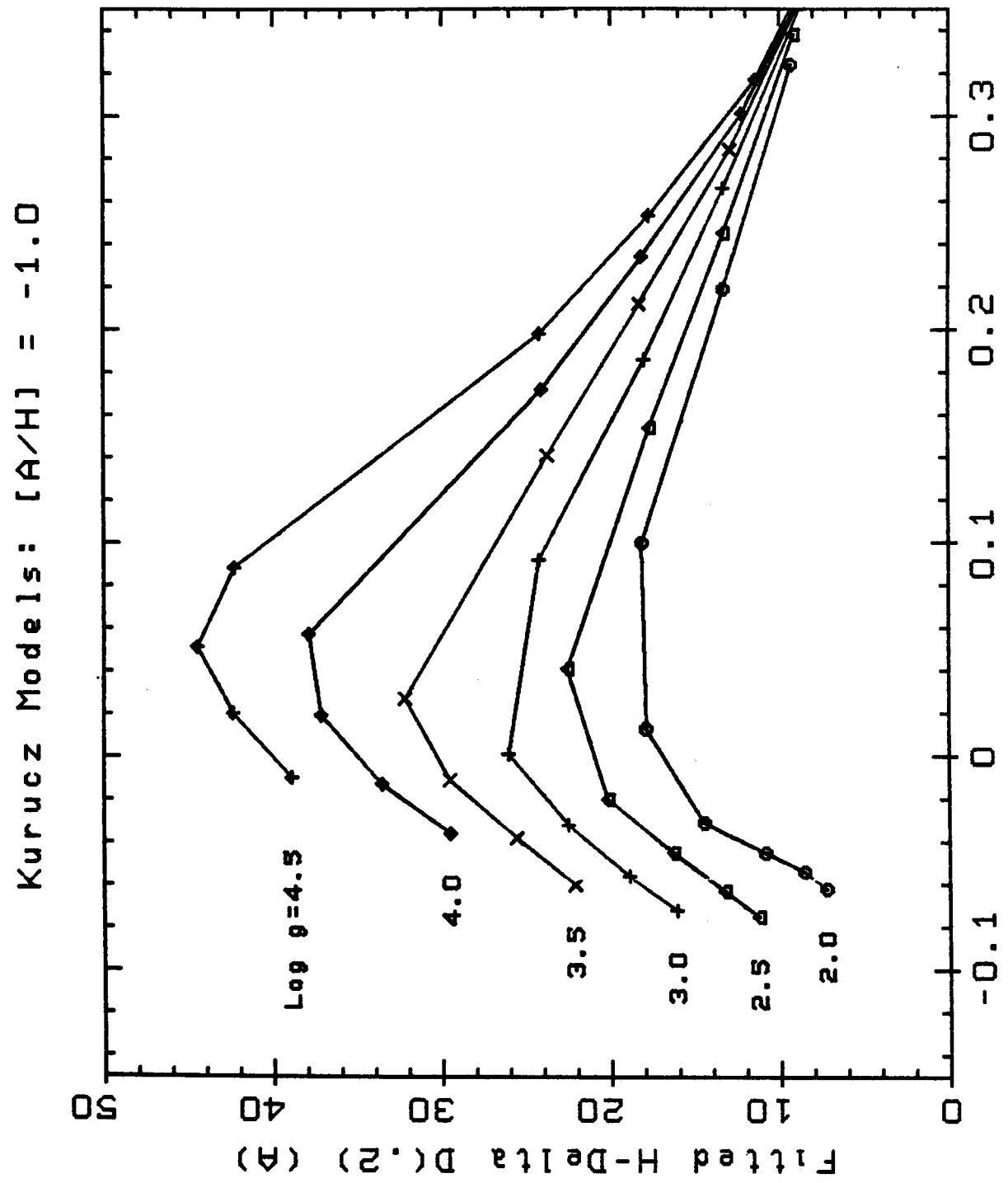
Kurucz Models: [A/H] = -1.0
Fitted H-Delta D(.2) (A)
B-V
Log g=4.5
4.0
3.5
3.0
2.5
2.0
0
10
20
30
40
50
-0.1
0
0.1
0.2
0.3

Figure 12

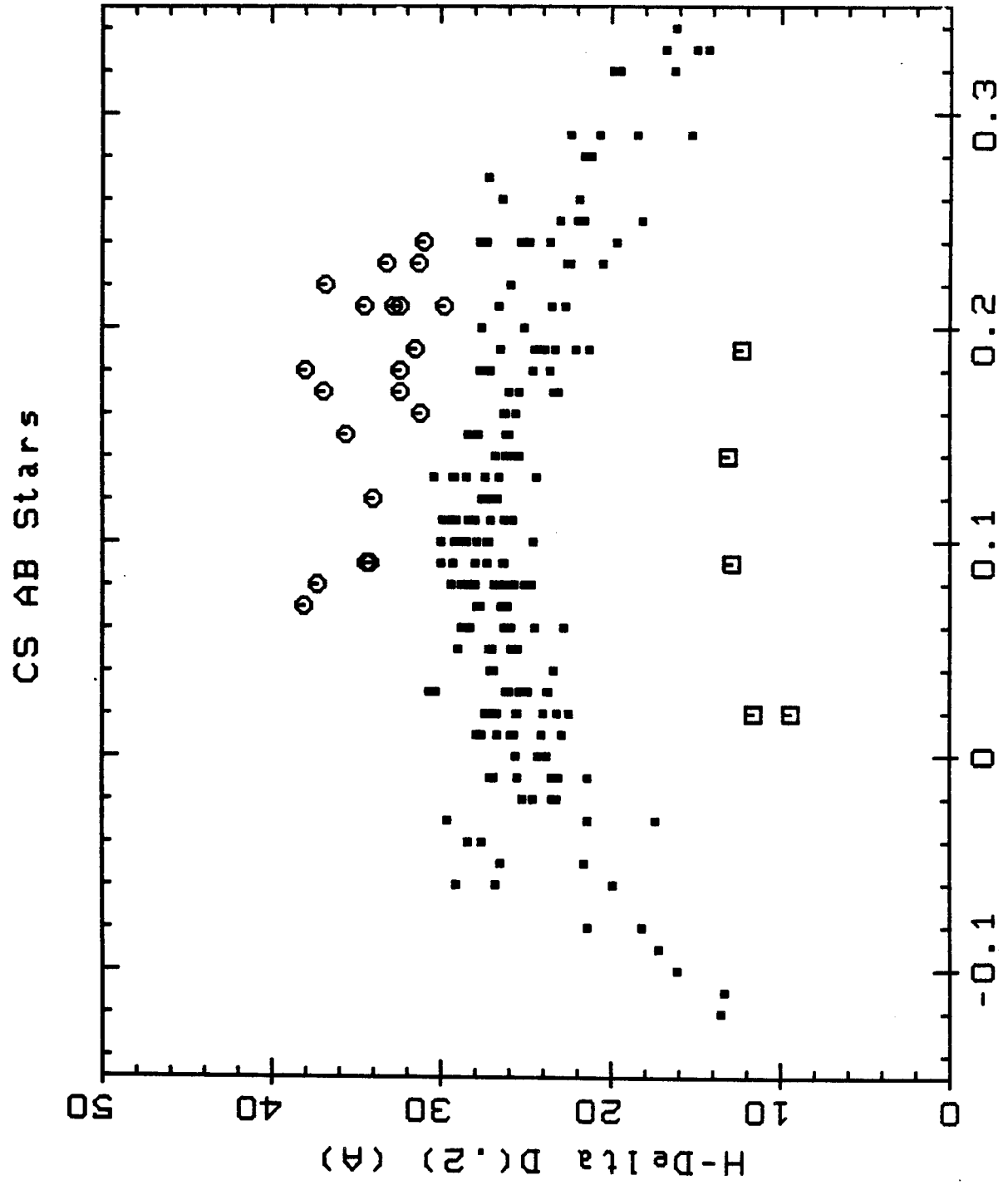

Figure 13

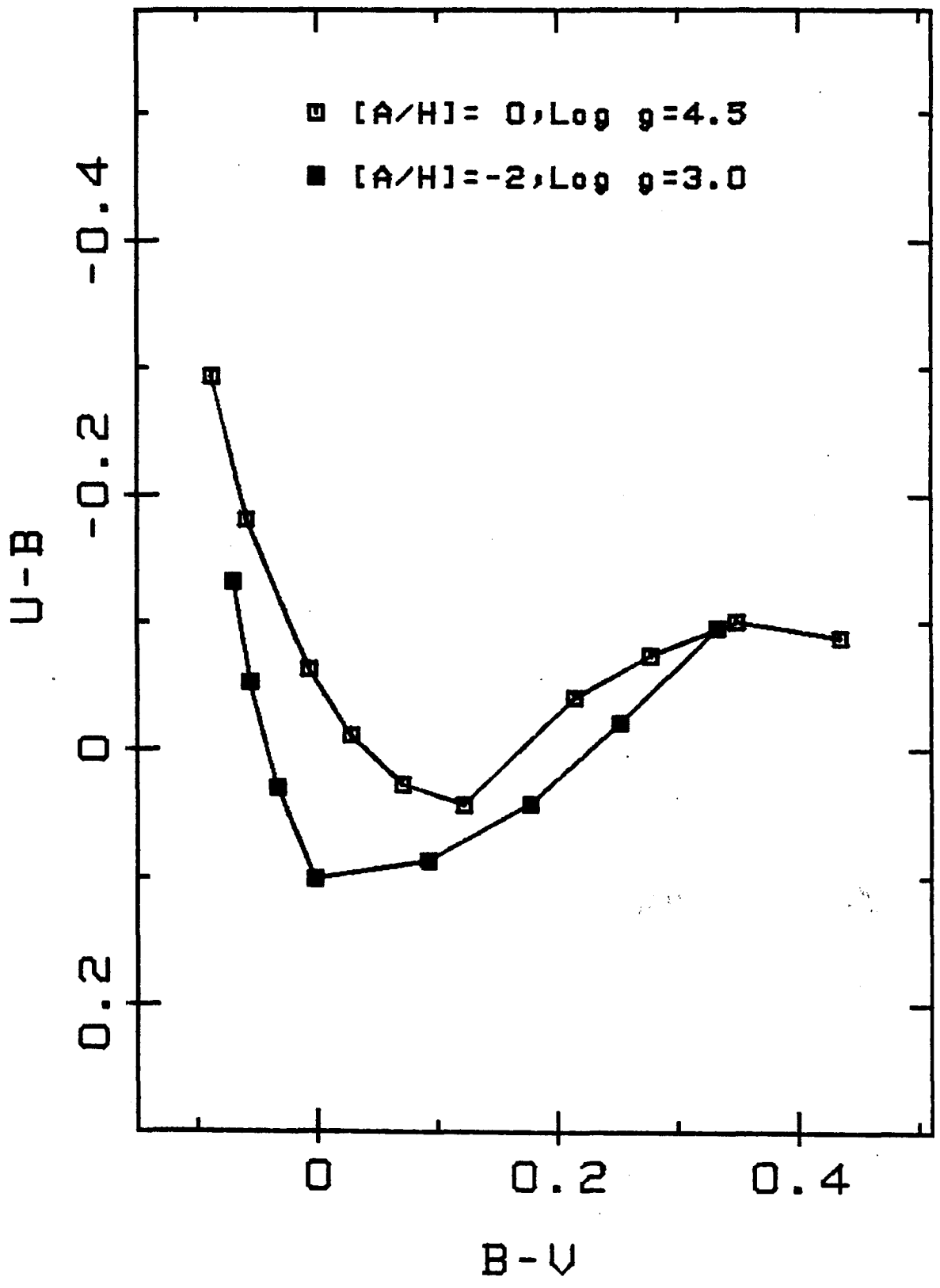

Figure 14

Chapter 3

THE KINEMATICS OF HALO AB STARS

I. INTRODUCTION

Studies of the kinematics of halo objects within the Galaxy include results for globular clusters, subdwarfs and RR Lyrae stars. Kinman (1959) found a solar motion of 167 km s^{-1} with respect to the globular cluster system. Adopting a rotational velocity of the Local Standard of Rest (LSR) of 220 km s^{-1} (Gunn, Knapp and Tremaine 1979), it then follows that the globular cluster system is itself rotating, albeit with a much more modest velocity. More recently, Frenk and White (1980) solved directly for the systematic rotation of the globular cluster system and found a value of 60 km s^{-1} (again assuming 220 km s^{-1} for the circular velocity) which was found to be independent of the metallicities and positions of the clusters. They furthermore deduced that the observed globular cluster velocities are isotropic and that the rotation curve for the Galaxy either remains flat or increases slightly with radius to the limit of their sample (33 kpc). Hartwick and Sargent (1978) found the velocity dispersion of the globular cluster system to remain constant out to a radius of 60 kpc.

Lynden-Bell and Frenk (1981) also find no evidence for anistropy in the globular cluster velocities but do find the Galaxy's rotational velocity at the sun as deduced from radial velocities of globular clusters to be dependent upon metallicity in the sense that use of a metal-poor-cluster sample produces a higher rotational velocity. The

metal-poor and metal-rich globular cluster samples have different mean galactocentric radii however, and so this result could be complicated by a radial gradient in the rotation.

Studies of subdwarfs are restricted to the solar neighborhood due to their low luminosities. In addition, they are often discovered by kinematic-dependent means (especially from high proper motion surveys). Nonetheless there is no apparent reason to doubt that they fairly represent the general field subdwarf population. A recent result from a carefully chosen subsample of the extreme subdwarfs (Carney 1979) yields a value for the solar motion very similar to that found by Kinman and by Frenk and White for the globular clusters (and thus implies a residual halo rotation). The subdwarfs, on the other hand, show considerable anistropy in the distribution of their velocities.

Woolley and Savage (1971) found the solar motion relative to a group of field RR Lyrae stars within ~ 3 kpc of the sun to be 225 km s^{-1} (from which it follows that these stars have negligible rotation). Woolley (1978) then solved for the velocity ellipsoid of the same group of stars and discovered that they had significant anisotropy in the sense that the mean squared velocities decrease from the radial direction to the azimuthal to the third mutually orthogonal direction roughly as 3:2:1.

This chapter presents a kinematic analysis of the halo Curtis Schmidt (CS) AB stars and a comparison of the results with those found for other halo objects. Section II discusses the solar motion solution and §III the velocity ellipsoid determination. Similar computations have been made for other constituents of the halo and the relationships

among the results are discussed in §IV. The implications of observed variations of the velocity dispersions of AB stars is addressed in §V while §VI discusses the anisotropy in the velocity ellipsoid. A summary of the conclusions appears in §VII.

II. SOLAR MOTION

From the observed heliocentric radial velocities the average motion of the AB stars relative to the sun has been determined. Following Woolley and Savage (1971) the observed heliocentric radial velocity ρ can be related to rectangular velocity components centered at the sun of $u = -\dot{x}$ towards the galactic center (galactic longitude $l = 0$, galactic latitude $b = 0$), $v = \dot{y}$ in the plane of the galaxy towards the direction of the circular motion of the (LSR) ($l = 90$, $b = 0$) and $w = \dot{z}$ towards the north galactic pole ($b = +90$) via:

$$\rho = (\underset{\sim}{V}_* - \underset{\sim}{V}_0) \cdot \underset{\sim}{g} + K \tag{1}$$

$$\text{where } \underset{\sim}{V}_* = \begin{vmatrix} u \\ v \\ w \end{vmatrix}, \text{ and } \underset{\sim}{V}_0 = \begin{vmatrix} u_0 \\ v_0 \\ w_0 \end{vmatrix} \tag{2}$$

and in which u_0, v_0, and w_0 represent the sun's peculiar motion

relative to the LSR. The values adopted here and used throughout this chapter are $u_0 = 9$, $v_0 = 12$ and $w_0 = 7$ km s^{-1} (Mihalas and Binney, 1981, p. 400). The K term allows for either systematic errors or expansion of the system, and the direction cosines are:

$$\underset{\sim}{g} = \begin{vmatrix} \cos(l)\cos(b) \\ \sin(l)\cos(b) \\ \sin(b) \end{vmatrix} . \qquad (3)$$

In order to provide a sample of homogeneous halo objects the CS AB star list was limited to those with $B-V \leq 0.25$ (spectra were available for very few stars redder than this). In addition, those stars classified in Chapter 2 as being (1) normal main-sequence, (2) metallic-line, or (3) high-luminosity were culled from the list. The remaining subsample contains 171 stars.

For this subsample, the least squares solution to equation (1) gives 0, -235, 4, and 8 km s^{-1} for u, v, w, and K respectively. Since the u, w, and K values do not differ significantly from zero it is appropriate to set them identically equal to zero in equation (1) and redo the calculation, solving only for v. The result is $v = -236 \pm 39$ km s^{-1} with a line-of-sight velocity dispersion of 100 ± 5 km s^{-1}.

Frenk and White (1980) point out that equation (1) and its solution are based upon the assumption that the system has either no systematic rotation relative to a frame of reference at rest with respect to the center of the galaxy or else the system rotates with constant angular velocity (i.e. solid body rotation). By assuming instead a constant rotational velocity for the system one can solve directly for systematic rotation as Frenk and White did for the globular cluster system.

In order to perform a calculation of this type it is necessary to assign distances to the objects. The absolute V magnitudes were determined using two separate color-magnitude relations. One, appropriate for Population II BHB stars, was drawn from Sandage (1970) and Philip, Cullen and White (1976). The other, for Population I main sequence stars, was taken from Chiu (1980). The BHB relation was used for all but the few higher-gravity stars for which it is thought that the Pop I relation is more appropriate.

For the purposes of this calculation, and througout this chapter, values adopted for the solar radius and the velocity of the LSR are ϖ_0 = 8.5 kpc and Θ_0 = 220 km s^{-1} (Gunn, Knapp and Tremain 1979). Solving directly for the rotation of the AB sample gives $V_{rot} = -36 \pm 32$ km s^{-1}, a result which perhaps could have been predicted by comparing the solar motion value with the adopted Θ_0. No statistically significant evidence for a systematic expansion was found.

III. THE VELOCITY ELLIPSOID

From the radial velocities and galactic coordinates presented in the preceding chapters and distances derived from photometric parallaxes, the dispersion in velocities in spherical polar coordinates (r,θ,ϕ) relative to the center of the galaxy can be determined. Woolley (1978) presented the relevant algebra (note that in this paper the definitions of the two angular coordinates have been interchanged relative to Woolley's usage). Refer to Figure 1 to aid in visualizing the relations:

$$\begin{aligned} x &= r\ \sin(\phi)\cos(\theta) \\ y &= r\ \sin(\phi)\sin(\theta) \\ z &= r\ \cos(\phi) \end{aligned} \qquad (5a,b,c)$$

where the sun is located at $(r,\theta,\phi) = (\varpi_0,0,0)$. $\tilde{\omega}$ is the projection of r (the distance to a star from the galactic center) onto $\phi = 90^o$ (the plane of the galaxy). These two distances can be determined from l, b and h (the distance of the star from the sun) via:

$$\varpi^2 = \varpi_0^2 + h^2\cos^2(b) - 2\ \varpi_0\ h\ \cos(b)\cos(l) \qquad (6a)$$

$$r^2 = \varpi_0^2 + h^2 - 2\varpi_0\ h\ \cos(b)\cos(l)\ . \qquad (6b)$$

The angular coordinates are then found from:

$$\begin{aligned} \sin(\phi) &= \varpi/r \\ \cos(\phi) &= [h\ \sin(b)]/r \\ \sin(\theta) &= [h\ \cos(b)\sin(l)]/\varpi \\ \cos(\theta) &= [\varpi_0 - h\ \cos(b)\cos(l)]/\tilde{\omega}\ . \end{aligned} \qquad (7a,b,c,d)$$

In order to obtain the velocity components at each star's position in the radial direction ($\dot{r} \equiv R$), azimuthal in the sense of galactic rotation ($r \sin(\phi)\dot{\theta} \equiv \Theta$) and the third mutually orthogonal direction ($r\,\dot{\phi} \equiv \dot{\Phi}$) it is necessary to perform a rotation of axes. Then,

$$\rho + \underset{\sim}{V'} \cdot \underset{\sim}{g} = \underset{\sim}{Q}\ \underset{\sim}{Y} \tag{8}$$

$$\text{where} \quad \underset{\sim}{V'} = \begin{vmatrix} u_0 \\ v_0 + \Theta_0 \\ w_0 \end{vmatrix} \quad \text{and} \quad \underset{\sim}{Y} = \begin{vmatrix} R \\ \Theta \\ \dot{\Phi} \end{vmatrix} . \tag{9a,b}$$

$\Theta_0 = 220$ km s^{-1} is the adopted circular rotation velocity at ϖ_0. The rotation elements are defined by $\underset{\sim}{Q} = \underset{\sim}{H}\,\underset{\sim}{g}$ where $\underset{\sim}{H}$ (given explicitly by Woolley [1978]) is the Jacobian matrix:

$$\underset{\sim}{H} = \begin{vmatrix} -\frac{\partial \dot{x}}{\partial R} & \frac{\partial \dot{y}}{\partial R} & \frac{\partial \dot{z}}{\partial R} \\ -\frac{\partial \dot{x}}{\partial \Theta} & \frac{\partial \dot{y}}{\partial \Theta} & \frac{\partial \dot{z}}{\partial \Theta} \\ -\frac{\partial \dot{x}}{\partial \dot{\Phi}} & \frac{\partial \dot{y}}{\partial \dot{\Phi}} & \frac{\partial \dot{z}}{\partial \dot{\Phi}} \end{vmatrix} , \tag{10}$$

and $\underset{\sim}{g}$ is as defined in equation (3). The negative signs in the $\dot{x}$ terms result from adopting Woolley's convention that $u = -\dot{x}$. Specifically then, the resulting direction cosine vector is $\underset{\sim}{Q} =$

$$\begin{vmatrix} -\cos(\theta)\sin(\phi)\cos(l)\cos(b)+\sin(\theta)\sin(\phi)\sin(l)\cos(b)+\cos(\phi)\sin(b) \\ \sin(\theta)\cos(l)\cos(b)+\cos(\theta)\sin(l)\cos(b) \\ -\cos(\theta)\cos(\phi)\cos(l)\cos(b)+\sin(\theta)\cos(\phi)\sin(l)\cos(b \quad \sin(\phi)\sin(b) \end{vmatrix} . \quad (11)$$

Squaring equation (8) and neglecting terms involving cross-products (such as $Q_1 Q_3 R\Theta$ which should sum to zero if the sample is well distributed) gives

$$X \equiv (\rho + \underset{\sim}{V}' \cdot \underset{\sim}{g})^2 = \underset{\sim}{A} \cdot \underset{\sim}{V} \quad (12)$$

$$\text{where} \quad \underset{\sim}{A} = \begin{vmatrix} Q_1^2 \\ Q_2^2 \\ Q_3^2 \end{vmatrix} \quad \text{and} \quad \underset{\sim}{V} = \begin{vmatrix} R^2 \\ \Theta^2 \\ \Phi^2 \end{vmatrix} . \quad (13a,b)$$

The unweighted least squares solution to equation (12) is

$$\underset{\sim}{V} = (\underset{\sim}{A}^T \underset{\sim}{A})^{-1} \underset{\sim}{A}^T \underset{\sim}{X} . \quad (14)$$

The contribution of each observation was not weighted by the accuracy of the observations for two reasons: (1) in general the estimate of the velocity uncertainty of every star is the same; and (2) the uncertainty (11 km s^{-1} from Chapter 2) is much smaller than the widths of the velocity distributions involved (~ 100 km s^{-1}). Uncertainties

in the rotation elements come almost exclusively from the uncertainties in the distances to the stars (since the errors due to uncertainties in the coordinates of the stars are entirely negligible except for undetected typographical errors). In order to gauge the importance of errors from distance determinations, trial solutions were conducted in which distance moduli noise was applied to the observations. These errors were randomly drawn from normally distributed populations with various dispersions. The trials showed that random errors with σ_ε < 0.2 magnitudes do not noticeably affect the results. At $\sigma_\varepsilon \sim 0.3$ magnitudes results are changed by up to as much as 1/2 of one standard error as defined by equation (15) below (as determined with no added noise). Sandage and Katem (1982) found that the total width of BHB stars in the Globular Cluster M3 was 0.3 magnitudes. The combined effects of photometric errors, absorption, dispersion in the color-magnitude relation calibration and the intrinsic dispersion in the luminosities the stars themselves is thus probably reaching the level of an 0.3 magnitude variance and should only marginally affect the results.

The standard error for the velocity ellipsoid solution can be calculated from the sum of the squares of the differences between the observed squared radial velocities and those predicted by the solution. For convenience of notation, define $\underset{\sim}{P} = (\underset{\sim}{A}^T \underset{\sim}{A})^{-1}$; then for the ith of the n (=3) elements of $\underset{\sim}{V}$ the error is (see, for example, Clifford 1973)

$$\sigma_i = \sigma[(\underset{\sim}{P})_{ii}]^{1/2} \qquad (15)$$

$$\text{where} \quad \sigma = \left[\frac{\underset{\sim}{E}^T \underset{\sim}{E}}{m-n}\right]^{1/2}, \tag{16}$$

in which $\underset{\sim}{E}$ is a column vector of length m (=171) containing the differences. The correlation matrix $\underset{\sim}{C}$ can be constructed from $\underset{\sim}{P}$ via:

$$(\underset{\sim}{C})_{ij} = \frac{(\underset{\sim}{P})_{ij}}{\left[(\underset{\sim}{P})_{ii}(\underset{\sim}{P})_{jj}\right]^{1/2}} . \tag{17}$$

The values of the off-diagonal elements of $\underset{\sim}{C}$, namely $(\underset{\sim}{C})_{12}$, $(\underset{\sim}{C})_{13}$, and $(\underset{\sim}{C})_{23}$, are the correlation coefficients among the cross products of $R\Theta$, $R\Phi$, and $\Theta\Phi$ respectively. In all solutions the absolute values of these correlation coefficients were < 0.5. The solution for the subsample of AB stars (in units of 10^4 [km s^{-1}]^2) is:

$$\langle R^2 \rangle = 1.33 \pm 0.43$$

$$\langle \Theta^2 \rangle = 0.22 \pm 1.05$$

$$\langle \Phi^2 \rangle = 0.93 \pm 0.23 \ .$$

Since the large majority of the stars in this sample lie on the $l = 0 - 180^\circ$ great circle, the uncertainty in Θ^2 is very high and its mean value will not be considered further here. There is a mild ($\sim 1\ \sigma$) suggestion of anisotropy in the velocity ellipsoid with $\langle R^2 \rangle : \langle \Phi^2 \rangle :: 3:2$.

IV. COMPARISON WITH OTHER HALO CONSTITUENTS

a) The Samples

For the purpose of comparing the parameters of halo objects, data were taken from the literature on subdwarfs, RR Lyrae stars and globular clusters. The techniques described in §§II and III were employed to determine their solar motions and velocity ellipsoids.

Carney (1979) gives a list of 90 extreme subdwarfs redder than B-V = 0.38 (to prevent blue straggler contamination), brighter than V = 12 (to avoid serious reddening effects) and with normalized ultraviolet excess $\delta(U-B)_{.6} \geq 0.21$ (which limits the sample to very metal-poor objects and also excludes subgiants). From the recent list of newly identified subdwarfs (Sandage 1981) an addditional eleven subdwarfs were chosen which met the same selection criteria. Both authors listed all of the relevant data (coordinates, V, B-V, $\delta(U-B)_{.6}$, radial velocities plus proper motions and the deduced u, v, and w motions) for each subdwarf. In order to maintain the same basis of comparison, proper motion data were not utilized and the solutions were made with radial velocity information alone. Distance moduli for the subdwarfs were computed from the relation given by Carney (1979).

The sample of 66 globular clusters from Frenk and White (1980) was adopted. Their selection criteria demanded that firmly established velocities and distance moduli exist in the literature for inclusion in the sample. For the present work the globular clusters' colors, apparent distance moduli and color excesses were all drawn from the

recent review article by Harris and Racine (1979). Absorption of A_V = 3.2E(B-V) was applied to get the true distance moduli. Radial velocities were taken from Webbink (1981).

The two metal-poor groups in Woolley and Savage (1971) provide the basis for the RR Lyrae sample. These two groups had median ΔS of 6 and 9 respectively and were combined into one sample of 79 metal-poor RR Lyrae stars in the solar neighborhood. Mean V magnitudes were given by Woolley and Savage and, following Woolley (1978) an absolute magnitude of M_V = 0.4 was adopted (changing this value to as bright as M_V = 0.0 and as faint as 1.0 does not affect the solution in any significant way).

b) The Solar Motion of the Halo

The solar motion calculated for each sample is given in column 3 of Table 1 along with its standard error in column 4. Line-of-sight velocity dispersions σ_{los} and the standard error in its determination $\varepsilon_{los} = \sigma_{los}/(2N)^{1/2}$ are listed in columns 5 and 6. The number of objects comprising each sample can be found in column 2. The values obtained for the subdwarfs, RR Lyrae and globular clusters are all in good agreement with other recent results (from the sources cited in §I for example). The results for Woolley's RR Lyrae sample are obtained through the same solution and should be identical -- in fact they differ very slightly. Round-off errors and possible undetected typographical mistakes could easily account for the differences. The observed variance of the four solutions is 33 km s^{-1} and the standard

error computed from

$$\sigma^2_{tot} = \sum \sigma^2_i/(N-1) \qquad (18)$$

gives σ_{tot} = 35 km s^{-1}. Hence one cannot argue that these objects are kinematically distinct. The fifth line in Table 1 shows the solar motion obtained by solving equation (1) for all 425 objects. The value of 195 $\pm$ 35 km s^{-1} sets a firm lower limit on the circular velocity of the LSR (though a higher limit is set in what follows).

Having just argued that the halo objects are not drawn from different kinematic populations, it is nonetheless of interest to see if the variances in the kinematics and metallicities within that population are related. The last half of Table 1 shows results obtained by dividing each of the four groups into two metallicity classes (called MP for metal-poor and MR for metal-rich for simplicity of notation but these are, of course, only relative terms). The AB stars were divided by simply drawing a straight line on the W(K) -- (B-V) diagram (see Figures 9 and 10 in Chapter 2) which closely approximates the lower limit set by those synthetic spectra with [A/H] = -1.0 and divides the sample into two nearly equal subsets. The RR Lyrae groupings were taken from Woolley and Savage (1971). Subdwarfs were divided into roughly equal groups by $\delta(U-B)_{.6}$. Integrated spectral types assigned to the globular clusters by Hartwick and Sargent (1978 -- which were in turned derived largely from the work of Harris 1976) were used to differentiate the metal-poor clusters (type F) from the relatively metal-rich (type G).

For all but the RR Lyrae stars both the solar motion and line-of-sight velocity dispersion increase with decreasing metallicity. Although the errors are large (each of the results is barely significant at the 1 σ level) the results are suggestive. The resulting values lend support to the long-recognized relationships between the metallicities and kinematics of halo objects (see, for example, Eggen, Lynden-Bell and Sandage 1962, hereinafter ELS). If one adopts a standard formation scenario for the Galaxy in which metallicity increases with time it then follows that those stars that are most metal-deficient and hence are the oldest have lower circular velocities and hence lower angular momenta than younger, more metal-rich stars (also a result by ELS). There is no clear-cut dividing point seen in any of the halo data. Rather there is a continuous progression from lower to higher metallicities in step with their kinematic signatures.

The last line of Table 1 shows the solar motion for 211 extremely metal-poor halo objects to be -208 ± 20 km s^{-1}. This sets an even greater lower speed limit for the circular velocity at the solar radius.

c) The Halo Velocity Ellipsoid

The last six columns of Table 1 present the velocity ellipsoid solutions for halo objects. Anisotropy seen here in the RR Lyrae velocities was reported by Woolley (1978). That in the subdwarfs has long been known from $\langle u^2 \rangle$, $\langle v^2 \rangle$, and $\langle w^2 \rangle$ -- which in the solar

neighborhood is nearly the same as $\langle R^2 \rangle$, $\langle \Theta^2 \rangle$, and $\langle \underline{\Phi}^2 \rangle$. The globular cluster result is not well determined owing principally to their distribution on the sky. Frenk and White (1980) and Lynden-Bell and Frenk (1981) see no evidence for anisotropy. Little can be said from the numbers here. For completeness, results for all of the samples and subsamples have been calculated, although in general the results are not well determined. The solution for all 425 halo objects does argue, however, for an anisotropic velocity distribution on the order of ~ $R^2:\Theta^2:\underline{\Phi}^2::2.4:2:1$. Although the formal anisotropy between R and Θ is not statistically significant, that between R and $\underline{\Phi}$ is firmly established. This anisotropy is seen to prevail in both metal-poor and metal-rich groups.

V. VARIATIONS WITH POSITION

a) Velocity Dispersions Perpendicular to the Plane

A number of AB stars are situated in fields towards the south galactic pole (SGP). To determine the variation of $Z \equiv \dot{z}$ with distance from the plane a subset of stars was chosen which have $\sin(|b|) > 0.9$ (i.e. $|b| > 65^\circ$). There are 39 such stars in the list and for them $\langle Z^2 \rangle^{1/2} = 79 \pm 9$ km s^{-1}. Further dividing the subset in half (at z = 6 kpc) and computing the velocity dispersion for each group yields 69 ± 11 km s^{-1} for $|z| < 6$ kpc (a result very similar to that found by Rodgers [1971] for another sample of A stars near the SGP) and 90 ± 15

km s^{-1} for those with $|z| \geq 6$ kpc. Taken at first glance, this is evidence for an increase in $\langle Z^2 \rangle^{1/2}$ with $|z|$. This result is, however, exactly what one would expect if the velocity ellipsoid were elongated in the radial direction. In the plane of the Galaxy Z and Φ are the same quantity. But at greater and greater distances from the plane Z becomes less and less a measure of Φ and more and more a measure of R. Define α to be the angle formed at the star between lines drawn to the sun and the galactic center. Then the contributions R and Φ make to the observed Z are $Z_R = R\cos(\alpha)$ and $Z_\Phi = \Phi\sin(\alpha)$, with $Z_R^2 + Z_\Phi^2 = Z^2$ (ignoring contributions from the θ direction which are negligible near the pole). For the low $|z|$ group the mean distance from the plane is 3.9 kpc and for the more distant group it is just twice that. With the adopted ϖ_0 it follows that the lower group's Z velocity is, on average, comprised of ~ 83% of the stars' Φ and only 17% R. But for the upper group the two components are represented nearly equally, at 54% for Φ and 46% for R. This result suggests that the anisotropy in velocities is a global, not just a local, phenomenon.

b) Velocity Dispersions at Different Galactic Radii

A star's distance from the galactic center (R_g) can be determined from the adopted distance modulus discussed in §III and from application of equation (6b). The sample was sorted by R_g and then divided into four roughly equal groups. The dispersion in the radial velocities for the groups was found to be

$$124 \pm 14 \text{ km s}^{-1} \text{ at } \langle R_g \rangle = 3.2 \text{ kpc},$$

$$96 \pm 10 \text{ km s}^{-1} \text{ at } \langle R_g \rangle = 6.0 \text{ kpc},$$

$$74 \pm 8 \text{ km s}^{-1} \text{ at } \langle R_g \rangle = 9.4 \text{ kpc},$$

and

$$102 \pm 11 \text{ km s}^{-1} \text{ at } \langle R_g \rangle = 12.0 \text{ kpc}.$$

At first blush these results seem to indicate that the velocity dispersion is high near the center, decreases to a minimum near the solar position, and then rises again. This not only puts the sun in a very special location but also is at odds with other indications (e.g. from rotation curve studies) which show no such pathological behavior in the gravitational potential. Once again a wholly satisfactory answer to this distribution comes by invoking anisotropy. The observed velocities for stars near the galactic center are dominated by the R component (the stars comprising this inner group are all in two fields with b = -16 and -29°). The next group is made up of stars with b = -29 and -55° so that the R component is still large although somewhat diminished. At $\langle R_g \rangle$ = 9.4 kpc the stars are largely towards the SGP where Φ claims most of the credit. The far field includes some stars at the pole far from the plane and some towards the anticenter at b = -58° where R again begins to dominate. The result is consistent with that of a velocity ellipsoid which remains essentially constant in size and is elongated towards the galactic center at all positions sampled.

c) A Note on Metallicity Spatial Distributions

As discussed in Chapter 2, the sample of AB stars may well be biased towards metal-poor stars due to the classification criteria used in their selection. Furthermore, the observational fact that significant numbers of BHB stars seem to occur only in metal-poor globular clusters almost certainly seriously biases the sample. Nonetheless a search was made for variations in mean metallicity with $\langle R_g \rangle$ and $\langle |z| \rangle$. None was found. All groupings showed the same mean value for the index employed (the ratio of the observed K line strength to that a normal A star of the same B-V would have) and all had roughly the same variance.

VI. IMPLICATIONS OF ANISOTROPY

A possible interpretation of the observed anisotropy of stars in the solar neighborhood (the subdwarf and RR Lyrae star samples, for example) is that the distribution of such stars is flattened towards the plane due to the added gravitational potential of the disk (Woolley 1978; van der Kruit and Searle 1981a,b). Van der Kruit and Searle conclude that it is the flattening of halo Population II rather than the extended scale height of an old disk Population I that gives rise to the thick disks observed in some external galaxies (Burstein 1979).

The observational evidence for flattening of the halo component in our Galaxy is controversial (see Mihalas and Binney 1981, pp. 259-262 for a recent discussion). Harris (1976) found the distribution of globular clusters to be well represented by a spherically-symmetric

distribution with a power-law density function and index ~ -3.5 for $R_g > 3$ kpc. Oort and Plaut (1975) found a similar result for RR Lyrae stars near the galactic center. For the halo AB stars, however, Shectman (1982, private communication) finds the number counts are best fit by a power-law with index ~ -3.4 and a flattened distribution with axial ration of 0.7. He rules out, at the 90% confidence level, axial ratios > 0.9 and < 0.5.

The data at hand are not sufficient to settle the issue. There is, however, a point to be made. It is that although a flattened halo would give rise to the observed velocity anisotropy locally, evidence for global anisotropy negates the conclusion. That is, if the halo velocities are everywhere anisotropic (as the halo AB star results indicate), then the observed anisotropy in the solar vicinity is simply a measure of global anisotropy and says nothing about flattening.

Furthermore it seems difficult to explain the anistropy to be a result of flattening. If the initial collapse of the Galaxy was radial and at some later time the disk was formed how would it affect the z component of the velocities of the spheroidal stars? Consider first a star that is passing through the proto-plane with velocity Z_0 as an increment of mass is added to the plane. As the star climbs toward higher z it will be decelerated by the additional mass and will not reach as high as it would have without the addition of the disk mass (thus flattening its orbit). However, when the star returns to the plane it will have regained the kinetic energy that it had given up to potential energy and again pass through with a velocity of Z_0. Alternatively, consider a star situated away from the plane when an

increment of mass is added to the disk. Such a star will receive an acceleration in z and pass through the plane at a Z_0 higher than it had on its previous passage. Hence the result of concentrating mass in the disk is either to leave Z_0 unaffected or to increase it. An anisotropic velocity ellipsoid implies that before the disk was formed the anisotropy was even more pronounced -- i.e. the stars which partook in the early collapse were on highly eccentric, predominantly radial orbits and the disk formation has played a role in making their velocities more isotropic. In short, local anisotropy does not necessarily imply flattening, rather flattening may even result in decreased anisotropy.

VII. CONCLUSIONS

The kinematic analyses presented here of the halo AB star sample and of other halo objects drawn from the literature have

1) lent support to the long-recognized coupling of the metallicities and kinematic properties of halo objects;

2) established a lower limit of 208 $\pm$ 20 km s^{-1} for the circular velocity at the solar radius;

3) shown that anisotropy in the velocity

ellipsoid is not limited to objects near the plane but reaches far out into the halo; and

4) suggested that the formation of the disk causes the velocity ellipsoid to become more isotropic which supports the hypothesis of an initial radial collapse of the Galaxy.

TABLE 1. KINEMATIC PARAMETERS FOR HALO OBJECTS

Sample	N	Solar Motion (km/s)	σ_{los}	$\langle R^2 \rangle$	$\langle \theta^2 \rangle$	$\langle \Phi^2 \rangle$
				10^4 (km/s)^2		
Halo AB	171	-236±39	100± 5	1.33±0.43	0.22±1.05	0.93±0.23
RR Lyrae	79	-224 25	110 9	2.14 0.54	1.51 0.55	0.52 0.37
Subdwarfs	109	-178 25	134 9	3.04 0.64	1.16 0.79	1.09 0.64
Glob. Cl.	66	-170 30	122 11	1.37 0.33	2.52 0.65	0.64 0.93
ALL	425	-195 35	115 4	1.91 0.24	1.60 0.36	0.80 0.20
AB-MR	82	-209 45	81 6	1.05 0.46	-- --	0.54 0.25
AB-MP	86	-264 64	115 9	1.69 0.74	0.39 1.69	1.25 0.40
RR-MR	54	-226 31	115 11	2.13 0.70	1.43 0.67	0.81 0.46
RR-MP	25	-223 39	98 14	2.24 0.89	1.84 1.03	-- --
SD-MR	46	-155 39	128 13	2.98 0.77	0.76 1.07	0.98 0.89
SD-MP	54	-204 35	139 13	3.38 1.19	1.23 1.24	1.34 0.98
GC-MR	19	-36 66	93 15	0.79 0.41	3.22 1.16	1.03 1.17
GC-MP	46	-190 35	130 14	1.86 0.46	2.15 0.80	0.21 1.28
ALL-MR	201	-181 20	106 5	1.69 0.29	1.52 0.46	0.61 0.23
ALL-MP	211	-208 20	123 6	2.20 0.40	1.53 0.57	0.99 0.32

REFERENCES

Burstein, D. 1979, Ap. J., 234, 829.

Carney, B. W., 1979, Ap. J., 233, 877.

Chiu, L.-T. G., 1980, Ap. J. Suppl., 44, 31.

Clifford, A. A. 1973, Multivariate Error Analysis, (New York:John Wiley and Sons), pp. 78-79.

Eggen, O. J., Lynden-Bell, D., and Sandage, A. 1962, Ap. J., 136, 748 (ELS).

Frenk, C. S., and White, S. D. M. 1980, M.N.R.A.S., 193, 295.

Gunn, J. E., Knapp, G. R., and Tremaine, S. D. 1979, A. J., 84, 1181.

Harris, W. E. 1976, A. J., 81, 1095.

Harris, W. E., and Racine, R. 1979, Ann. Rev. Astr. Ap., 17, 241.

Hartwick, F. D. A., and Sargent W. L. W. 1978, Ap. J., 221, 512.

Kinman, T. D. 1959, M.N.R.A.S., 119, 559.

Lynden-Bell, D., and Frenk, C. S. 1981, The Observatory, 101, 200.

Mihalas, D., and Binney, J. 1981, Galactic Astronomy, (2d ed.; San Francisco:W. H. Freeman).

Oort, J. H., and Plaut, L. 1975, Astr. Ap., 41, 71.

Philip, A. G. D., Cullen, M. F., and White, R. E. 1976, Dudley. Obs. Rpt., No. 11.

Rodgers. A. W. 1971, Ap. J., 165, 581.

Sandage, A. 1970, Ap. J., 162, 841.

-----1981, A. J., 86, 1643.

Sandage, A., and Katem, B. 1982, A. J., 87, 537.

van der Kruit, P. C., and Searle, L. 1981a, Astr. Ap., 95, 105.

-----1981b, Astr. Ap., 95, 116.

Webbink, R. F. 1981, Ap. J. Suppl., 45, 259.

Woolley, R. 1978, M.N.R.A.S., 184, 311.

Woolley, R., and Savage, A. 1971, R. Obs. Bull., No. 170.

FIGURE CAPTION

Fig. 1. - The angles and distances used in the analysis are defined as shown.

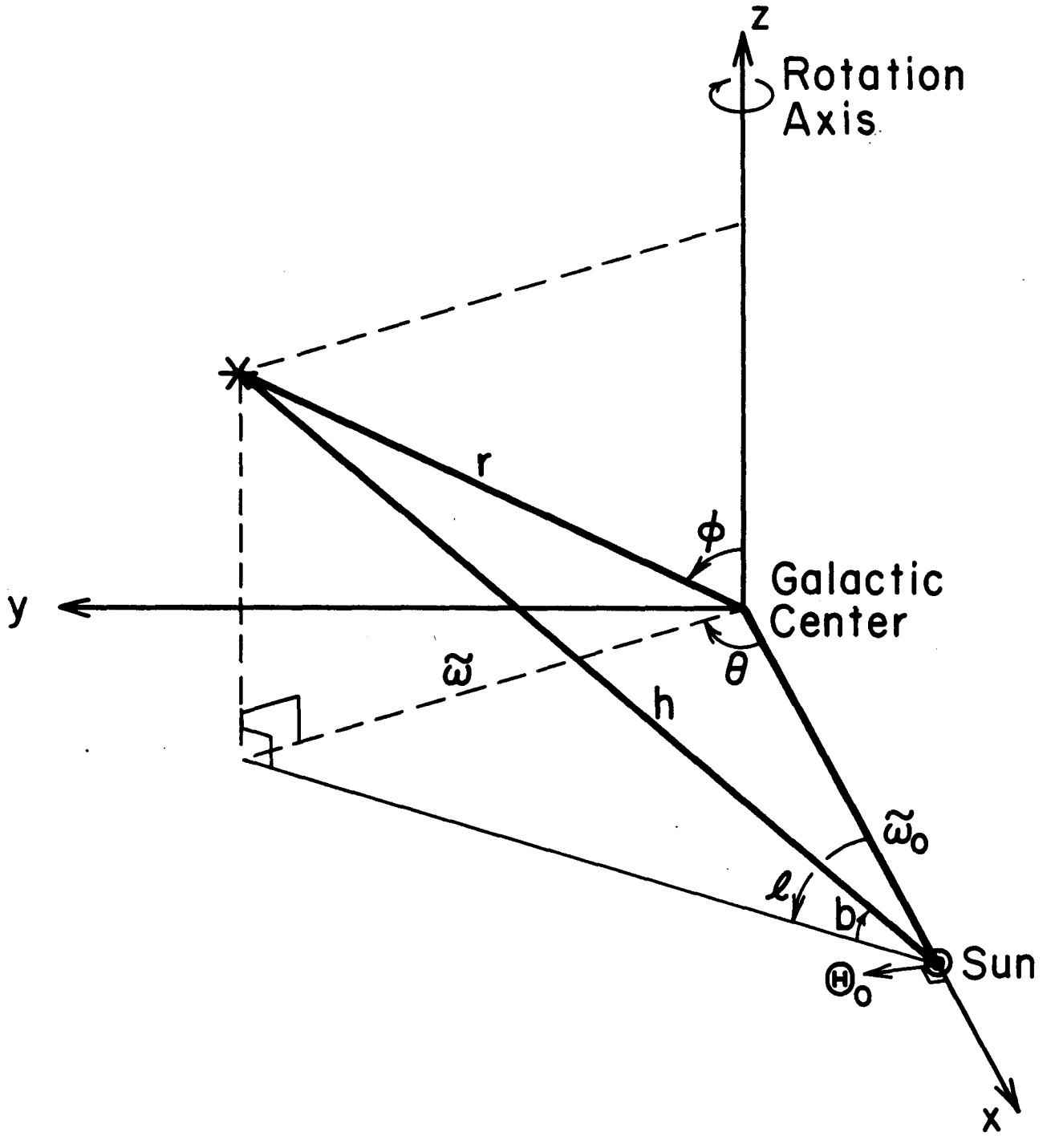

Figure 1